Accurate ab initio theoretical studies of rovibronic states of some simple diatomic molecules

Kazutoshi Okada

Doctor of Philosophy

Department of Structual Molecular Science

School of Mathematical and Physical Science

The Graduate University for Advanced Studies

Contents

Chapter 1

General Introduction

Some of diatomic molecules are known to be the most important molecules in the fields of gas-phase reaction, atmospheric chemistry and quantum chemistry. They have been the subject of numerouns experimental and theoretical studies for many years. In the early stage of development in quantum theory, together with the atomic spectra, the electronic, vibrational and rotational spectra of diatomic molecules played a historic role. The spectra give information of the energy difference between the initial and the final quantum states, which is called transition energy. By analyzing the transition energy, the electronic, vibrational and rotational states of the molecules, and the energy levels of the states are determined. The motion of the electron and nuclei are analyzed from the obtained electronic, vibration and rotational levels.

The studies of electronic spectra have lead to the theoretical understanding of chemical valence. The studies of vibrational spectra have lead to vibrational frequencies and force constants, which provide not only the microscopic properties of the molecule but also information about the macroscopic properties of gaseous phase. The studies of rotational spectra give accurate information about the geometrical arrangement of the nuclei in the molecule, especially about the knowledge of rotational constants B_v. From experimental B_v, the equilibrium structure of the molecule, such as equilibrium bond length R_e, can be obtained. The knowledge of the various spectroscopic properties allows us to understand many of the physical and chemical properties of molecules. During many years of improvement of experimental studies such as light source, detector, and the experimental technique, the resolution of the spectra was substantially improved. Rotationally resolved spectral pattern was observed even for the electronic excited states. As the resolution

improves, irregularities of spectral pattern from conventional vibrational and rotational levels becomes evident, which is due to the existence of the interaction with other electronic states; it implies the partial breakdown of the Born-Oppenheimer description.

Theoretically, ab initio SCF MO and CI calculations of diatomic molecules were started more than 40 years ago. From these calculations, many properties, such as potential energy and dipole moment, were directly obtained from a given geometric structure and electronic state of a molecule. The calculated results were compared with the experimental data. At first, the accuracy of calculations was, however, very limited. As the power of the computer increases, more accurate theoretical calculations became possible. The accurate calculated results were comparable with experimental data. The calculated results reasonably reproduced experimental data, often gave predictions and sometimes gave new insights to experimental studies. Theoretical studies now play an important role in the studies of diatomic molecules in the quantitative sense.

In accordance with the development of both experimental and theoretical studies, ionic states of diatomic molecule have also been paid attention to. Experimentally, there are many studies on diatomic molecular ion using photoelectron spectroscopy. Recently, the pulsed field ionization zero kinetic energy (PFI-ZEKE) spectroscopy has made it possible to obtain rotationally resolved spectra. Theoretical studies also paid attention to the ionic states. As the experimental techniques being well established, the obtained rovibronic spectra becomes more and more complicated, and more and more important properties of diatomic molecules and molecular ions are being studied. The studies on diatomic molecules, both experimentally and

theoretically, still remain important.

To analyze the complicated experimental data, more accurate theoretical studies are required. However, the previous theoretical studies on diatomic molecules are usually old and the results are not very accurate to reproduce the recent experimental data quantitatively. With the rapid development of computational power and techniques, theoretical studies on diatomic molecule are required to be updated.

In this study, a new state-of-the-art theoretical studies are presented for some diatomic molecules and molecular ions. Accurate potential energy and dipole moment curves are obtained. Vibrational and rotational energies and wavefunctions on the calculated potential energy curves are calculated. Vibrational and rotational spectroscopic constants are obtained. With the obtained vibronic wavefunctions and dipole moment curves, Einstein's A and B coefficients for rovibronic transitions are calculated, and the radiative lifetimes of the rovibronic levels are also evaluated. All calculated results are compared with available experimental data and previous calculated results. Especially in chapter 4, for the ground state of carbon monoxide molecule, accurate calculations of rovibrational levels up to very high rotational quantum number $J \sim 150$ are performed. Absorption energies and intensities for the rovibrational transitions $(v', J') \leftarrow (v'', J'')$ are simulated and compared with experimental data obtained on an interferometric spectrometer on a satellite.

Chapter 2

Accurate potential energy and transition dipole moment curves of the $X^2\Sigma^+$, $A^2\Pi$ and $B^2\Sigma^+$ states CO^+

The Journal of Chemical Physics **112**, 1804 (2000).

I. INTRODUCTION

The carbon monoxide cation is one of the basic diatomic cations. Wanberg et al [1] reported vibrationally resolved photoelectron spectra for the $X^2\Sigma^+$,$A^2\Pi$, and $B^2\Sigma^+$ states of CO^+ by HeI, HeII, NeI, and NeII excitations. More recently, Hepburn et al obtained rotational structures of $X^2\Sigma^+$, [2] and $A^2\Pi$ [3] state of CO^+ with the resolution of about $1.5cm^{-1}$ by pulsed field ionization photoelectron (PFI-PE) spectroscopy. Also Evans and Ng determined vibrational spacings and rotational constants of the $X^2\Sigma^+$ state by observing the rovibrational levels up to near dissociation limit. [4] Accurate theoretical calculations are required to explore these new experimental results.

There are numerous theoretical studies for low-lying doublet and quartet states. For instance, Marian et al calculated the potential energy curves as well as the transition dipole functions along with the lifetime measurement. [5] Lavendy et al also reported the transition probability among the low-lying states. [6] Both works evaluated the spectroscopic constants such as R_e, ω_e, and $\omega_e x_e$, which were in fairly good agreement with the then-available experimental constants. In the present theoretical works, we attempt to respond to the latest experimental data on the $X^2\Sigma^+$ and $A^2\Pi$ states, and have attained quantitative agreement with them up to the highest vibrational levels. We further extend the works to the other doublet and quartet states with nearly the same accuracy to stimulate detailed experimental studies.

II. CALCULATION

Multi-reference configuration interaction (MRCI) calculations were performed for low-lying electronic states of CO^+ and the neutral ground state. Two types of basis set were employed. The one was derived from Huzinaga's (8s,5p) [7] contracted to [5111/2111], augmented with two d function and one f function by Noro et al [8] ; the basis set becomes [5111/2111/21/2]. The other was the augmented valence quadruple zeta (aug-ccpVQZ, AVQZ) basis set of Dunning [9] The latter was employed to obtain accurate potential energy and property curves for $X^2\Sigma^+$, $A^2\Pi$, $B^2\Sigma^+$, and $C^2\Delta$ state of CO^+, and the neutral ground state ($X^1\Sigma^+$). The valence-type vacant orbitals, 2π and 6σ, were determined by the VALVAC (valence-type-vacant) method of Iwata. [10] The method requires only a single Fock matrix generation, and provides us with a proper anti-bonding nature of molecular orbitals. In this method we need not solve the state-averaged MCSCF. The occupied orbitals (1σ to 5σ and 1π) were determined with the closed shell SCF calculation for the neutral ground state. With a single set of molecular orbitals thus determined, MRCI calculations were carried out for all the other states.

The outline of the VALVAC method is described below.

In the basis set expansion, the molecular orbital (one-electron function) ζ_t is written as

$$\zeta_t = \sum_{p=1}^{N_{basis}} \chi_p v_{p,t} \equiv \tilde{\chi}\mathbf{v_t},$$

where $\tilde{\chi}$ is the row vector of the basis function, and $\mathbf{v_t}$ is the column vector of the coefficients. The atomic occupied orbitals in the present case, 1s, 2s and 2p orbitals

of carbon and oxygen atoms, are expanded with the same (or a part of) basis set, χ. The set of atomic occupied orbitals, φ_i^{at}, defines a space Ω^{at}, and the projection operator $\widehat{P}_{at}$ on to the space is defined as

$$\widehat{P}_{at} = \sum_{i=1}^{N_{at}} |\varphi_i^{at} >< \varphi_i^{at}|$$

where N_{at} is the number of the occupied orbitals in the atoms; in the present case, $N_{at} = 5 + 5 = 10$. For a molecule concerned, N_{moc} corresponds to the number of occupied molecular orbitals $\{\phi_k; k = 1, , , N_{moc}\}$, and define a space Ω^{moc}. The projection operator $\widehat{P}_{moc}$ is written as

$$\widehat{P}_{moc} = \sum_{k=1}^{N_{moc}} |\phi_k >< \phi_k| \ .$$

As chemists, we know that the electron distribution around each atom in a molecule is not very much different from that of an isolated atom. Therefore, the space Ω^{moc} is almost included in the space Ω^{at}. The vacant orbital space is represented as Ω^{mvac} and its projection operator is defined as

$$\widehat{P}_{mvac} = 1 - \widehat{P}_{moc} = \sum_{k=N_{moc}+1}^{N_{basis}} |\phi_k >< \phi_k| \quad .$$

Now, the valence type vacant orbitals are the orbitals (one-electron functions) which are included both in Ω^{at} and Ω^{mvac}. The projection operator $\widehat{P}_{vv}$ on to the space which includes both Ω^{at} and Ω^{mvac} is written as

$$\widehat{P}_{vv} = \widehat{P}_{at}\widehat{P}_{mvac} \ .$$

Now, the valence vacant orbitals ψ_s can be defined as

$$\widehat{P}_{vv}\psi_s = 1 \cdot \psi_s \ ,$$

that is, to determine the valence vacant orbitals, we look for the orbitals whose eigenvalue of $\widehat{P}_{vv}$ is 1. It can be proved in general that the eigenvalues of a projection

operator should be less than or equal to 1.

In the basis set expansion, a projection operator $\widehat{P}$ is written as

$$\widehat{P} = \sum_{t}^{N_P} |\zeta_t >< \zeta_t| = \widetilde{\chi}(\sum_{t}^{\mathbf{N_P}} \mathbf{v_t}\widetilde{\mathbf{v}}_\mathbf{t})\chi$$

If $\psi_s = \widetilde{\chi}\mathbf{u_s}$, the equation to be satisfied is

$$< \psi_s|\widehat{P}|\psi_s >= \tilde{\mathbf{u}}_s\mathbf{S}(\sum_{t}^{\mathbf{N_P}} \mathbf{v_t}\widetilde{\mathbf{v}}_\mathbf{t})\mathbf{S}\mathbf{u_s} = \mathbf{1} \ ,$$

where $\mathbf{S}$ is an overlap matrix $\langle\chi|\widetilde{\chi}\rangle$. In other words, we look for the eigenvectors of the symmetric matrix,

$$\mathbf{SPS} \equiv \mathbf{S}(\sum_{t}^{\mathbf{N_P}} \mathbf{v_t}\widetilde{\mathbf{v}}_\mathbf{t})\mathbf{S} \ ,$$

whose eigenvalue is 1. If the space Ω^{moc} is completely outside of Ω^{at}, there exist N_{at} eigenvectors with an eigenvalue of 1. On the other hand, if the space Ω^{moc} is almost included in Ω^{at}, which happens in most of the cases as mentioned above, N_{at} - N_{moc} eigenvectors with an eigenvalue of 1 are expected. In CO, 10 - 7 = 3 is the number of eigenvectors with an eigenvalue 1; they correspond to π^* and σ^* anti-bonding orbitals. To avoid the symmetry broken solution we need a little care in the computer code. In our code, starting with a set of proper guess vectors, we use the maximum eigenvalue method. In our experience, the expected number of vectors with an eigenvalue 1 is $N_{at} - N_{moc}$, unless there are input errors in the geometry, basis set, or the atomic orbitals φ_i^{at}.

MRCI calculations were performed with MOLPRO internally contracted CI method. [11,12] The reference configurations were all electronic configurations generated from [$1\sigma^2$, $2\sigma^2$, $3\sigma^{0-2}$, $4\sigma^{0-2}$, $1\pi^{0-4}$, $5\sigma^{0-2}$, $2\pi^{0-4}$, $6\sigma^{0-2}$, $7\sigma^{0-1}$], where 7σ orbital is a Rydberg type orbital. The calculations were performed under C_{2v} symmetry.

Vibrational energies and wavefunctions on each adiabatic potential energy curve were calculated by solving the one-dimension nuclear Schrödinger equation with the FEM1D program of Kimura et al. [13] The integration region was between 1.6 a.u. and 10.0 a.u.. Vibrational spectroscopic constants ω_e, $\omega_e x_e$, $\omega_e y_e$, and $\omega_e z_e$ were obtained using the least-squares fitting of $\Delta G_{v+\frac{1}{2}} = G(v+1) - G(v)$, $G(v)$ being the vibrational energy relative to the lowest vibrational level. $G(v)$ is expressed as

$$G_v = \omega_e\left(v+\tfrac{1}{2}\right) - \omega_e x_e\left(v+\tfrac{1}{2}\right)^2 + \omega_e y_e\left(v+\tfrac{1}{2}\right)^3 + \omega_e z_e\left(v+\tfrac{1}{2}\right)^4 + \ldots$$

Rotational constants B_v were evaluated using the vibrational wavefunction as

$$B_v = \tfrac{h}{8\pi^2 c\mu}\left\langle \Psi(R;v)\left|\tfrac{1}{R^2}\right|\Psi(R;v)\right\rangle$$

where μ is the reduced mass of the molecule, and $\Psi(R;v)$ is the vibrational wavefunction of the vibrational quantum number v. Rotational constants, B_e, α, γ, and δ, were evaluated by the least-squares fitting to

$$B_v(v) = B_e - \alpha\left(v+\tfrac{1}{2}\right) + \gamma\left(v+\tfrac{1}{2}\right)^2 + \delta\left(v+\tfrac{1}{2}\right)^3$$

The dipole moment function of each state and the transition moment function between the states were evaluated, and by integrating them over the vibrational wavefunctions, the Einstein's A and B coefficients of the vibrational transitions as well as the vibronic transitions were evaluated.

III. RESULTS AND DISCUSSION

A. Potential energy curves

Figure 1 shows the potential energy curves (PEC) of CO^+ calculated by AVQZ basis set. The potential energy curves lying below 70000 cm^{-1} relative to the $v = 0$

level of the $X\ ^2\Sigma^+$ state are shown. The horizontal lines on each potential energy curve are the calculated vibrational levels. Equilibrium bond length, excitation energy, dissociation energy, and vibrational constants are also calculated from the potential energy curves, and are summarized in Table 1. More detailed calculational results are available on the web site. [14]

Figure 2 shows the potential energy curves of the other doublet states and the low-lying quartet states and $^2\Sigma^-$ states, calculated by Noro basis set. These states dissociate to $C^+(^2P)$+$O(^3P)$ or $C^+(^2P)$+$O(^1D)$. From the figures, all of the calculated potential energy curves properly converge to the correct dissociation limit. The calculated energy difference at the dissociation limit between $C^+(^2P)$+$O(^3P)$ and $C^+(^2P)$+$O(^1D)$ is 16524 cm^{-1} by Noro basis set and 16118 cm^{-1} for AVQZ basis set. This is in good agreement with the corresponding experimental value 15789.9 cm^{-1}. [15] Figure 1 and Table 1 show that the PECs are accurate both near the equilibrium bond length and to the dissociation limit. Even the PECs by NOROs are reasonably accurate. It should be emphasized that a single set of molecular orbitals are used in these MRCI calculations.

B. Vibrational and rotational constants

Figure 3 shows $\Delta G_{v+\frac{1}{2}} \equiv G(v+1) - G(v)$ for the $X^2\Sigma^+$ state, plotted against $v+1/2$. In the figure, $\Delta G_{v+\frac{1}{2}}$ calculated with both basis sets are compared with the latest experimental values of Evans and Ng. [4,17] Dashed lines and a solid line are the least-squares fitted lines below $v \leq 14$ to determine spectroscopic constants ω_e

and $\omega_e x_e$. The agreement of AVQZ plot is almost perfect. As shown in Figure 1, the $v = 10$ of $X^2\Sigma^+$ state lies just above the $v = 0$ of the $A^2\Pi$ state. Coxon et al [18] and also Kong and Hepburn [19] decoupled the perturbation by assuming that the $v = 10$ level of the $X^2\Sigma^+$ state coincides with the $v = 0$ level of the $^2\Pi_{1/2}$ in $3cm^{-1}$. The $v = 0$ level of the $^2\Pi_{3/2}$ state is 120 cm^{-1} below the the $v = 0$ level of the $^2\Pi_{3/2}$ state In our calculations the spin-orbit coupling in the $A^2\Pi$ state is not taken into account. The calculated error in the energy difference between the $v = 10$ of $X^2\Sigma^+$ state and the $v = 0$ of the $A^2\Pi$ state is as large as the splitting of two multiplets of the $A^2\Pi$ state.

Evans and Ng determined the vibrational spacings up to $v = 41$. The experimental and AVQZ $\Delta G_{v+\frac{1}{2}}$ are plotted to the third order polynomial for $v \leq 40$ to obtain the ω_e, $\omega_e x_e$, $\omega_e y_e$ and $\omega_e z_e$. Their experimental (AVQZ) values are 2225.8 (2237.6), 17.07(18.34), 0.111(0.189) and $-0.00232(-0.00359)$, respectively. Above $v = 34$, the deviation from the data points becomes large. If we use the data below $v = 34$, they become 2221.1(2226.8), 16.44(16.86), 0.081(0.0120), $-0.00189(-0.002657)$, respectively. The agreement of the corresponding values is substantially improved. In the experimental plot, the other irregularities are found at $\Delta G_{27+1/2}$ and $\Delta G_{28+1/2}$. In the inserted figure of Figure 4, the plots between $v = 25$ and 34 are shown in an expanded scale. The experimental energy of the $v = 28$ of the X state is at 49498 cm^{-1}. In our calculated vibrational energies of the $v = 2$ and 3 of the $B^2\Sigma^+$ state are $49044cm^{-1}$ and $50627cm^{-1}$. As Table 1 shows, the calculated T_e for the $B^2\Sigma^+$ state is only $100cm^{-1}$ higher than the experimental value, and also the vibrational constants for the $B^2\Sigma^+$ states are in good agreement with the experimental ones.

Therefore, the perturbing state is either $v = 2$ or 3.

The vibrational levels are also calculated for the other electronic states, and their spectroscopic constants are compared with the corresponding experimental data. The $\Delta G_{v+\frac{1}{2}}$ plots with the AVQZ basis set for the $A^2\Pi$, and $B^2\Sigma^+$ states are expected to be in a similar accuracy with that for the $X^2\Sigma^+$ state. The calculated curve of the $C^2\Delta$ state supports only four vibrational states.

Figure 4 shows the v dependence of rotational constant B_v of the $X^2\Sigma^+$ state. B_v is fitted by third order polynomial for $v \leq 40$ to obtain B_e, α, γ and δ. Their experimental (AVQZ) values are 1.9798(1.981), 0.0202(0.0234), $-1.2\times10^{-4}(3.80\times10^{-4})$ and $-5.3\times10^{-6}(-9.94\times10^{-6})$, respectively. When we use the data only below $v = 34$, they become 1.976(1.971), 0.0187(0.0198), $-3.9\times10^{-6}(1.0\times10^{-4})$ and $-2.6\times10^{-6}(-4.5\times10^{-6})$, respectively. Evans and Ng [4] noticed the wavy structure in the plot of B_v between $v = 25$ and 35, which becomes more evident when the plot of the theoretical B_v, as shown in the inserted figure of Figure 4.

C. Franck-Condon factors

In the PFI-PE [4] and HeI photoelectron [1] spectra, the relative intensity in the vibrational progression is measured. They might be compared with Franck-Condon factors $< v'' = 0; X^1\Sigma^+|v'; X^2\Sigma^+ >$. But, the relative FCFs are always much smaller than the observed relative intensity; for instance, the ratio for $v' = 1$ is 18.18 in PFI-PE, 4.819 in HeI PES and 2.86 in FCF, the ratio for $v' = 3$ is 5.87 in PFI-PE, 1.386 in HeI PES and 0.00015 in FCF, and the ration for $v' = 11$ is 0.3455

in PFI-PE, 1.566 in HeI PES and the order of 10^{-6} in FCF. It is obvious that the bond length dependence of the electronic matrix element must be taken into account in evaluating the vibrational dependence of photoionization cross section.

D. Lifetime and Einstein's A coefficients of the vibronic states of the $A^2\Pi$ and $B^2\Sigma^+$ states

Figure 5 shows the square of transition dipole moment functions between the $X^2\Sigma^+$and $A^2\Pi$ states, between the $X^2\Sigma^+$and $B^2\Sigma^+$ states, and between the $A^2\Pi$ and $B^2\Sigma^+$ states. Marian et al [5] and Lavendy et al [6] also calculated the transition dipole moment functions. Roughly speaking, the shapes of their curves are in agreement with ours, but in detail the bond length dependence of the functions is different. In Table 2, the calculated lifetimes of the vibronic states of the $A^2\Pi$ state are compared with the experimental and previously calculational ones. Our values up to $v = 10$ are in excellent agreement with the experimental ones by Möhlmann and Heer. [21] The accuracy in our calculations is expected to persist for higher vibrational quanta and for the higher electronic states. For instance, as shown in Table 3, the calculated lifetimes of the vibrational levels of the $B^2\Sigma^+$ state are in perfect agreement with the available experimental data within the experimental error. Our calculations confirm the lifetime measurement by Marian et al. [5] These agreements imply that the calculated Einstein's A coefficients to the lower electronic states are accurate. The calculated A coefficients can be used to estimate the vibrational temperature of the excited states, by observing the relative intensity of the vibronic bands in the emission spectra. The vibrational temperature enables

us to discuss the formation and decay mechanisms of the ions. Furthermore, if the absolute intensity of the emission bands could be estimated from the observation, we could determine the ion density of the light source in the atmosphere and in interstellar space. Because the rotational constants of the vibrational levels are accurately calculated, the A and B coefficients of the rovibronic states can be accurately predicted, if necessary. In fact, we have simulated the rovibrational $\Delta v = 2$ spectrum from very hot neutral CO molecules in the sun, and the results will be published separately. [22, Okada K, Iwata S in preparation]

IV. CONCLUDING REMARKS

Using an appropriate set of molecular orbitals with an extensive basis set, we have demonstrated that MR SDCI calculations provide accurate potential energy and dipole moment function curves for several low-lying electronic states. The calculated physical properties of the rovibronic states, such as the Einstein's A and B coefficients, can be substituted for the experimentally unavailable data in simulating the microscopic and macroscopic properties of molecular gases.

V. ACKNOWLEDGMENT

The authors acknowledge professor Ng and Dr. Evans for sending their new experimental data prior to the publication. This project is partially supported by the Grant-in-Aids for Scientific Research (No. 11166270) by the Ministry of Education, Science, Sports, and Culture, Japan, and by the project "Computational

Chemistry of Molecules in Atmospheric Environment" of Research and Development Applying Advanced Computational Science and Technology under Japan Science and Technology Corporation.

REFERENCES

[1] B. Wannberg, D. Nordfors, K. L. Tan, L. Karlsson and L. Mattsson, J. Electron Spectroscopy and Related Phenomena **47,** 147 (1988).

[2] W. Kong, D. Rodgers, and J. W. Hepburn, K. Wang, and V. McKoy, J. Chem. Phys. **99,** 3159 (1993).

[3] W. Kong and J. W. Hepburn, J. Phys Chem. **99,** 1637 (1995)

[4] M. Evans and C. Y. Ng, J. Chem. Phys. in press (1999).

[5] C. M. Marian, M. Larsson, B. J. Olsson and P. Sigray, Chem. Phys. **130,** 361 (1989).

[6] H. Lavendy, J. M. Robbe and J. P. Flament, Chem. Phys. Lett. **205,** 456 (1993)

[7] S. Huzinaga, J. Andzelm, M. Klobukowski, E. RadzioAndzelm, Y. Sakai and H. Tatewaki, eds. Physical Sciences Data, Vol. 16, *Gaussian basis sets for molecular calculations* (Elsevier, Amsterdam, 1985)

[8] T. Noro, M. Sekiya and T. Koga, Theor. Chem. Acc. **98,** 25 (1997).

[9] T. H. Dunning Jr, J. Chem. Phys. **90,** 1007 (1989).

[10] S. Iwata, Chem. Phys. Lett. **83,** 134 (1981).

[11] H. -J. Werner and P. J. Knowles, J. Chem. Phys. **89,** 5803 (1988).

[12] P. J. Knowles and H. -J. Werner, Chem. Phys. Lett. **145,** 514 (1988).

[13] T. Kimura, N. Sato, and S. Iwata, J. Comp. Chem. **9,** 827 (1988).

[14] http://www.kadmos.ims.ac.jp/

[15] A. A. Radzig and B. M. Smironv *Reference Data on Atomes, Molecules, and Ions* (1985); The proper average is taken among the multiplets.

[16] K. P. Huber and G. Herzberg, Molecular Spectra and Molecular Structure IV. *Constants of Diatomic Molecules* (Litton Educational Publishing Inc. 1979).

[17] R. C. Shiell, M. Evans, C-W. Hsu, C. Y. Ng and J. W. Hepburn, Chem. Phys. Lett. in press.

[18] J. A. Coxon and S. C. Foster, J. Mol. Spectro. **93,** 117 (1982).

[19] W. Kong and J. W. Hepburn, J. Phys. Chem. **99,** 1637 (1995).

[20] V. E. Bondybey and T. A. Miller, J. Chem. Phys. **69,** 3597 (1978).

[21] G. R. Möhlmann and F. J. De Heer, Chem. Phys. Lett. **43,** 170 (1976).

[22] K. Okada and S. Iwata in preparation

FIGURE CAPTION

Figure 1. The potential energy curves of the $X^2\Sigma^+$, $A^2\Pi$, and $B^2\Sigma^+$states of CO^+.

Figure 2. The potential energy curves of several low-lying electronic states calculated with the Noro basis set. a) The curves of the $^2\Sigma^+$, $^2\Pi$, and $^2\Delta$ states. b) The curves of the $^2\Sigma^-$ states and of the quartet states.

Figure 3. The energy spacing between two adjacent vibrational levels of the $X^2\Sigma^+$ state, $\Delta G(v+\frac{1}{2})$, plotted against the vibrational quantum number $2v$. Black and white circles are the calculated results from the Noro and AVQZ basis sets, respectively. Black boxes are from experiment [4]. The plot of $\Delta G(v+\frac{1}{2})$ starts at $G(1) - G(0)$. The inserted figure expands the plots between $v = 25$ and 34.

Figure 4. v dependence of rotational constant, B_v, of the $X^2\Sigma^+$ state. The inserted figure expands the plots between $v = 25$ and 35.

Figure 5. Square of transition dipole moments between $X^2\Sigma^+$ and $A^2\Pi$ states, between $X^2\Sigma^+$ and $B^2\Sigma^+$ states, and between $A^2\Pi$ and $B^2\Sigma^+$ states

Fig. 1

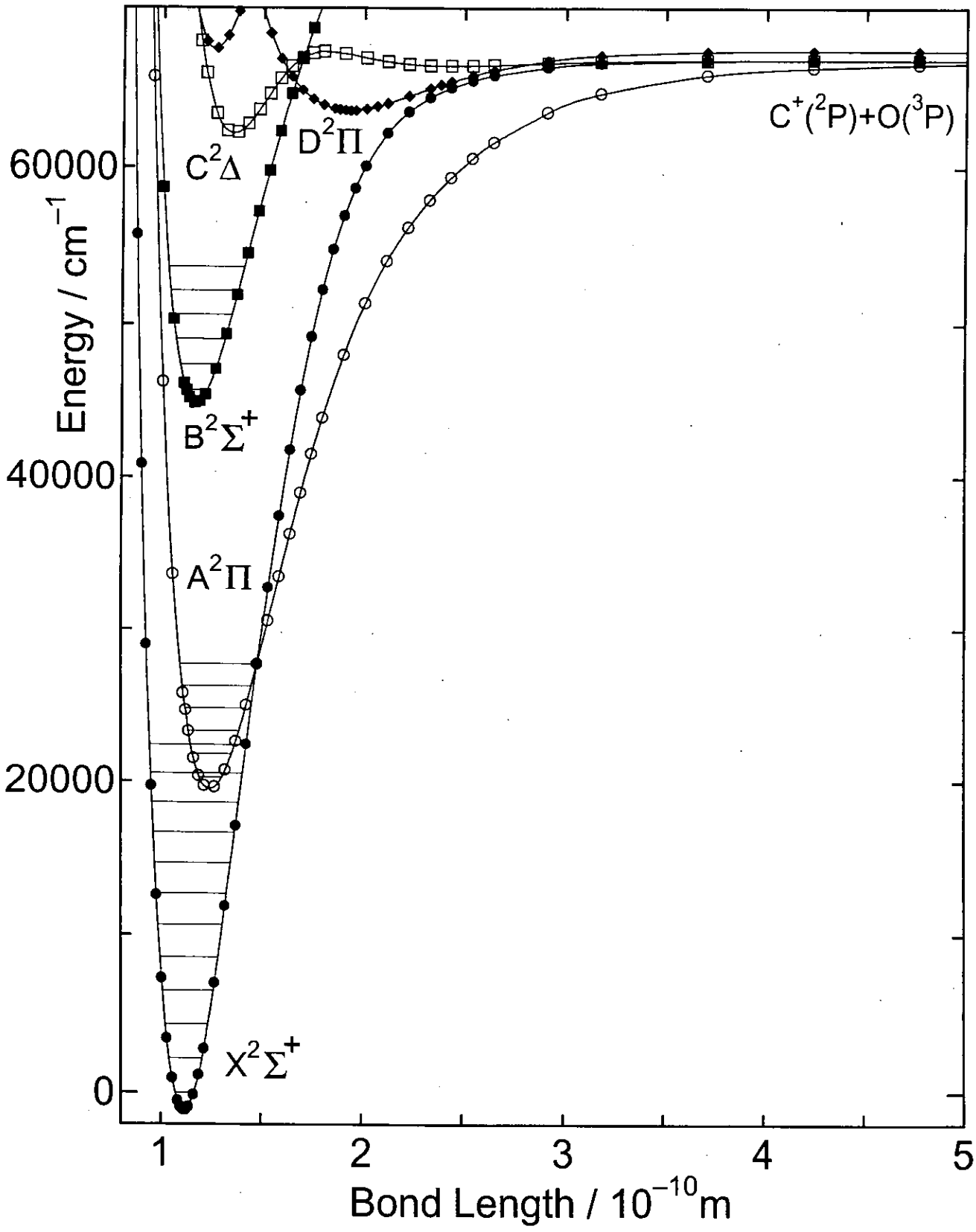
Energy / cm^{-1}
60000
40000
20000
0
1
2
3
4
5
Bond Length / 10^{-10}m
$C^2\Delta$
$D^2\Pi$
$B^2\Sigma^+$
$A^2\Pi$
$X^2\Sigma^+$
$C^+(^2P)+O(^3P)$

Fig. 2.1

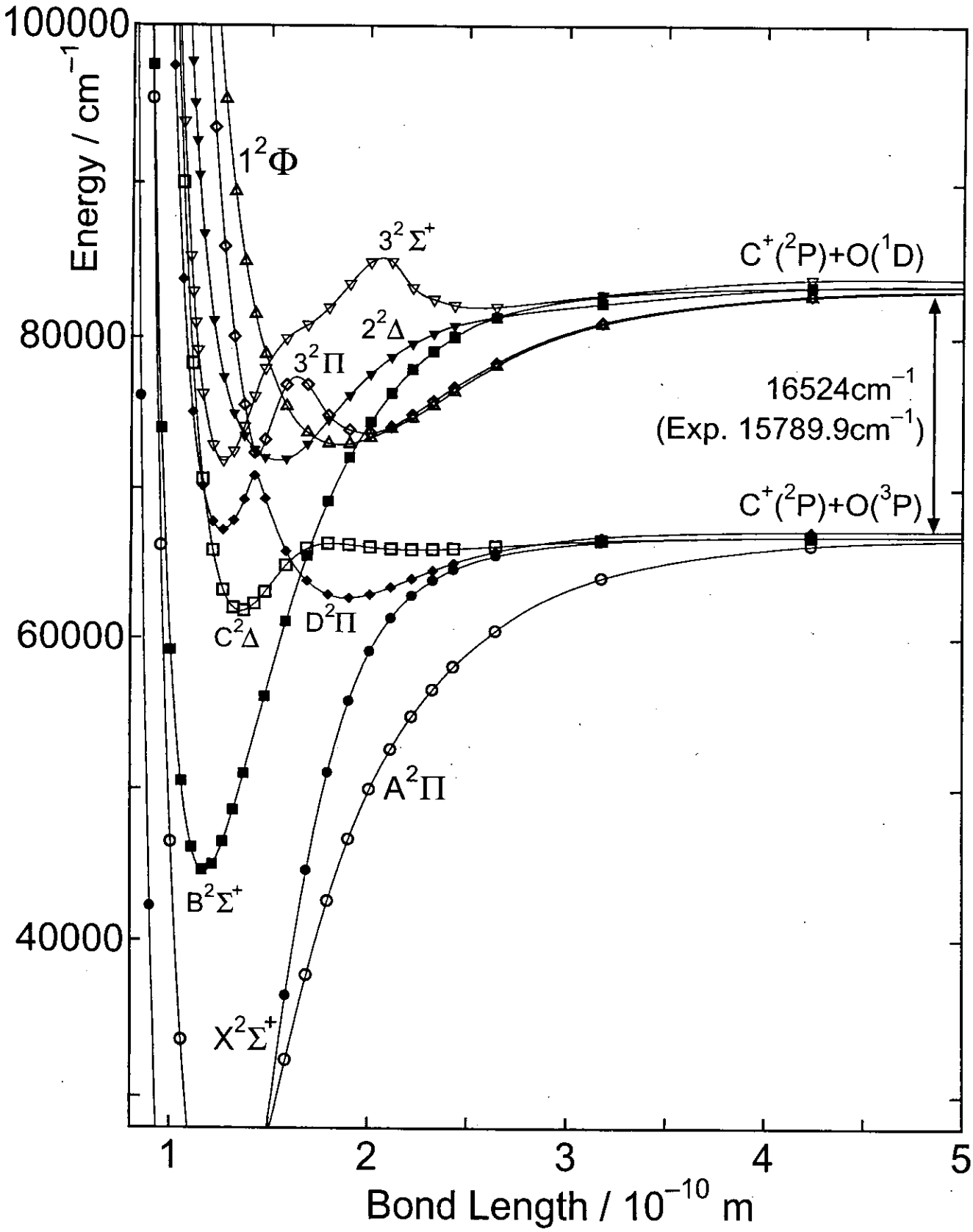
100000
80000
60000
40000
Energy / cm^{-1}
1$^2\Phi$
3$^2\Sigma^+$
2$^2\Delta$
3$^2\Pi$
C$^2\Delta$
D$^2\Pi$
B$^2\Sigma^+$
A$^2\Pi$
X$^2\Sigma^+$
C$^+$(^{2}P)+O(^{1}D)
16524cm^{-1}
(Exp. 15789.9cm^{-1})
C$^+$(^{2}P)+O(^{3}P)
1
2
3
4
5
Bond Length / 10^{-10} m

Fig. 2.2

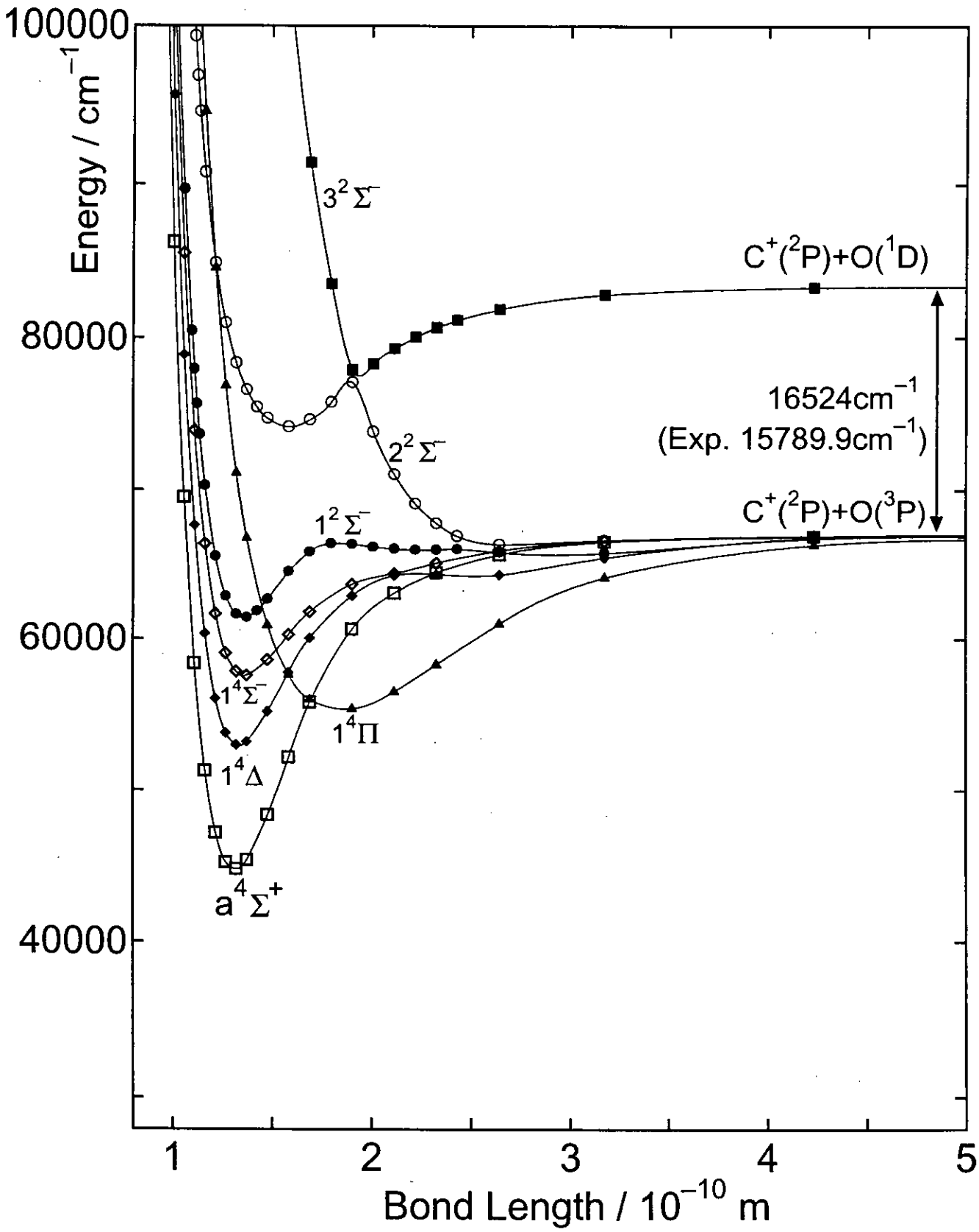
100000
80000
60000
40000
Energy / cm^{-1}
1
2
3
4
5
Bond Length / 10^{-10} m
$3^2\Sigma^-$
$2^2\Sigma^-$
$1^2\Sigma^-$
$1^4\Sigma^-$
$1^4\Delta$
$1^4\Pi$
$a^4\Sigma^+$
$C^+(^2P)+O(^1D)$
$C^+(^2P)+O(^3P)$
16524cm^{-1}
(Exp. 15789.9cm^{-1})

Fig. 3

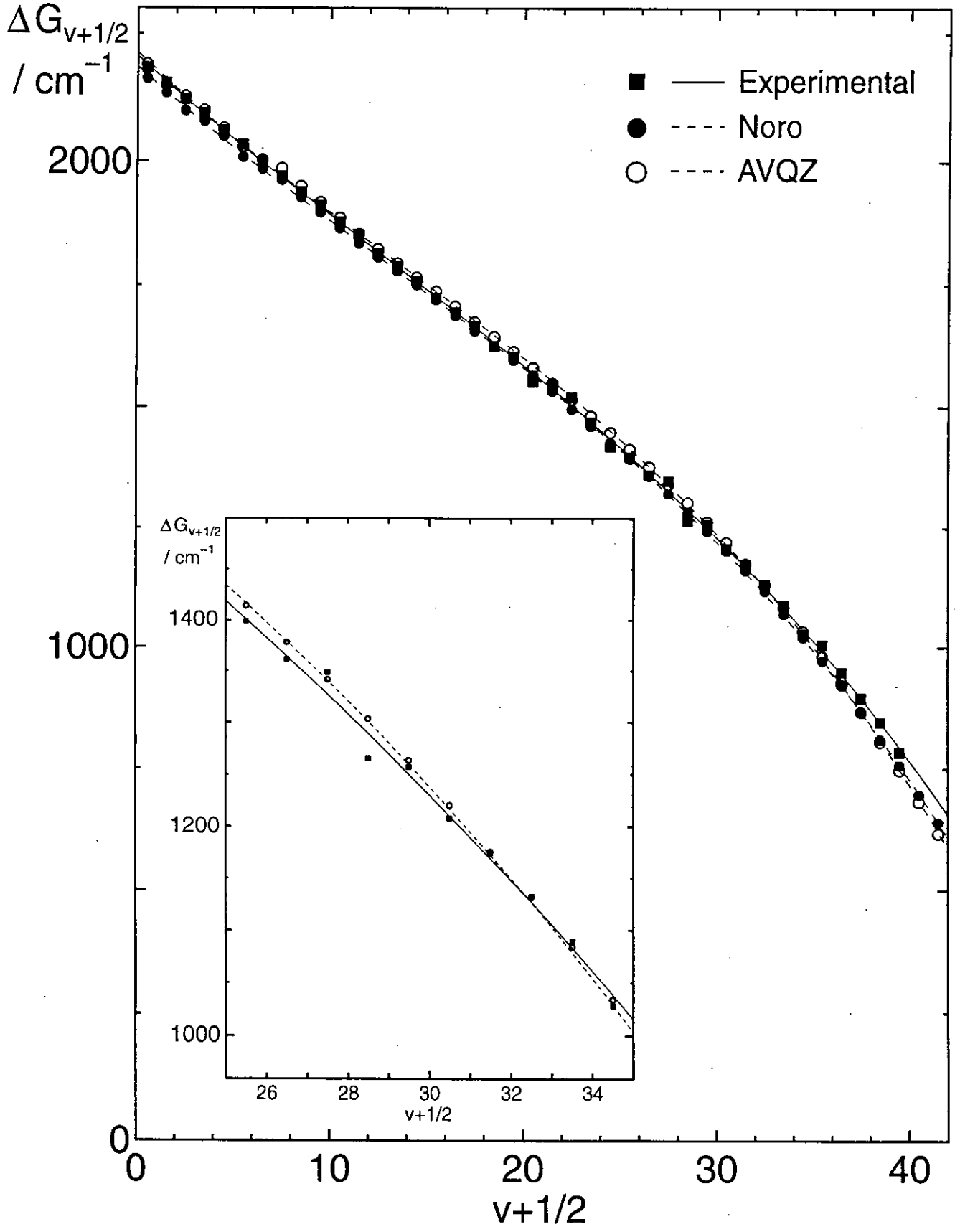
ΔG v+1/2
/ cm−1
2000
1000
0
0
10
20
30
40
v+1/2
Experimental
Noro
AVQZ
ΔG v+1/2
/ cm−1
1400
1200
1000
26
28
30
32
34
v+1/2

Fig. 4

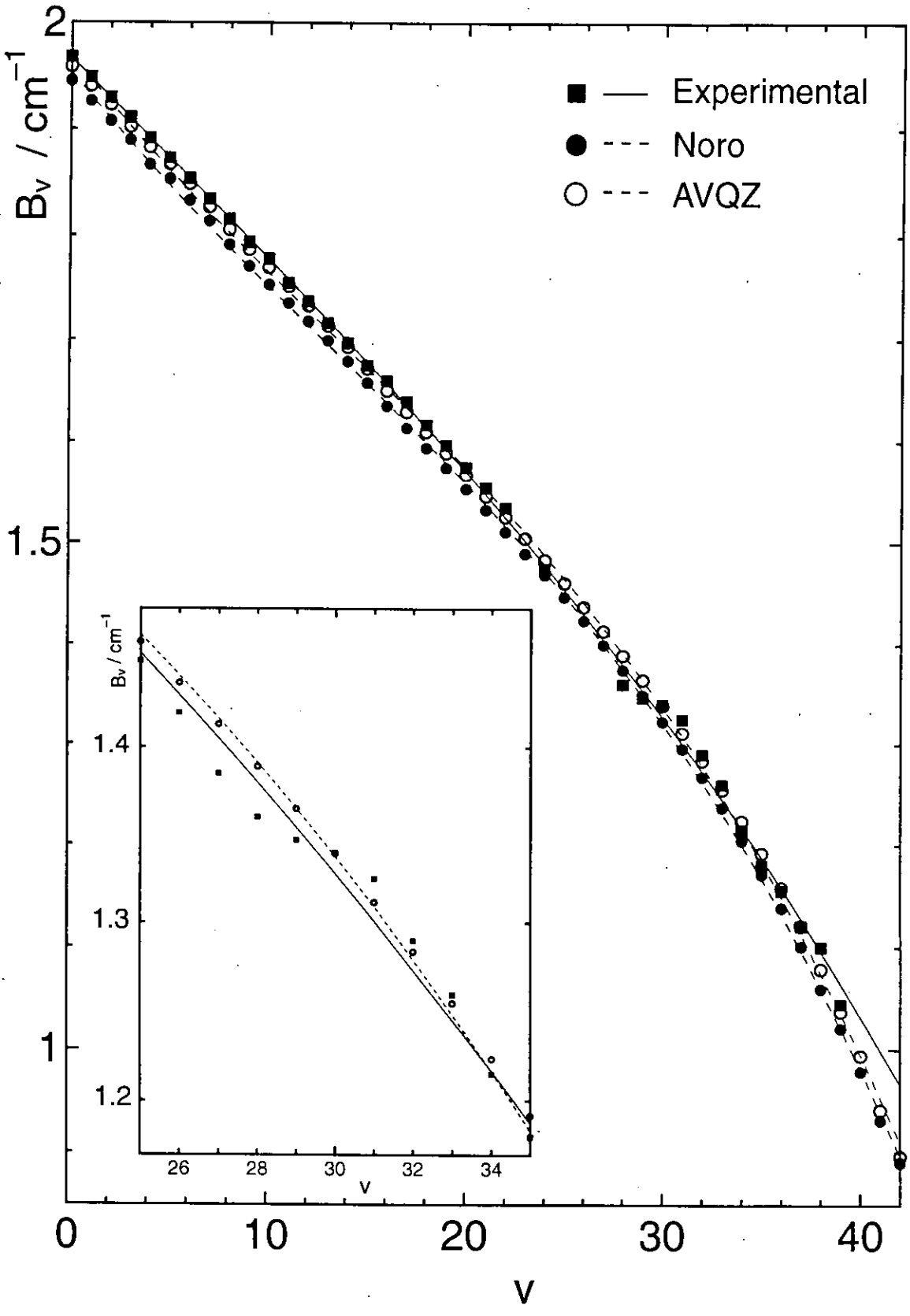
Experimental
Noro
AVQZ
B_v / cm^{-1}
v
2
1.5
1
0
10
20
30
40
1.4
1.3
1.2
26
28
30
32
34

Fig. 5

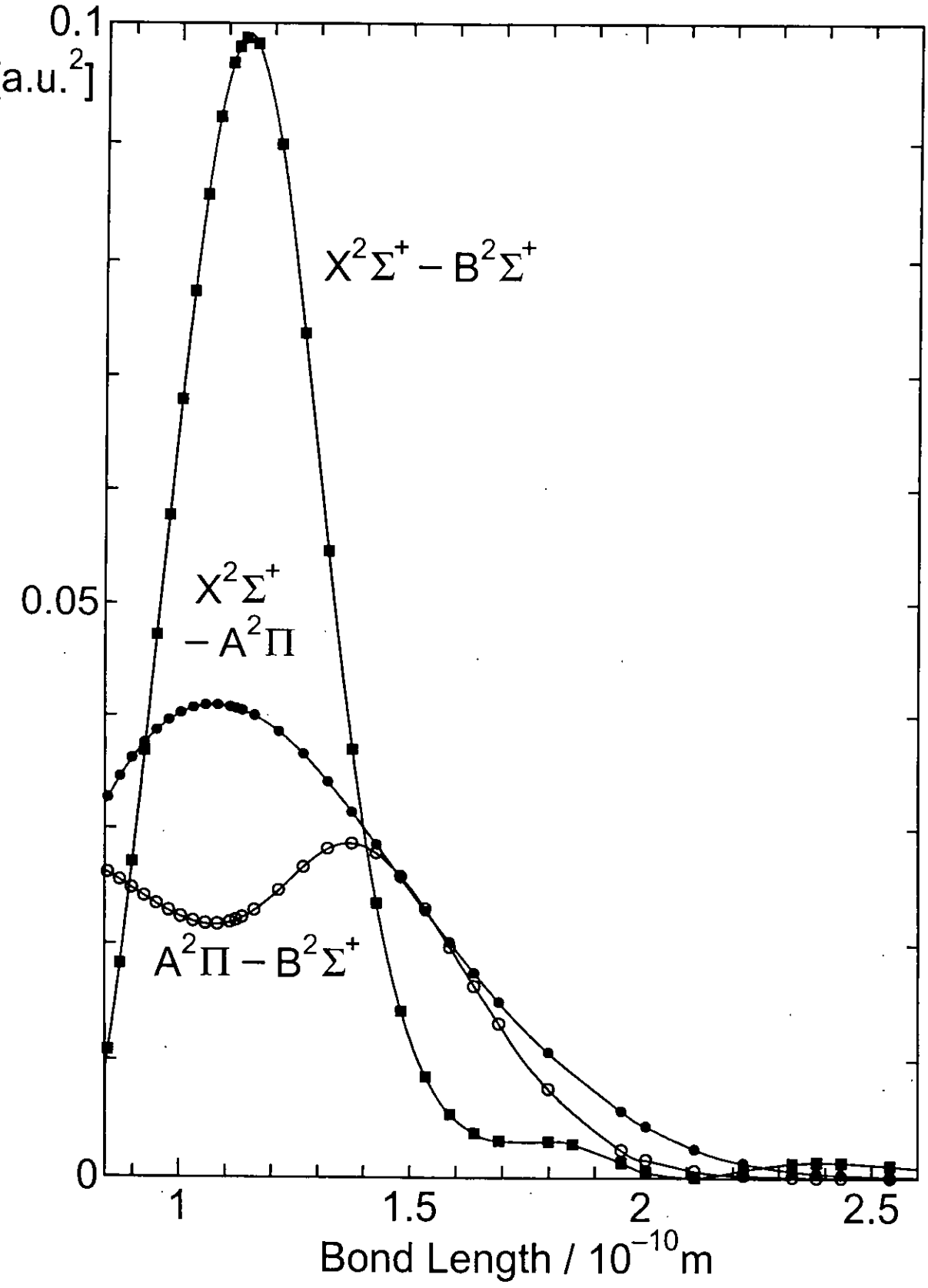
0.1
[a.u.^{2}]
0.05
0
$X^2\Sigma^+ - B^2\Sigma^+$
$X^2\Sigma^+ - A^2\Pi$
$A^2\Pi - B^2\Sigma^+$
1
1.5
2
2.5
Bond Length / 10^{-10}m

Table 1 Electronic, vibrational, and rotational spectroscopic constants of CO^+ and $X^1\Sigma^+$ state of neutral CO molecule. Potential energy curves and $\Delta G_{v+\frac{1}{2}}$ plot were fitted and spectroscopic constants were obtained.

state	$R_e/10^{-10}$m $exp^{(a)}$	$R_e/10^{-10}$m $present^{(b)}$	T_e/cm^{-1} $exp^{(a)}$	T_e/cm^{-1} $present^{(b)}$	$\omega_e/\mathrm{cm}^{-1}$ $exp^{(a)}$	$\omega_e/\mathrm{cm}^{-1}$ $present^{(b)}$	$\omega_e x_e/\mathrm{cm}^{-1}$ $exp^{(a)}$	$\omega_e x_e/\mathrm{cm}^{-1}$ $present^{(b)}$	D_{00}/cm^{-1} $exp^{(a)}$	D_{00}/cm^{-1} $present^{(b)}$
$CO\ X^1\Sigma^+$	1.128323	1.130	$-113034^{(c)}$	-112830	2169.81	2175.1	13.29	13.31	89446	89032
		(1.132)		(-111070)		(2168.7)		(12.98)		(88476)
$CO^+X^2\Sigma^+$	1.1151	1.119	0	0	$2215.1^{(c)}$	2214.6	$15.27^{(c)}$	14.75	$67535^{(c)}$	66731
		(1.121)		(0)		(2194.9)		(14.62)		(66835)
$CO^+A^2\Pi$	1.2437	1.246	20733.3	20594	1562.0	1570.0	13.53	12.86	$47128^{(d)}$	46473
		(1.250)		(19980)		(1556.9)		(13.08)		(47179)
$CO^+B^2\Sigma^+$	1.1687	1.170	45876.7	45979	1734.1	1742.7	27.92	25.99	$37692^{(d)}$	37123
		(1.176)		(45674)		(1693.7)		(23.74)		(37933)
$CO^+C^2\Delta$	1.34	1.355	63012	63275	1144	1167.5	33	36.43	$5063^{(d)}$	4003
		(1.356)		(62924)		(1147.92)		(42.58)		(4438)
$CO^+D^2\Pi^{(e)}$		1.936		64691		417.8		10.78		3026
		(1.891)		(63828)		(462.0)		(11.22)		(3891)
$CO^+D^2\Pi^{(e)}$		1.258	$67783^{(e)}$	68575	$1532^{(e,f)}$	1519.35	$26^{(e,f)}$	27.38		3334
		(1.263)		(68335)		(1487.74)		(26.22)		(2911)
$CO^+a^4\Sigma^+$		(1.315)		(45857)		(1405.6)		(20.01)		(47179)
$CO^+b^4\Pi$		(1.842)		(56340)		(495.1)		(5.02)		(11321)
$CO^+1^4\Delta$		(1.336)		(54063)		(1274.0)		(30.74)		(13250)
$CO^+1^4\Sigma^-$		(1.367)		(58773)		(1096.2)		(34.24)		(8735)

(a) Reference 16.

(b) For $X^2\Sigma^+$, $A^2\Pi$, $B^2\Sigma^+$, $C^2\Delta$ and $D^2\Pi$ states, the values are calculated by AVQZ basis set. The values in parentheses are calculated by Noro basis set.

(c) The data are taken from Reference 4. The T_e is estimated from the reported T_0. The Dunham coefficients ω_e and $\omega_e x_e$ are evaluated by fitting the spacings below $v = 14$ to the first order polynomial.

(d) Experimental D_{00} of $A^2\Pi$ and $C^2\Delta$ states were obtained by D_{00} of $X^2\Sigma^+$ state and T_e, ω_e and $\omega_e x_e$ of $A^2\Pi$ and $C^2\Delta$ states. For $B^2\Sigma^+$ state, the experimentally obtained energy difference between $C^+(^2P) + O(^3P)$ and $C^+(^2P) + O(^1D)$ in the dissociation limit (Reference 15) is also used.

(e) Because the $D^2\Pi$ state has double minima, the constants for two minima are given. The global minimum of the potential energy curve is at the outer well.

(f) The data in reference 17 are used and evaluated by fitting the spacings below $v = 8$.

Table 2 The lifetime (in μ sec.) of the vibrational levels of the $A^2\Pi_u$ state of nitrogen.

v	exp[a]	exp[b]	present	Langhoff et al [c]
0	16.57		16.98	16.04
1	13.88	13.9 ± 1.0	13.97	13.47
2	12.04	11.9 ± 0.4	11.93	11.74
3	10.70	10.7 ± 0.4	10.50	10.49
4	9.68	9.7 ± 0.4	9.49	9.54
5	8.89	9.1 ± 0.4	8.70	8.81
6	8.25	8.4 ± 0.5	8.10	8.24
7	7.72	7.8 ± 0.5	7.58	7.78
8	7.28	7.3 ± 0.5	7.15	7.40
9	6.91		6.77	7.10
10	6.58		6.54	6.85

(a) Reference 20.
(b) Reference 21.
(c) Reference 5.

Table 3 The lifetime (in n sec.) of the vibrational levels of $B^2\Sigma^+$ state. and Einstein's A coefficients of the vibronic transition($A^2\Pi$ state or $X^2\Sigma^+$ state v$''$) $\leftarrow$ ($B^2\Sigma^+$ state v$'$)

$B^2\Sigma^+$ state v'	$v'=0$	1	2	3	4	5
lifetime	56.40	61.48	66.87	72.31	78.32	83.34
Marian et al[(a)](exp.)	57.1±1.0	61.8±1.0	68.9±1.6	72.5 ±2.7		
Marian et al[(a)](theo.)	50.00	54.9	59.7	64.9		
A coefficient / $10^6 s^{-1}$						
$X^2\Sigma^+$ state v$''$						
$v''=0$	10.205	6.587	2.370	0.612	0.128	0.024
1	5.407	1.120	5.522	4.238	1.808	0.579
2	1.266	4.763	0.221	2.206	4.249	3.059
3	0.173	2.424	2.218	1.390	0.174	2.684
$A^2\Pi$ state v$''$						
$v''=0$	0.332	0.452	0.198	0.030	0.001	0.000
1	0.203	0.006	0.384	0.374	0.080	0.002
2	0.083	0.099	0.032	0.234	0.489	0.134
3	0.028	0.092	0.020	0.090	0.117	0.541
4	0.009	0.050	0.060	0.000	0.115	0.049
5	0.002	0.022	0.054	0.027	0.010	0.110

(a) Reference 5.

Chapter 3

Accurate ab initio MO studies of three $^2\Pi$ states of CO^+

Journal of Electron Spectroscopy and Related Phenomena, in press.

1 Introduction

Molecular spectroscopies of carbon monoxide have been studied for many years both experimentally and theoretically. Recently, high resolution photoelectron spectroscopies with the use of atomic resonance lines, laser and synchrotron radiations as ionizing sources have made it possible to scrutinize several excited states of the cation in more detail. Wanberg et al [1] observed the photoelectron spectra of CO by He I, He II, Ne I, and Ne II excitations, and Baltzer et al [2] reported the spectra including the higher electronic states such as $C^2\Delta$, $D^2\Pi$, $3^2\Sigma^+$ and $4^2\Sigma^+$ states by HeII excitations. More recently Ng and his collaboraters published a sereis of papers [3-6], in which rotationally resolved pulsed field ionization photoelectron (PFI-PE) spectra were observed using the synchrotron radiation as a light source.

There are also theoretical studies using the multi-reference configuration interaction method for low-lying doublet and quartet states. Marian et al [7] calculated the $X^2\Sigma^+$, $A^2\Pi$, and $B^2\Sigma^+$ states of CO^+ and obtained potential energy curves, spectroscopic constants, vibrational levels and their lifetimes. Lavendy et al [8] also calculated some low-lying doublet and quartet states of CO^+ and obtained spectroscopic constants, oscillator strengths, and few other properties. Recently, we reported [9] accurate calculations of ground state of CO $X^1\Sigma^+$ and some low-lying doublet and quartet states of CO^+. The calculated vibrational and rotational constants of the $X^2\Sigma^+$ state were in very good agreement with the recent experimental data of Evans and Ng [5].

In this study, the adiabatic potential energy curves of $X^2\Sigma^+$, $A^2\Pi$, $B^2\Sigma^+$, $C^2\Delta$

and $D^2\Pi$ of CO^+ were calculated, and the vibrational levels of each state and spectroscopic constants were obtained. Recently, Shiell et al [6] reported a peculiar vibrational progression assigned to the $D^2\Pi$ states. To compare this with our theoretical results, we focused our discussion particularly on the three lowest $^2\Pi$ states.

2 Theoretical Methods

Multireference configuration interaction (MRCI) calculations were performed for several electronic states of CO^+. The augmented valence quadruple zeta (aug-cc$p$VQZ, AVQZ) basis set of Dunning [10] was used for all the calculations. MRCI calculations were performed with MOLPRO internally contracted CI method [11,12]. The reference configurations were all electronic configurations generated from [$1\sigma^2$, $2\sigma^2$, $3\sigma^{0-2}$, $4\sigma^{0-2}$, $1\pi^{0-4}$, $5\sigma^{0-2}$, $2\pi^{0-4}$, $6\sigma^{0-2}$, $7\sigma^{0-1}$], where 7σ orbital is a Rydberg type orbital. The calculations were performed with C_{2v} symmetry constraints. The valence-type vacant orbitals, 2π and 6σ, were determined by the VALVAC (valence-type-vacant) method of Iwata. [13] The method requires only a single Fock matrix generation, and provides us with a proper anti-bonding nature of molecular orbitals. In this method, we need not solve the state-averaged MCSCF.

Vibrational energies and wavefunctions on each adiabatic potential energy curve were calculated by solving the one-dimension nuclear Schrödinger equation with the FEM1D program of Kimura et al [14]. Vibrational spectroscopic constants ω_e and $\omega_e x_e$ were obtained using the least-squares fitting of $\Delta G_{v+\frac{1}{2}} = G(v+1) - G(v)$, $G(v)$ being the vibrational energy relative to the lowest vibrational level.

3 Results and Discussion

Table 1 shows the electronic and vibrational spectroscopic constants of the $X^2\Sigma^+$, $A^2\Pi$, $B^2\Sigma^+$, $C^2\Delta$ and $D^2\Pi$ states of CO^+ and the $X^1\Sigma^+$ state of neutral CO. Experimental data are also shown in the table for comparison. All calculated spectroscopic constants are in excellent agreement with experimental data. Table 2 shows the calculated rotationless vibronic levels of the $X^2\Sigma^+$, $A^2\Pi$, $B^2\Sigma^+$, $C^2\Delta$ and $D^2\Pi$ states of CO^+. In this table, G stands for the vibrational energy relative to $R = R_e$ of the $X^2\Sigma^+$ state, and ΔG is the energy spacing between adjacent vibrational levels.

Figure 1 shows the experimental and theoretical Sponer plots, $\Delta G_{v+1/2} = G(v+1) - G(v)$, for the $X^2\Sigma^+$, $A^2\Pi$ and $B^2\Sigma^+$ states. Experimental data for the $X^2\Sigma^+$ state are taken from the recent high resolution PFI-PE spectra of Evans and Ng [5]. The experimental and theoretical Sponer plots for the $X^2\Sigma^+$ state are in very good agreement with each other. The calculated energy difference between $v = 0$ levels of the ionic and neutral ground state is 112,827 cm^{-1} (13.989 eV), which also agrees well with the experimental energy reported by Evans and Ng, 113,026 cm^{-1} (14.0136 eV).

The data for the $A^2\Pi$ and $B^2\Sigma^+$ states are taken from the less resolved spectra reported by Wannberg et al [1]. As is seen in Fig. 1, the experimental plots for the $A^2\Pi$ state and $B^2\Sigma^+$ states deviate from the linear line. For the $A^2\Pi$ state, there should exist the $A^2\Pi_{1/2}$ and $A^2\Pi_{3/2}$ states due to the spin-orbit splitting. The resolution of the spectrum of Wannberg et al is not high enough to resolve the splitting. The irregularity in $\Delta G_{v+1/2}$ of the $A^2\Pi$ state might result from the

unresolved splittings. Very recently, Fedorov et al [17] reported the experimental and theoretical studies of the spin-orbit interaction for each vibrational level of the $A^2\Pi$ state. In their analysis they assumed a Morse function for each spin state and determined the spectroscopic constants, R_e, D_e, ω_e and $\omega_e x_e$, which are compared with our results in Table 1. Although our calculations do not include the spin-orbit interaction, the agreement is satisfactory except for D_e; our calculated value of D_e is 47,250 cm^{-1}, while the reported value of Fedrov et al [16] is 45,000 cm^{-1}. This difference is bigger than our expectation. One of the possible reasons for this apparent large difference between the experimentally estimated and the calculated D_e values might be the assumption that a Morse function to represent the potential energy curve of the state is not proper. This is because for $R > 2.5\mathring{A}$, the curve deviates from the Morse function, which results from the configuration mixing of the first and second $^2\Pi$ states. The Sponer plot for large v deviates from a linear line, although it is not shown in Fig.1.

In our previous paper, we noticed that the vibronic levels of $26 \leq v \leq 33$ of the $X^2\Sigma^+$ state are perturbed by the vibronic levels of the $B^2\Sigma^+$ state [9]. The effects were seen in the vibrational level spacings $\Delta G_{v+1/2}$ and the rotational constants B_v of the $X^2\Sigma^+$ state. The first and third columns of Table 2 show that the rotationless levels above $v = 0$ of the $B^2\Sigma^+$ state are inter-mixed with the levels above $v = 26$ of the $X^2\Sigma^+$ states. The coupling strength among the rovibronic levels depends not only on the electronic wavefunctions but also on the overlap matrix of the wavefunctions of rovibrational part. Figure 1, along with Figures 3 and 4 of the

previous paper [9], indicates that the perturbation becomes significant between $v = 3$ and 7 of the $B^2\Sigma^+$ state.

Figure 2 shows the calculated adiabatic potential energy curves of CO^+. The origin of energy is set to be at $R = R_e$ of the $X^2\Sigma^+$ state. The equilibrium bond lengths of the ground $X^1\Sigma^+$ state of neutral CO and the $X^2\Sigma^+$, $A^2\Pi$, and $B^2\Sigma^+$ states of CO^+ are close to each other. Therefore, these states are clearly observed in the photoelectron spectra, and the high Rydberg states converging to these states are also accessible by PFI-PE(ZEKE) spectroscopy. Visible and near-ultraviolet spectra excited from the $X^2\Sigma^+$ state of CO^+ are also observed. The transition to the $C^2\Delta$ state from the $X^2\Sigma^+$ state of CO^+ is forbidden. However, the transition from $A^2\Pi$ is observed which allows to determine at least a few spectroscopic constants. The $C^2\Delta$ state has been known as the final state for one of the shake-up bands in the photoelectron spectrum.

For the second $^2\Pi$ state, there are two potential minima inside and outside the Franck-Condon region of the neutral ground state, and the vibrational levels for both minima are evaluated. In Fig. 2, the horizontal lines show the rotationless vibrational levels of the adiabatic second and third $^2\Pi$ states. The potential minima of the second $^2\Pi$ state are at $R \sim 1.26$ Å at the inner well, and at $R \sim 1.93$ Å (3.65 a.u.) in the outer well. Our calculated $v = 0$ level on the adiabatic potential energy curve at the inner well state lies above 182,200 cm^{-1}(22.584 eV) from the $v = 0$ of the neutral ground state. The corresponding experimental value by Ng et al [6] is 180,500 cm^{-1} (22.375 eV).

As is seen in Fig. 2, the double minima results from a strong avoided crossing. In Table 3, the coefficients of the main electronic configurations are given. The character of the state changes after the avoided crossing; at the inner well the wavefunction is a linear combination of $(1\pi)^{-1}(5\sigma)^{-2}(2\pi)^2$ and $(4\sigma)^{-1}(1\pi)^{-1}(5\sigma)^{-1}(2\pi)^2$, and at their outer well it is found to be a linear combination of $(1\pi)^{-1}$ and $(1\pi)^{-1}(5\sigma)^{-1}(6\sigma)^1$. The number of π electrons changes from five to three, and the character of the $2^2\Pi$ and the $3^2\Pi$ states interchanges at $R = 1.44$ Å. To examine the strength of the coupling, a few more calculations have been performed near $R \sim 1.44$ Å, and as is seen in Fig. 2, the splitting at 1.44 Å is as large as 1200 cm^{-1}(0.15 eV). Experimentally, Shiell et al [6] and Balzer et al [2] reported a vibrational progression of the D (second) $^2\Pi$ state; the progression reaches up to $v = 9$ at 23.78 eV (191,800 cm^{-1}), which is 79,880 cm^{-1} above the energy at the equilibrium bond length of the $X^2\Sigma^+$ state. It is shown in Fig. 2 that the experimentally assigned $v = 9$ level lies well above the barrier of the adiabatic potential energy curve of the third $^2\Pi$ state. However it should be noted that our calculations overestimate the $v = 0$ level of second $(D)^2\Pi$ state by 1700 cm^{-1}. Thus, if the experimental assignment to the vibrational progression is correct, the vibrational levels above $v = 2$ have to be on the diabatic potential energy curve. Both experimental reports noticed that the broadening starts at $v = 3$, although their spectroscopies are different; one is the HeII PE [2], and the other one is PFI-PE [6]. The observed broadening at $v = 3$ is consistent with our calculated potential energy curves. However, as mentioned above, the splitting at the top of the barrier is as large as 1200 cm^{-1}. The experimental

assignment is based on the assumption that the diabatic representation of the states is a good approximation to describe the rovibrational levels. To investigate this, a proper quantum treatment is required. Starting from the vibrational wavefunction of $v'' = 0$ of the neutral ground state, we evaluated Franck-Condon factor (FCF) spectrum of the transitions to two strongly-coupled diabatic second and third $^2\Pi$ states. The details of the method to calculate the FCF of the coupled states will be published separately[17]. In Figure 3 the calculated spectrum is compared with the PFI-PE spectrum observed by Shiell et al [6]. In the calculations, the rotational excitation is not taken into account. The broadening in the theoretical spectrum starts at $v^{+\prime\prime} = 3$, and then the bands are slightly sharpened as exactly seen in the experimental spectrum. From our present and previous papers, it is observed that there is only one more electronic state, $3^2\Sigma^+$, exists around this energy range. The energy of the $2^2\Delta$ state is also closer, but the equilibrium distance is 1.355 Å [9], which is not accessible from the neutral ground state. So the only possibility is that the experimental assignment is correct, and thus, although the adiabatic potential energy curves of the second and third $^2\Pi$ states seem to be well defined in Fig. 2, the observed rovibronic levels are described well as resonant states on the diabatic potential energy curve.

Table 3 shows the main electronic configurations of the $X^2\Sigma^+$, $A^2\Pi$, $B^2\Sigma^+$, $C^2\Delta$ and $D^2\Pi$ states of CO^+. Three bond lengths, 2.125 a.u.(Franck-Condon region of photoexcitation), 3.65 a.u.(intermediate) and 10.5 a.u.(near dissociation limit) are considered for the calculation. The weights, $\sqrt{\sum(\mathbf{C}_{\mu,I})^2}$, are also shown, where the

sum is taken over the configuration state functions (CSF) having the same electronic configuration.

In near equiliblium region, the main electronic configuration for the $X^2\Sigma^+$, $A^2\Pi$, and $B^2\Sigma^+$ states is found to be a single hole state, $(5\sigma)^{-1}$, $(1\pi)^{-1}$ and $(4\sigma)^{-1}$, respectively. Yet a significant contribution from two-hole one-electron configurations, such as $(1\pi)^{-1}(5\sigma)^{-1}(2\pi)^1$ in the $B^2\Sigma^+$ state, should also be noticed. It has been known [18] that to calculate the correct ordering of the ground $^2\Sigma_g^+$ and the first excited $^2\Pi_u$ states of nitrogen molecular cation, the mixing of the two-hole one-electron configurations to the single hole state is essential. This is also true for the first three states of CO^+. As shown in Table 3, the weights of the two-hole one-electron configurations significantly increase with bond length, and so the single determinant description for these states fails in evaluating the spectroscopic constants.

The $C^2\Delta$ state is a typical two-hole one-electron state near R_e. Because of its symmetry, the wavefunction has no contribution from a single-hole configuration. The photoelectron spectrum of this state has also been observed. The photoelectron intensity arises from the so-called ground state correlation. As already mentioned, the $D^2\Pi$ state at the inner well is described by three-hole two-electron configurations, and has almost no contribution from a single-hole configuration $(1\pi)^{-1}$. Since the wavefunction of the neutral ground state contains $(1\pi)^4(5\sigma)^0(2\pi)^2$ configuration, this state becomes accessible by the photoionization.

4 Conclusion

With MR-SDCI calculations using an extended basis set, the potential energy curves of several doublet states of CO^+ are obtained, and spectroscopic constants and vibrational levels are compared with recent experimental data. The calculated spectroscopic constants are in excellent agreement with experimental data. For the $D^2\Pi$ state, the observed vibrational progression up to $v = 9$ is understood only by the non-adiabatic couplings among the second(D) and the third $^2\Pi$ states.

5 Acknowledgment

The authors acknowledge professor Ng for sending their experimental data even before publication. The work is partially supported by the Grant-in-Aids for Scientific Research (No. 11166270) by the Ministry of Education, Science, Sports, and Culture, Japan, and by the project "Computational Chemistry of Molecules in the Atmospheric Environment" of Research and Development Applying Advanced Computational Science and Technology under Japan Science and Technology Corporation.

References

[1] B. Wannberg, D. Nordfors, K. L. Tan, L. Karlsson, and L. Mattsson, J. Electron Spectroscopy and Related Phenomena 47 (1988) 147.

[2] P. Balzer, M. Lundqvist, B. Wannberg, L. Karlsson, M. Larsson, M. A. Hayes, J.B. West, M. R. F. Siggel, A. C. Parr, and J. L. Dehmer, J. Phys. B 27 (1994) 4915.

[3] W. Kong, D. Rodgers, J. W. Hepburn, K. Wang, and V. McKoy, J. Chem. Phys. 99 (1993) 3159.

[4] W. Kong and J. W. Hepburn, J. Phys. Chem. 99 (1995) 1637.

[5] M. Evans and C. Y. Ng. J. Chem. Phys., in press.

[6] R. C. Shiell, M. Evans, S. Stimson, C-W. Hsu, C. Y. Ng, and J. W. Hepburn, Submitted to Chem. Phys. Lett.

[7] C. M. Marian, M. Larsson, B. J. Olsson, and P. Sigray, Chem. Phys. 130 (1989) 361.

[8] H. Lavendy, J. M. Robbe, and J. P. Flament, Chem. Phys. Lett. 205 (1993) 456.

[9] K. Okada and S. Iwata, J. Chem. Phys. in press.

[10] T. H. Dunning Jr, J. Chem. Phys. 90 (1989) 1007.

[11] H. -J. Werner and P. J. Knowles, J. Chem. Phys. 89 (1988) 5803.

[12] P. J. Knowles and H. -J. Werner, Chem. Phys. Lett. 145 (1988) 514.

[13] S. Iwata, Chem. Phys. Lett. 83 (1981) 134.

[14] T. Kimura, N. Sato, and S. Iwata, J. Comp. Chem. 9 (1988) 827.

[15] K. P. Huber and G. Herzberg, Molecular Spectra and Molecular Structure IV. *Constants of Diatomic Molecules* (Litton Educational Publishing Inc. 1979).

[16] D. G. Fedorov, M. Evans, Y. Song, M. S. Gordon, and C. Y. Ng, J. Chem. Phys. in press

[17] T. Ikegami, K. Okada, and S. Iwata, in preparation.

[18] N. Kosugi, H. Kuroda, and S. Iwata, Chem. Phys. 39 (1979) 337.

6 Figure Captions

Figure 1.

The experimental and theoretical Sponer plots, $\Delta G_{v+1/2} = G(v+1) - G(v)$, for the $X^2\Sigma^+[5]$, $A^2\Pi[1]$ and $B^2\Sigma^+[1]$ states of CO^+.

Figure 2.

Potential energy curves of excited states of CO^+. The reference energy is the zero point vibrational level of the $X^2\Sigma^+$ state.

Figure 3.

Upper part: The calculated Franck-Condon factor (FCF) spectrum of the transitions to two strongly-coupled diabatic second and third $^2\Pi$ states from the $v" = 0$ level of the neutral ground state.

Lower part: The PFI-PE spectrum reported in reference [6].

Fig. 1

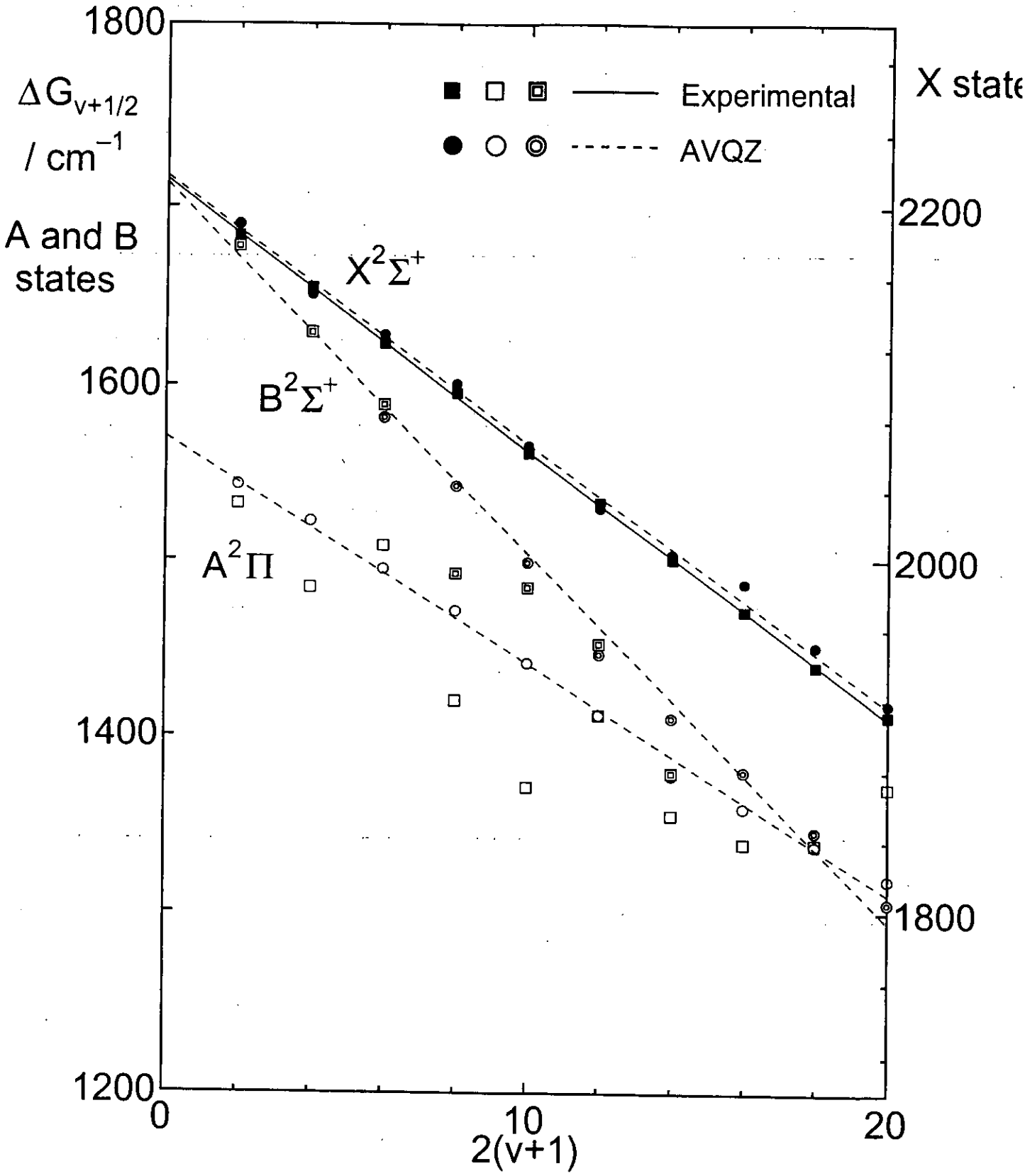
1800
$\Delta G_{v+1/2}$
/ cm^{-1}
A and B states
1600
1400
1200
0
10
20
2(v+1)
Experimental
AVQZ
$X^2\Sigma^+$
$B^2\Sigma^+$
$A^2\Pi$
X state
2200
2000
1800

Fig. 2

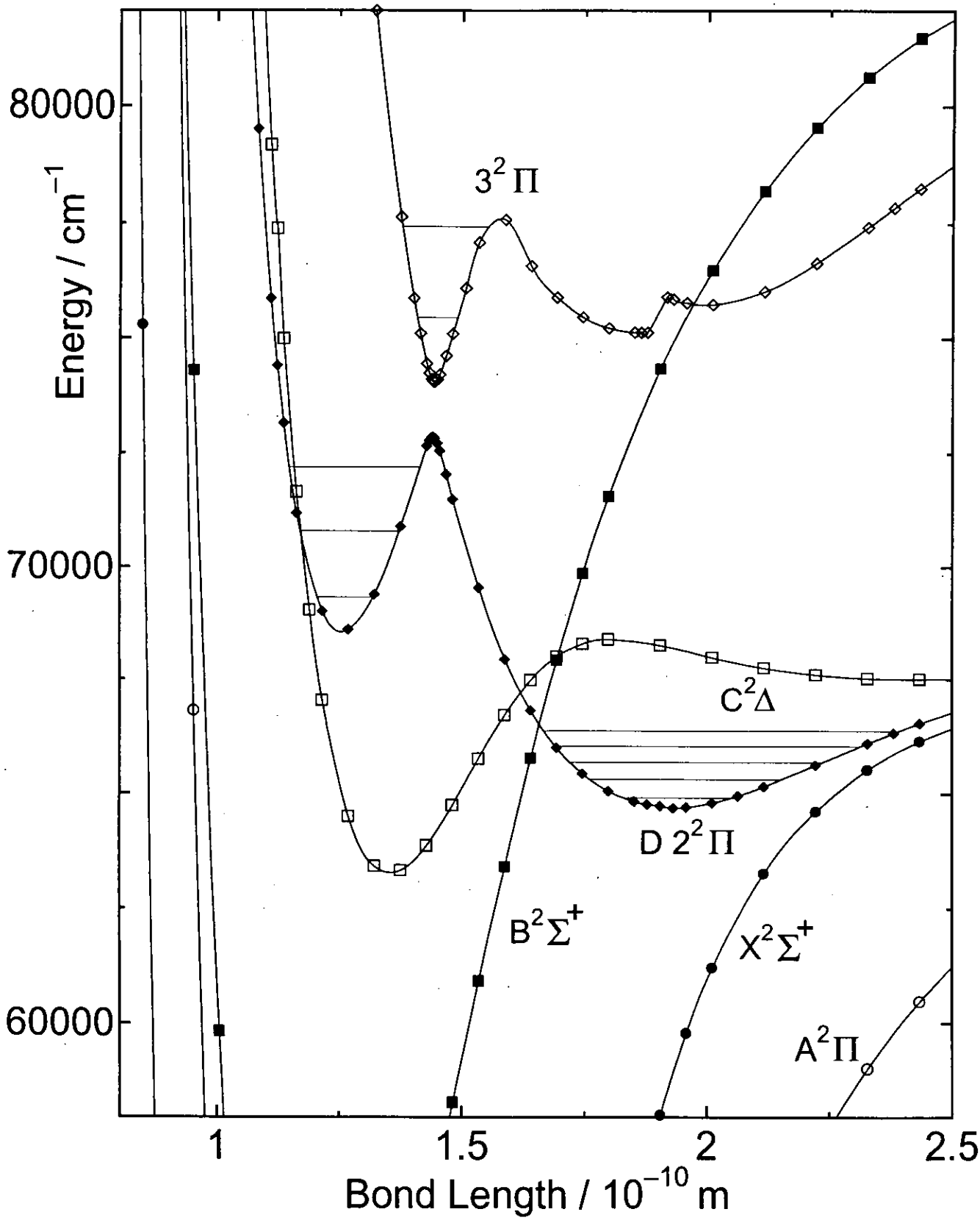
80000
70000
60000
Energy / cm^{-1}
$3^2\Pi$
$C^2\Delta$
$D\,2^2\Pi$
$B^2\Sigma^+$
$X^2\Sigma^+$
$A^2\Pi$
1
1.5
2
2.5
Bond Length / 10^{-10} m

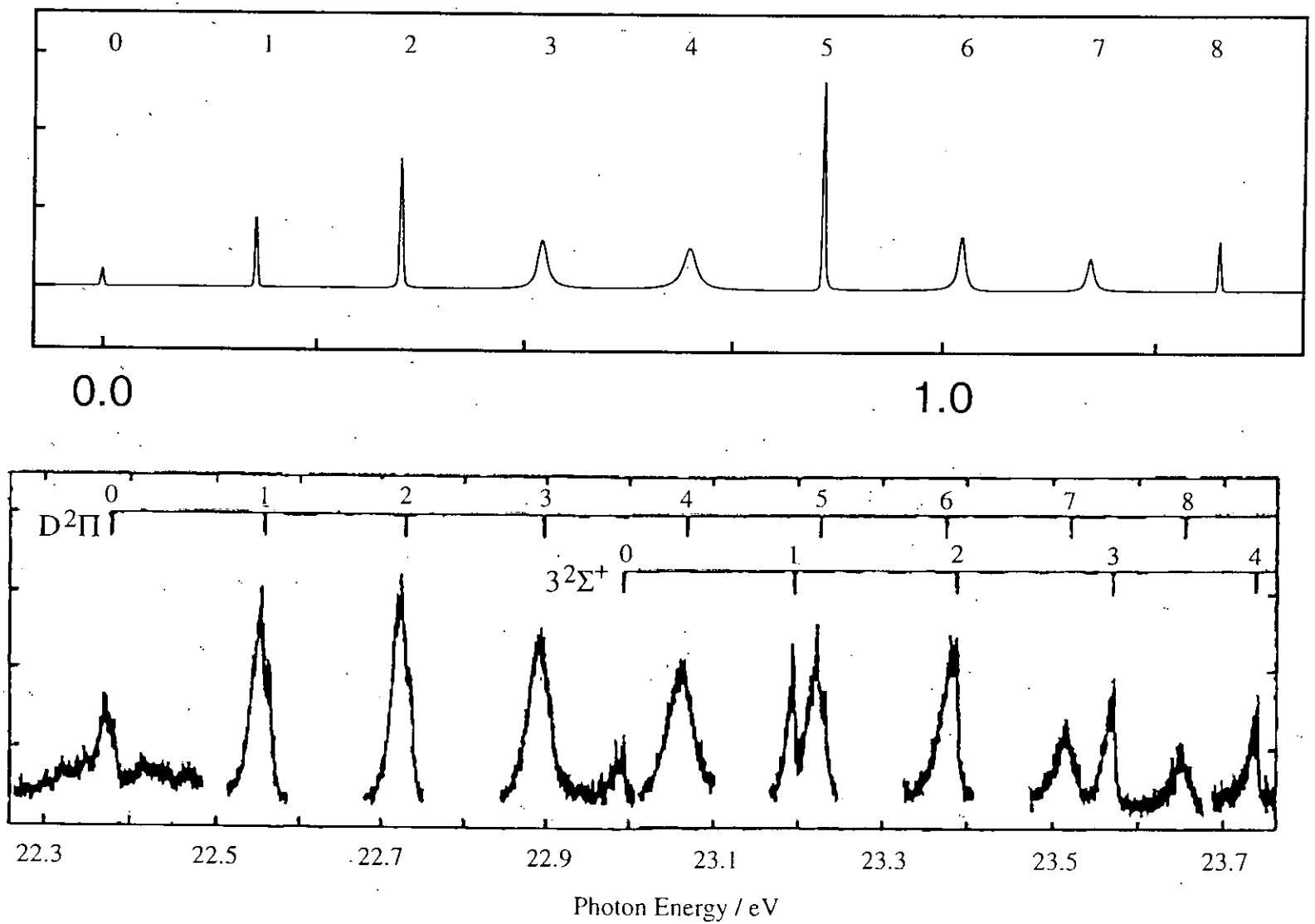
0
1
2
3
4
5
6
7
8
0.0
1.0
D²Π
3²Σ⁺
22.3
22.5
22.7
22.9
23.1
23.3
23.5
23.7
Photon Energy / eV

Fig 3.

Table 1 Electronic and vibrational spectroscopic constants of CO^+ and $X^1\Sigma^+$ state of neutral CO molecule. Potential energy curves and $\Delta G_{v+\frac{1}{2}}$ plot were fitted and spectroscopic constants were obtained.

state	$R_e/10^{-10}$m $exp^{(a)}$	$R_e/10^{-10}$m *present*	$\omega_e/\mathrm{cm}^{-1}$ $exp^{(a)}$	$\omega_e/\mathrm{cm}^{-1}$ *present*	$\omega_e x_e/\mathrm{cm}^{-1}$ $exp^{(a)}$	$\omega_e x_e/\mathrm{cm}^{-1}$ *present*
$CO\ X^1\Sigma^+$	1.128323	1.130	2169.81	2175.1	13.29	13.31
$CO^+X^2\Sigma^+$	1.1151	1.119	2215.1[(b)]	2214.6	15.27[(b)]	14.75
$CO^+A^2\Pi$[(c)]	1.2436	1.246	1562.1	1570.0	13.52	12.86
$CO^+B^2\Sigma^+$	1.1687	1.170	1734.1	1742.7	27.92	25.99
$CO^+C^2\Delta$	1.34	1.355	1144	1167.5	33	36.43
$CO^+D^2\Pi$[(d,e)]		1.936		10.8		417.8
$CO^+D^2\Pi$[(d,e)]		1.258	1532	1519.4	26	27.4

(a) Reference 15.

(b) The data are taken from Evans and Ng[5]. T_e is estimated from the reported T_0. The Dunham coefficients ω_e and $\omega_e x_e$ are evaluated by fitting the spacings below $v = 14$ to the first order polynomial.

(c) The experimental data by Fedrov et al[16] are used.

(d) Since the $D^2\Pi$ state has double minima, the constants for two minima are given. The global minimum of the potential energy curve is at the outer well.

(e) The experimental data by Shiell et al[6] are used and evaluated by fitting the spacings below $v = 8$.

Table 2 The calculated rotationless vibronic levels of the $X^2\Sigma^+$, $A^2\Pi$, $B^2\Sigma^+$, $C^2\Delta$ and $D^2\Pi$ states.

	$X^2\Sigma^+$ state		$A^2\Pi$ state		$B^2\Sigma^+$ state		$C^2\Delta$ state		$D^2\Pi$ state (Inner)		
v	G(cm^{-1})	$\Delta G(cm^{-1})$	G	ΔG	G	ΔG	G	ΔG	v	G	ΔG
0	1116		21374		46841		63843		0	69321	
1	3305	2189	22917	1543	48531	1690	64935	1092	1	70788	1467
2	5456	2151	24440	1523	50161	1630	65963	1028	2	72194	1406
3	7584	2128	25934	1494	51742	1581	66909	946			
4	9684	2100	27405	1471	53285	1543	67570	661			(Outer)
5	11750	2066	28845	1440	54783	1498	67682	112			
6	13780	2030	30257	1412	56229	1446	67736	54	0	64910	
7	15783	2003	31634	1377	57639	1410	67774	38	1	65306	396
8	17770	1987	32994	1360	59019	1380	67844	70	2	65677	371
9	19720	1950	34331	1337	60365	1346	67880	36	3	66032	355
10	21638	1918	35650	1319	61670	1305	67887	7	4	66365	333
11	23524	1886	36938	1288	62937	1267			5	66676	311
12	25378	1854	38197	1259	64169	1232			6	66966	290
13	27200	1822	39427	1230	65368	1199			7	67234	268
14	28994	1794	40631	1204	66535	1167			8	67479	245
15	30761	1767	41813	1182	67670	1135			9	67700	221
16	32498	1737	42970	1157	68770	1100			10	67900	200
17	34205	1707	44100	1130	69824	1054			11	68075	175
18	35880	1675	45201	1101	70830	1006			12	68222	147
19	37525	1645	46271	1070	71800	970			13	68336	114
20	39140	1615	47311	1040	72733	933			14	68423	87
21	40721	1581	48323	1012	73621	888			15	68464	41
22	42270	1549	49306	983	74466	845					
23	43787	1517	50259	953	75271	805					
24	45269	1482	51182	923	76037	766					
25	46717	1448	52073	891	76764	727					
26	48131	1414	52932	859	77454	690					
27	49509	1378	53759	827	78108	654					
28	50851	1342	54558	799	78729	621					

$X^1\Sigma^+$ state v=0 of neutral CO lies below 112858 cm^{-1} of $X^2\Sigma^+$ state v=0 of CO^+

Table 3 The weights of the main configurations. (a) see text

	R	3σ	4σ	1π	5σ	2π	6σ	Weight[a]
$X^2\Sigma^+$ state								
	2.125 a.u.							
	(1.12 Å)	2	2	4	1	0	0	0.904
		2	2	3	1	1	0	0.189
		2	2	2	1	2	0	0.143
	3.65 a.u.							
	(1.93 Å)	2	2	4	1	0	0	0.518
		2	2	3	1	1	0	0.506
		2	2	3	0	1	1	0.470
		2	2	4	0	0	1	0.205
	10.5 a.u.							
	(5.56 Å)	2	2	3	0	1	1	0.941
$A^2\Pi$ state								
	2.125 a.u.							
	(1.12 Å)	2	2	3	2	0	0	0.919
	3.65 a.u.							
	(1.93 Å)	2	2	3	2	0	0	0.620
		2	2	2	1	1	1	0.413
		2	2	3	1	0	1	0.394
		2	2	2	2	1	0	0.281
	10.5 a.u.							
	(5.56 Å)	2	2	2	0	1	2	0.940
$B^2\Sigma^+$ state								
	2.125 a.u.							
	(1.12 Å)	2	1	4	2	0	0	0.877
		2	2	3	1	1	0	0.266
		2	1	4	0	2	0	0.128
	3.65 a.u.							
	(1.93 Å)	2	2	3	1	1	0	0.631
		2	2	3	0	1	1	0.382
		2	2	4	1	0	0	0.207
		2	2	3	1	1	0	0.267
	10.5 a.u.							
	(5.56 Å)	2	2	3	0	1	1	0.942
$C^2\Delta$ state								
	2.125 a.u.							
	(1.12 Å)	2	2	3	1	1	0	0.935
	3.65 a.u.							
	(1.93 Å)	2	2	3	1	1	0	0.705
		2	2	3	0	1	1	0.571
	10.5 a.u.							
	(5.56 Å)	2	2	3	0	1	1	0.941
$D^2\Pi$ state								
	2.125 a.u.							
	(1.12 Å)	2	2	3	0	2	0	0.792
		2	1	3	1	2	0	0.392
	3.65 a.u.							
	(1.93 Å)	2	2	3	2	0	0	0.677
		2	2	3	1	0	1	0.503
	10.5 a.u.							
	(5.56 Å)	2	2	3	1	0	1	0.935

Chapter 4

Theoretical studies of Einstein's A and B coefficients of rovibrational transitions for carbon monoxide: simulation of temperature distribution of CO in the solar atmosphere

1 Introduction

Carbon monoxide (CO) molecule is one of the most important diatomic molecules in atmospheric chemistry on our earth as well as in interstellar chemistry. There are numerous studies on the vibrational and rotational levels on the ground $X^1\Sigma_g^+$ state, which are largely based on infrared and microwave spectroscopies. Recently, extensive and accurate observation from the solar line was performed by an interferometric spectrometer on a satellite operated by NASA [1]. Because of very hot environment on sun, high rovibrational levels up to $v = 40$ and $J = 133$ were detected and identified. From the assigned bands, an accurate set of Dunham coefficients were deduced.

There are also many theoretical studies on the ground $X^1\Sigma_g^+$ state of CO. For instance, the sign and value of dipole moment at the equilibrium bond distance have been one of the hot topics in the history of ab initio electronic structure theories [2]. Recently, Dage et al [3] calculated the potential energy and one-photon and two-photon dipole moment functions, vibrational spectroscopic constants and oscillator strengths. Langhoff and Baucshlicher (LB) also calculated potential energy and dipole moment functions, and evaluated the radiative lifetime of rotationless vibrationally excited levels [4]. Their theoretical studies reproduce experimental data reasonably well. However, as far as the rovibrational levels are concerned, there have been few studies that are comparable with the recent experimental spectra in energy and spectral intensity.

In the present studies, we attempt more accurate calculations than the previous

studies for the ground $X^1\Sigma_g^+$ state of CO. The potential energy and dipole moment functions are calculated, and the rovibrational wavefunctions on the potential energy curve up to near vibrational dissociation limit and rotational levels $J \sim 100$ are evaluated. Einstein's A and B coefficients of rovibrational transitions are evaluated using the rovibrational energies and their wavefunctions. The rovibrational infrared spectra are constructed for $\Delta v = 1, 2$ and 3, and the calculated spectra are compared with the recent experimental data from the satellite as well as with the previous theoretical studies. By simulating the rovibrational spectra in the $\Delta v = 2$ region observed at the satellite [1], we could deduce the temperature distribution of CO molecule at the atmosphere of sun.

2 Calculation

Multireference configuration interaction (MRCI) calculations were performed for the ground state of CO. The basis set used was the augmented valence quadruple zeta (aug-cc*p*VQZ, AVQZ) basis set of Dunning [5]. MRCI calculations were performed with MOLPRO internally contracted CI method [6][7]. The reference configurations were all electronic configurations generated from [$1\sigma^2$, $2\sigma^2$, $3\sigma^{0-2}$, $4\sigma^{0-2}$, $1\pi^{0-4}$, $5\sigma^{0-2}$, $2\pi^{0-4}$, $6\sigma^{0-2}$, $7\sigma^{0-1}$], where 7σ orbital is a Rydberg type orbital. The calculations were performed under C_{2v} symmetry. The valence-type vacant orbitals, 2π and 6σ, were determined by the VALVAC (valence-type-vacant) method of Iwata [8]. The method requires only a single Fock matrix generation, and provides us with a proper anti-bonding nature of molecular orbitals. The other occupied orbitals

$(1\sigma - 5\sigma, 1\pi)$ are the closed shell SCF orbitals.

Vibrational energies and wavefunctions on the adiabatic potential energy curve were calculated by solving the one-dimension nuclear Schrödinger equation with the FEM1D program of Kimura et al [9]. The integration region was between 1.4 a.u. and 10.0 a.u.. Vibrational spectroscopic constants ω_e, $\omega_e x_e$ and $\omega_e y_e$ were obtained using the least-squares fitting of $\Delta G_{v+1/2} = G(v+1) - G(v)$, $G(v)$ being the vibrational energy relative to the lowest vibrational level. The spacing $G(v)$ is expressed as

$$G_v = \omega_e \left(v + \tfrac{1}{2}\right) - \omega_e x_e \left(v + \tfrac{1}{2}\right)^2 + \omega_e y_e \left(v + \tfrac{1}{2}\right)^3 + \ldots$$

By integrating the dipole moment function over the vibrational wavefunctions, Einstein's A and B coefficients of the vibrational transitions as well as the vibronic transitions were evaluated.

3 Results and discussion

3.1 Vibrational spectroscopic constants

Figure 1 shows potential energy and dipole moment curves of the neutral ground $X^1\Sigma_g^+$ state of CO. The calculated solid horizontal lines on the potential energy curve are the calculated vibrational levels. The origin of energy is set to be at the calculated $v = 0$ vibrational energy level. The vertical dashed line shows the equilibrium bond length, $R = R_e$, and the horizontal dashed line shows no permanent dipole moment. The positive sign of dipole moment represents C^+O^-. At $R = R_e$,

the sign of the dipole moment of the molecule is slightly negative as was known in the previous studies [2]. As the bond length increases, dipole moment becomes positive; the molecule is polarized as $C^{\delta+}O^{\delta-}$. At $R \sim 1.90$ Å, the dipole moment has a maximum positive value. At near dissociation limit, the dipole moment again decreases and asymptotically becomes zero.

Langhoff and Bauschlicher(LB) reported both potential energy and dipole moment curves with the then state-of-art level of calculation. To estimate the accuracy of calculated potential energy and dipole moment functions, spectroscopic constants R_e, D_e, ω_e, $\omega_e x_e$ and $\omega_e y_e$ are calculated using the functions of ours and LB's. The calculated spectroscopic constants are compared with the available experimental data in Table 1.

Figure 2 shows the spacings between adjacent vibrational levels, $\Delta G_{v+1/2}(v) = G(v+1) - G(v) = \omega_e - 2\omega_e x_e(v+1)$, plotted against $2(v+1)$. Experimental $\Delta G_{v+1/2}(v)$ plots in the figure are evaluated with a set of Dunham coefficients determined by the spectroscopic studies of solar carbon monoxide. The vibrational spectroscopic constant ω_e is obtained using the least-squares fitting of $\Delta G_{v+1/2}$. Dashed lines and a solid line are the least-squares fitted results of the vibrational levels $v \leq 9$ to determine spectroscopic constant ω_e. The calculated plots of ours and LB's agree with the experimental data. However, LB plot underestimate ω_e by about 20 cm^{-1}. In the present calculation, the error of $\omega_e x_e$ is about 2 cm^{-1}. The agreement with the experimental data is substantially improved in our calculations.

To obtain higher order spectroscopic constants, the spacing of $\Delta G(v)$, $\Delta\Delta G =$

$\Delta G(v+1)-\Delta G(v)$, which is $-2\omega_e x_e+6\omega_e y_e(v+3/2)$ in the Dunham expansion, is also calculated. Figure 3 shows $\Delta\Delta G(v)$, plotted against v. Vibrational spectroscopic constants $\omega_e x_e$ and $\omega_e y_e$ are obtained using the least squares fitting of $\Delta\Delta G(v)$. The rovibrational levels of $J = 0$ and $v \leq 25$ are used in these fittings. For the calculated results of Langhoff and Bauschlicher, $\Delta\Delta G(v)$ plots deviate much from the fitted line, because the calculation points are not enough. Our calculated $\Delta\Delta G(v)$ plots also have many zigzags for $v \leq 40$, but $\Delta\Delta G(v)$ plots of $v \leq 25$ are almost in a fitted line. Expected errors in the fitting of $\omega_e x_e$ and $\omega_e y_e$ of Langhoff and Bauschlicher are 0.20 cm^{-1} and 0.0046 cm^{-1}, respectively. The errors of $\omega_e x_e$ and $\omega_e y_e$ on the present results are 0.030 cm^{-1} and 0.00068 cm^{-1}, respectively. The present fitted results are expected to be more reliable. Near the dissociation limit, $v \geq 40$, the present calculation results reproduce experimental data. The constants $\omega_e x_e$ and $\omega_e y_e$ in Tbale 1 are determined in this way. As is seen from the table, for R_e and ω_e the present calculations are in better agreement with the experiments than BL's. The calculated set ($\omega_e x_e$, $\omega_e y_e$) is overall in good agreement with the experimentally determined parameters. It turned out the fit $\Delta\Delta G$ is very sensitive to the potential energy functions used in solving the nuclear Schödinger equation. In the present study we have used the 3rd order spline fitting in interpolating the potential energy. When a vibrational eigenvalue hits at the interpolating point, it deviates from the appropriate value. The analytical fitting is desired to obviate the zigzags in the higher order plot.

3.2 Einstein's A and B coefficinets

Figure 4 shows calculated Einstein's A coefficients of rotationless vibrational transition $v'' \leftarrow v'$ of $\Delta v = v' - v'' = 1, 2$ and 3, plotted against v''. Langhoff and Bauschlicher also calculated Einstein's A coefficients, and so both calculated results are compared. Both results are in very good agreement with each other. It is expected that the present calculated results are more accurate for higher v. An Einstein A coefficient can be compared with the experimentally obtained lifetime of vibrationally excited states $v = 1$. The experimentally observed lifetime of the transition $(v'' = 0) \leftarrow (v' = 1)$ is 33 milliseconds; the corresponding Einstein's A coefficient is 30 [10]. Both calculated results agree well with the experimental value. It should be noted that the A coefficient for $\Delta v = 2$ monotonically increases with v, and becomes comparable with that for $\Delta v = 1$ at $v = 30$. To estimate the radiative decay rate for higher vibrational levels, the $\Delta v = 2$ and 3 transitions cannot be neglected.

Figure 5 shows the vibrational quantum number (v) dependence of the calculated Einstein B coefficients of rotationless vibrational transitions $v' \leftarrow v''$ of $\Delta v = v' - v'' = 1, 2$ and 3, plotted against v''. For $\Delta v = 1, 2$ and 3, Einstein's B coefficients peak at $v'' = 33, 54$ and 58, respectively. For $\Delta v = 2$ and 3 transitions, Einstein's B coefficients are substantially large at high vibrational levels.

Large coefficients of A and B for higher vibrational levels reflect the functional form of the dipole moment shown in Figurel, Figure 2 b) and c) clearly indicate that the absorption bands for $\Delta v = 2$ and 3 are substantially strong. As is shown

below, the $\Delta v = 2$ ($v' = 2 \leftarrow v'' = 0$) transitions are observed between 4250 cm^{-1} and 4360 cm^{-1} in the solar spectra. This wave number region has less absorption bands from the other molecules than the fundamental ($\Delta v = 1$) region.

Figure 6 shows the rotational quantum number (J) dependence of the calculated Einstein's B coefficients for some rovibrational transitions of $\Delta v = 1$ and 2, for $\Delta J = +1$ (R-branch) and $\Delta J = -1$ (P-branch). For a given $v' \leftarrow v''$ transition of $\Delta v = 1$, Einstein's B coefficients of $\Delta J = +1$ are larger than $\Delta J = -1$ for low J'', and both coefficients become nearly equal to each other and constant for high J''. For a given $v' \leftarrow v''$ transition of $\Delta v = 2$, Einstein's B coefficients of $\Delta J = +1$ are substantially larger than $\Delta J = -1$ for all J''. Interestingly, at $J'' = 10$, the B coefficient for $\Delta J = +1$ transition is at the minimum, and that for $\Delta J = -1$ transition is at the maximum. For high J'', Einstein's B coefficients of $\Delta J = +1$ become extremely large.

With Einstien's B coefficients at hand, if the abundance of rovibrational levels (v'', J'') is known or assumed, the rovibrational absorption spectra are simulated. In turn, if the rovibrational spectra are observed, the population of the rovibronic levels are deduced. Based on the calculated Einstein's B coefficients of rovibrational transitions, the wide range of spectrum of the solar atmosphere, which were observed at the interferometer on the satellite by NASA, is analyzed. In the following subsection, the number of molecules in the rotational levels is assumed to be Boltzmann distribution, and several rotational temperatures are assumed in the analyses.

3.3 Temperature distribution of CO molecule at the atmosphere of sun

Figure 7 shows the simulated and experimentally observed absorption spectra between 4250 cm^{-1} and 4370 cm^{-1}. In the simulated spectrum, rotational and vibrational temperature was assumed to be at 5000 K. The simulated spectrum is shifted downward by 7 cm^{-1}. Note that no adjustable parameters other than 7 cm^{-1} shift and the temperature are used in the simulation. Rovibrational transitions $(v' = 4 \leftarrow v'' = 2; \Delta J = +1)$ and $(v' = 2 \leftarrow v'' = 0; \Delta J = +1)$ are compared in the figure. The simulated spectrum well reproduces the observed spectrum. The theoretical absorption spectra for $\Delta v = 1$ are also constructed, and are compared with the solar spectra. The spectra range around 2200 cm^{-1}, and therefore, the observed spectra are on the strong background. Without the proper subtraction of the background, the simulated spectra cannot be compared with the observed ones.

The theoretical absorption spectral intensity distribution $I(v', J' \leftarrow v'', J'')$ can be evaluated by the following formulae;

$$I(v', J' \leftarrow v'', J'') = \frac{B(v', J' \leftarrow v'', J'') \times \exp(-\Delta E_{vib}/kT_{vib}) \times (2J''+1) \exp(-\Delta E_{rot}/kT_{vib})}{\sum_{v'', J''} \exp(-\Delta E_{vib}/kT_{vib}) \times (2J''+1) \exp(-\Delta E_{rot}/kT_{vib})}$$

$$\Delta E_{vib}(v'', J'') = E(v'', 0) - E(0, 0)$$

$$\Delta E_{rot}(v'', J'') = E(v'', J'') - E(v'', 0)$$

where $B(v', J' \leftarrow v'', J'')$ is Einstein's B coefficient of the rovibrational transition $(v', J' \leftarrow v'', J'')$. Also we assume Boltzmann distribution with rotational temperature T_{rot} and vibrational temperature T_{vib}. Both the experimentally observed and the calculated absorption intensities $I(v', J' \leftarrow v'', J'')$ for $\Delta v = 2$ are well fit in to

an analytical function with three parameters a, b and c.

$$I(J''+1 \leftarrow J'', v' = v''+2 \leftarrow v'') = (a + b \times J'') \exp(-c \times J''^2)$$

Figure 8 shows the simulated and experimentally observed absorption intensity of rovibrational spectra for $v' = 4 \leftarrow v'' = 2$; $\Delta J = +1$ and for $v' = 2 \leftarrow v'' = 0$; $\Delta J = +1$, plotted against J''. In Figure 8, the experimentally obtained function is superimposed on the simulated results with assumed temperatures between 4000 K and 6000 K with 500 K interval. The fitted function of experimental data well superimpose on the calculated results of 4500 K at the peak of the graphs at $J \sim 30$, where the absorption intensities are the largest. For high J experimental data well superimpose on the calculated results of 5000 K. The figures indicate that the temperature of carbon monoxide molecules of the solar atmosphere distributes between 4500 K and 5000 K. The temperature of carbon monoxide molecules on the sun cannot fit to a single temperature, which might imply that the gas exist at a wide range of the altitude.

4 Concluding remarks

With the accurate potential energy and dipole moment curves, and rovibrational wavefunctions on the potential energy curve, Einstein's A and B coefficients are evaluated. The calculated spectroscopic constants and Einstein's coefficients quantitatively reproduce the experimental data, if ever exist.

With the quantitatively reproduced calculated results, simulation of rovibrational absorption spectra for some rotational and vibrational temperatures are per-

formed using the calculated Einstein's B coefficients. The simulated absorption spectra are compared with the experimental absorption spectra from the solar atmosphere. The vibrational and rotational temperatures of solar atmosphere are estimated. The vibrational and rotational temperatures of the carbon monoxide gas in the solar atmosphere are estimated to lie between $4500K$ and $5000\ K$.

References

[1] R. Farrenq, G. Guelachvili, A.J. Sauval, N. Grevesse and C. B. Farmer, J. Mol. Spectr. **149**, 375 (1991).

[2] F. Grimaldi, A. Lecourt, and C. Moser, Int. J. Quan. Chem. **S1** : 153 (1967).

[3] Dage Sundholm, Jeppe Olsen and Poul Jørgensen, J. Chem. Phys. **102**, 4143 (1995).

[4] Stephen. R. Langhoff and Charles W. Bauschlicher, Jr. , J. Chem. Phys. **102**, 5220 (1995).

[5] T. H. Dunning Jr, J. Chem. Phys. **90,** 1007 (1989).

[6] H. -J. Werner and P. J. Knowles, J. Chem. Phys. **89,** 5803 (1988).

[7] P. J. Knowles and H. -J. Werner, Chem. Phys. Lett. **145,** 514 (1988).

[8] S. Iwata, Chem. Phys. Lett. **83,** 134 (1981).

[9] T. Kimura, N. Sato, and S. Iwata, J. Comp. Chem. **9,** 827 (1988).

[10] R. Millikan. J. Chem. Phys. **38**, 2855 (1963).

Figure Caption

Figure 1. The potential energy and dipole moment curve of the ground $X^1\Sigma^+$ state. Positive sign on the dipole moment curve represents $C^{\delta+}O^{\delta-}$.

Figure 2. The spacings between adjacent vibrational levels, $\Delta G_{v+1/2}(v) = G(v+1) - G(v) = \omega_e - 2\omega_e x_e(v+1)$, plotted against $2(v+1)$.

Figure 3. The spacings of $\Delta G(v)$, $\Delta\Delta G = \Delta G(v+1) - \Delta G(v) = -2\omega_e x_e + 6\omega_e y_e(v+3/2)$, plotted against v.

Figure 4 Calculated Einstein's A coefficient of rotationless vibrational transition $v'' \leftarrow v'$ of $\Delta v = v' - v'' = 1$, 2 and 3, plotted against v''.

Figure 5 Calculated Einstein's B coefficient of rotationless vibrational transition $v' \leftarrow v''$ of $\Delta v = v' - v'' = 1$, 2 and 3, plotted against v''.

Figure 6. The rotational quantum number (J) dependence of the calculated Einstein's B coefficients. of $(v', J') \leftarrow (v'', J'')$ for some rovibrational transitions of $\Delta v = 1$ and 2, for $\Delta J = +1$ (R-branch) and $\Delta J = -1$ (P-branch).

Figure 7. The simulated and experimentally observed absorption spectra between 4250 cm^{-1} and 4370 cm^{-1}.

Figure 8. The simulated and experimentally observed absorption intensity of rovibrationa spectra for $v' = 4 \leftarrow v'' = 2$ and $v' = 2 \leftarrow v'' = 0$, and $\Delta J = +1$. The estimated rotational temperature in the solar atmosphere is between 4500 K and 5500 K.

Fig. 1

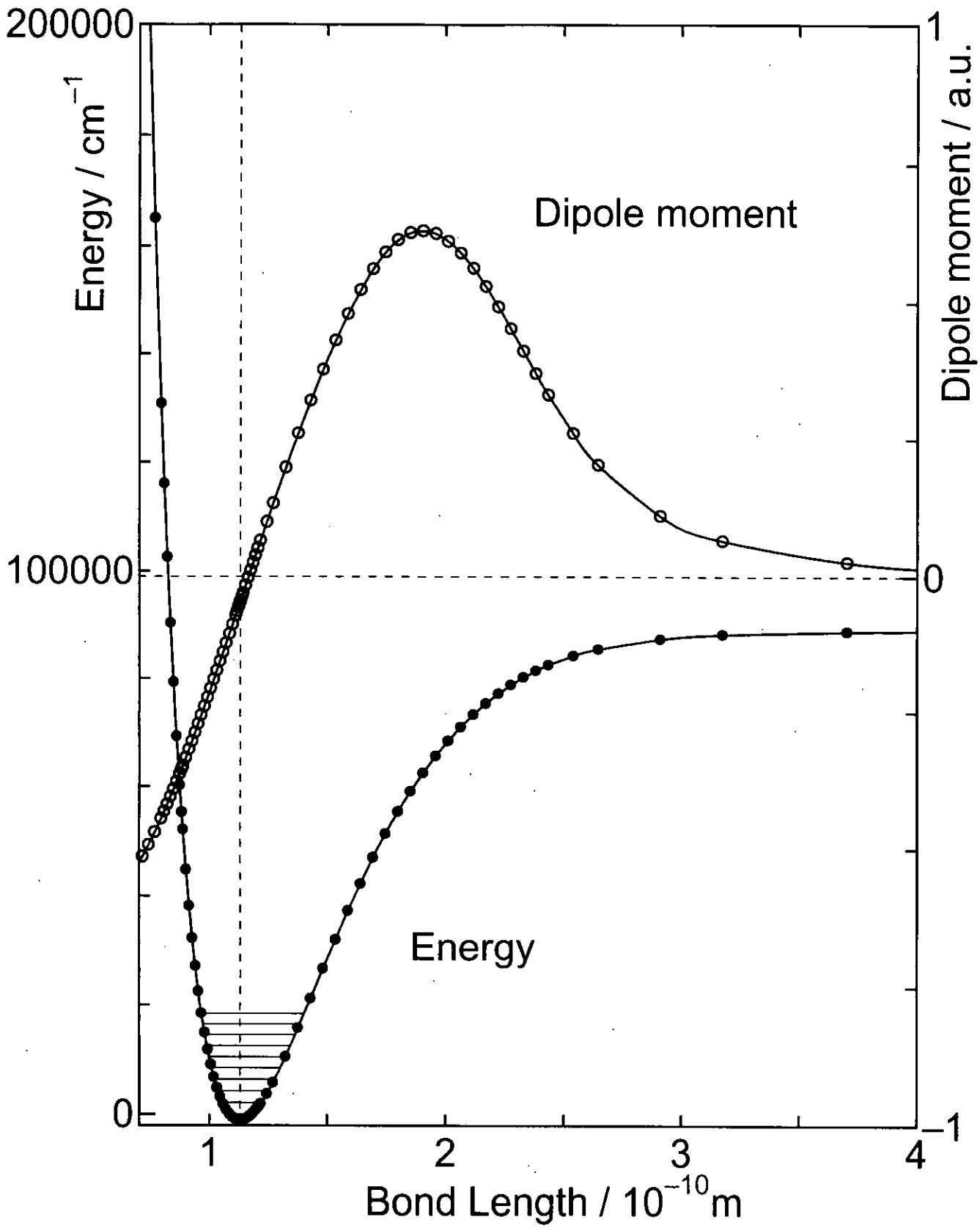
200000
100000
0
Energy / cm^{-1}
1
0
−1
Dipole moment / a.u.
Dipole moment
Energy
1
2
3
4
Bond Length / 10^{-10}m

Fig. 2

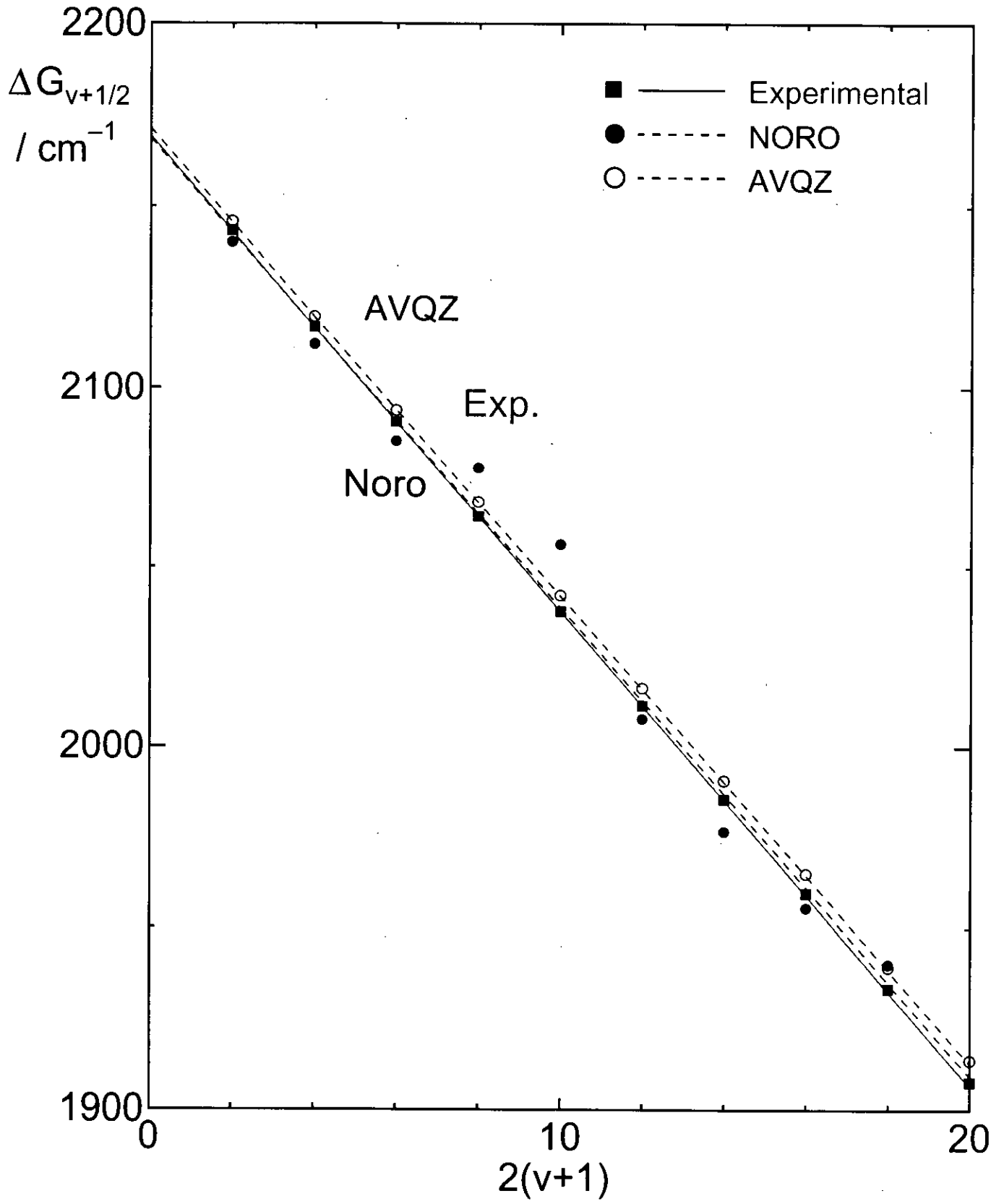
2200
2100
2000
1900
$\Delta G_{v+1/2}$ / cm^{-1}
Experimental
NORO
AVQZ
AVQZ
Exp.
Noro
0
10
20
2(v+1)

Fig. 3

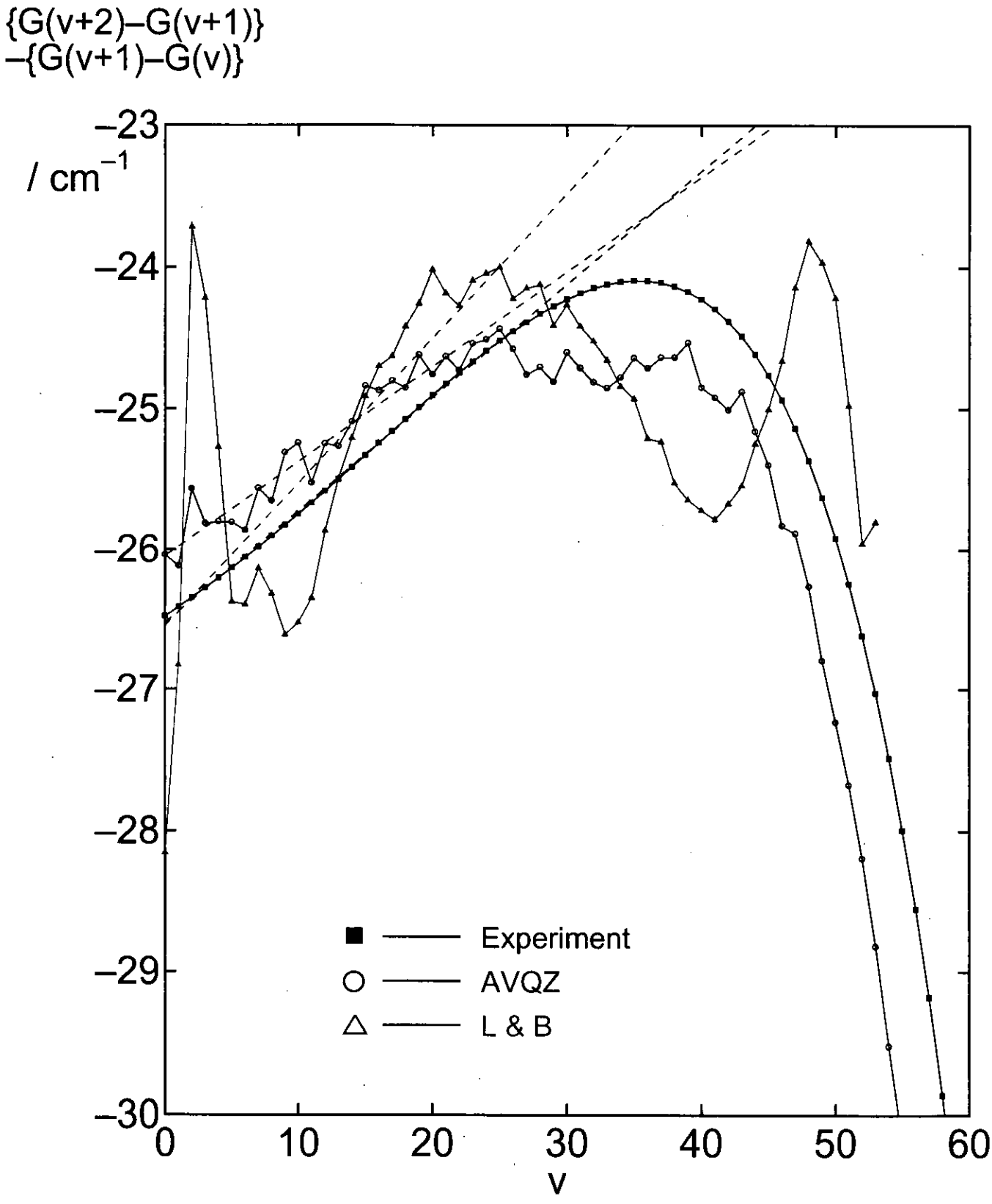
{G(v+2)–G(v+1)}
–{G(v+1)–G(v)}
/ cm^{-1}
–23
–24
–25
–26
–27
–28
–29
–30
0
10
20
30
40
50
60
v
Experiment
AVQZ
L & B

Fig. 4.1 $\Delta v = 1$

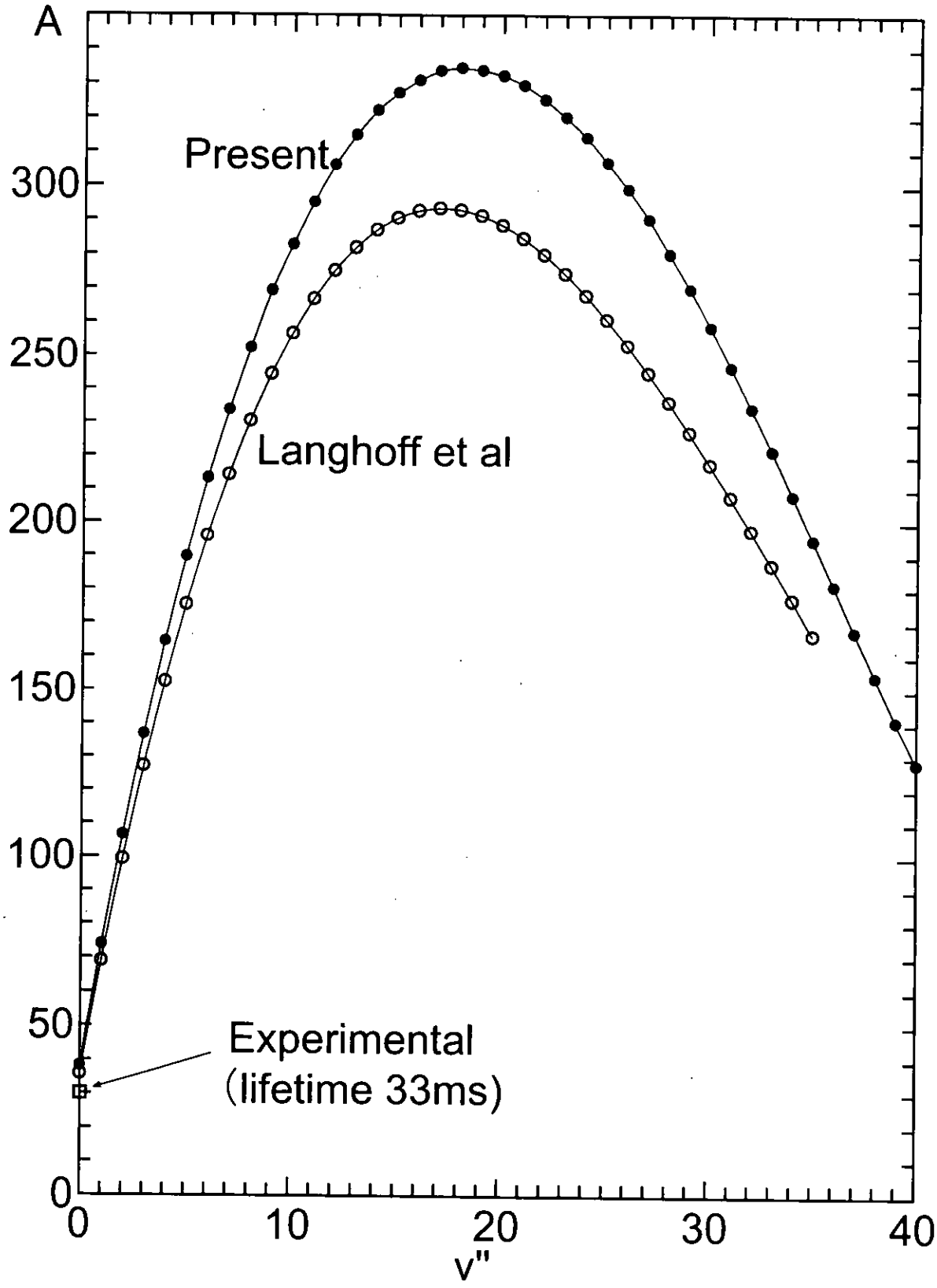

Fig. 4.2 $\Delta v = 2$

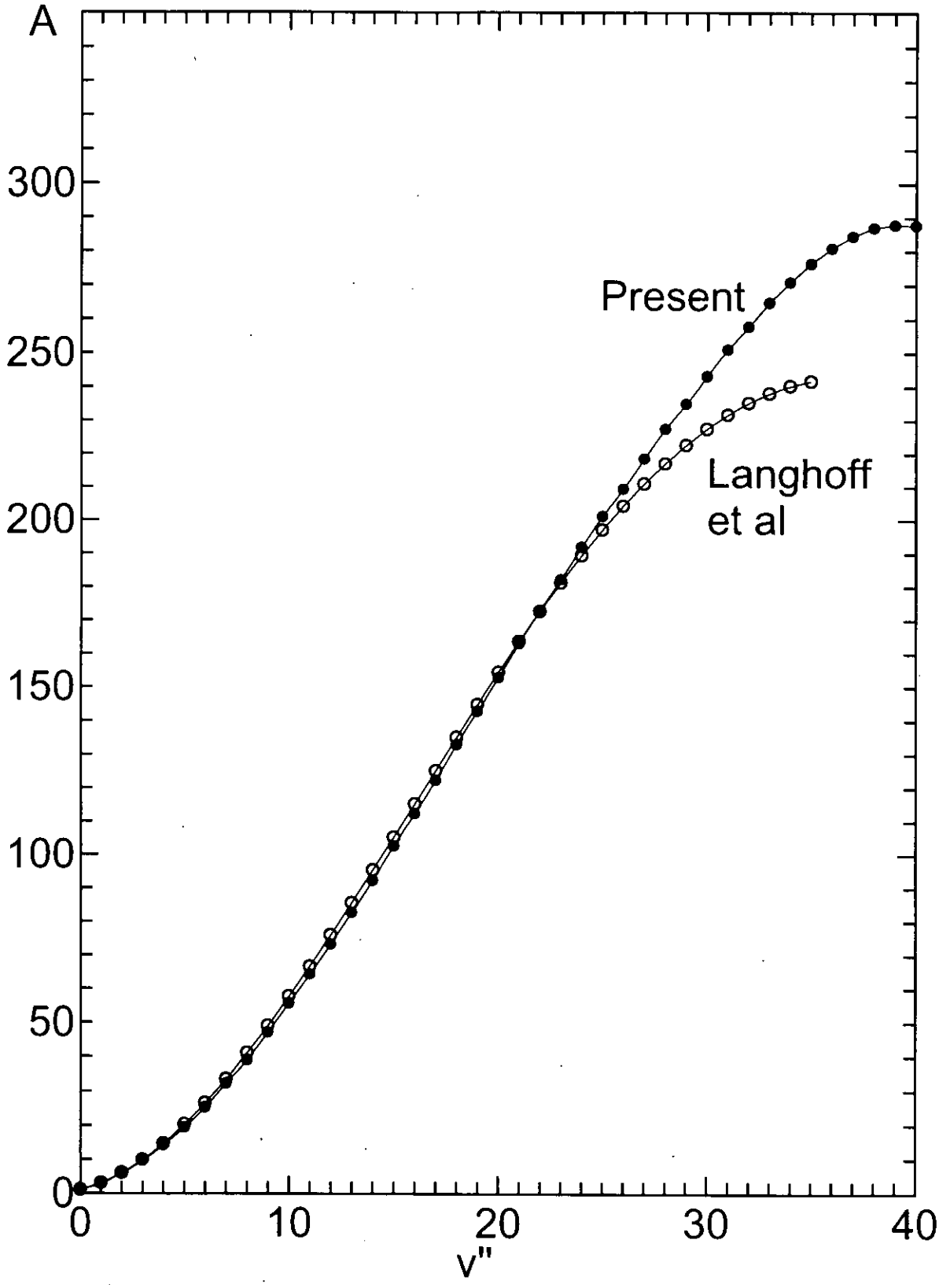

Fig. 4.3 $\Delta v = 3$

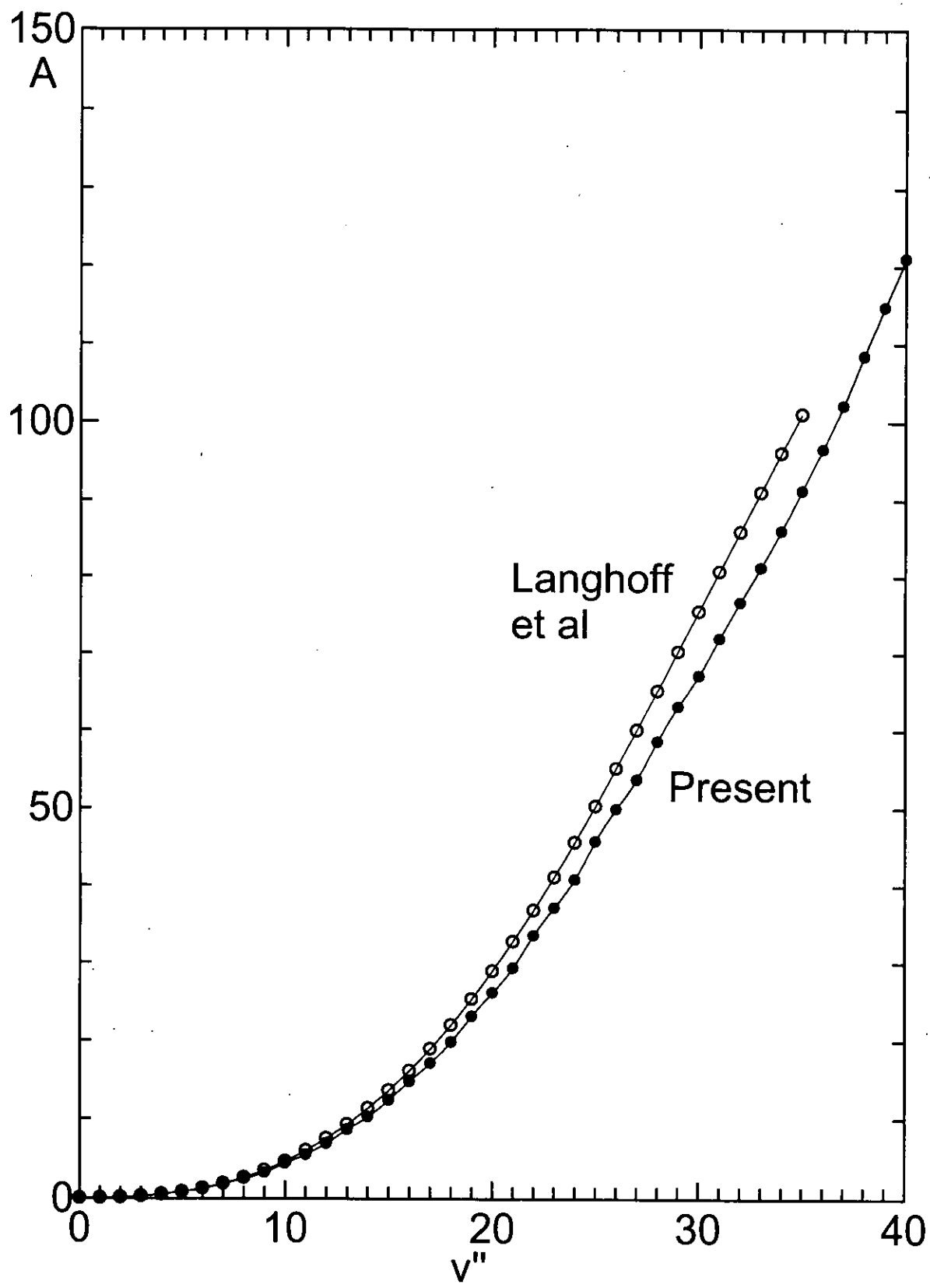

Fig. 5.1 $\Delta v = 1$

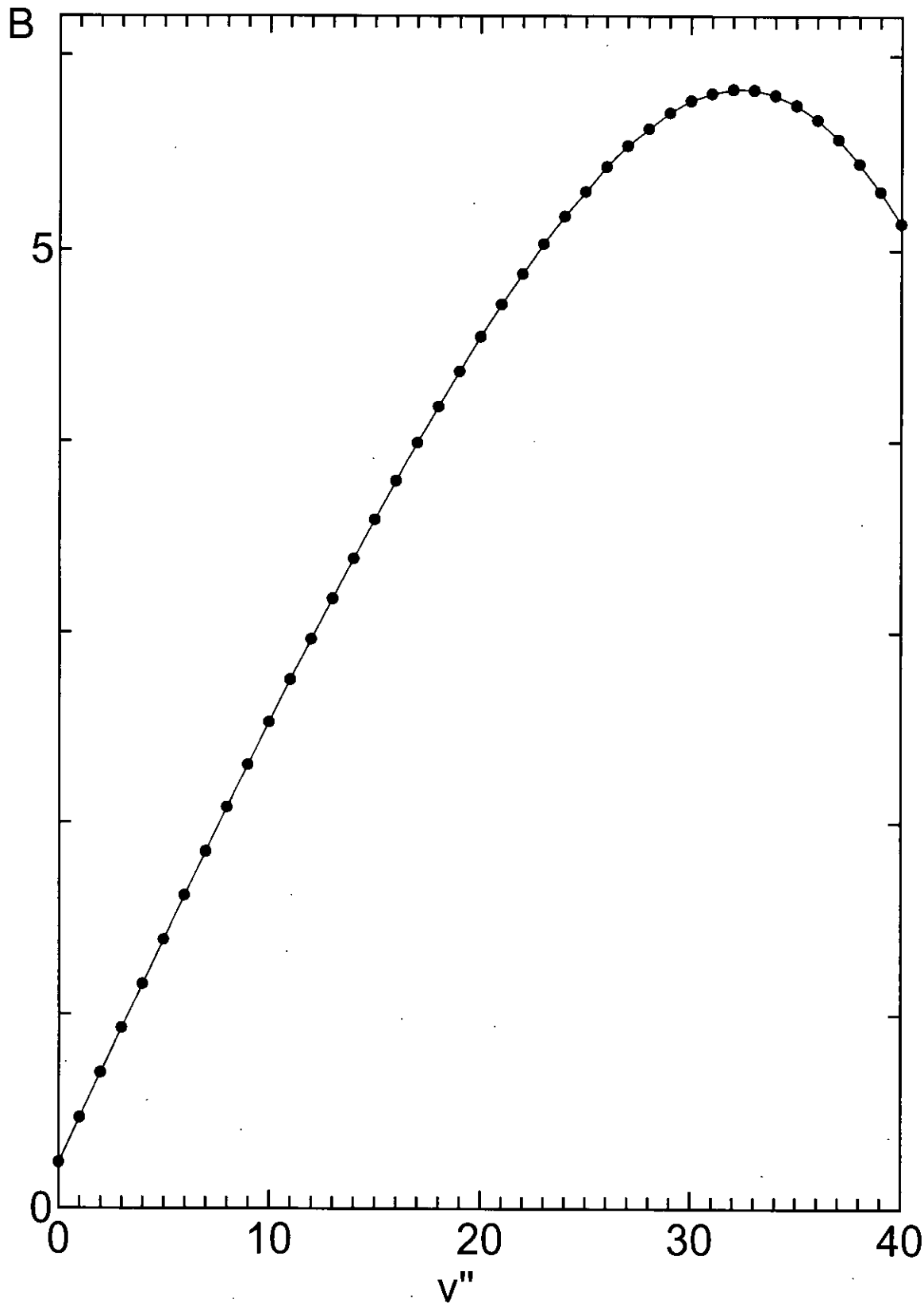

Fig. 5.2 $\Delta v = 2$

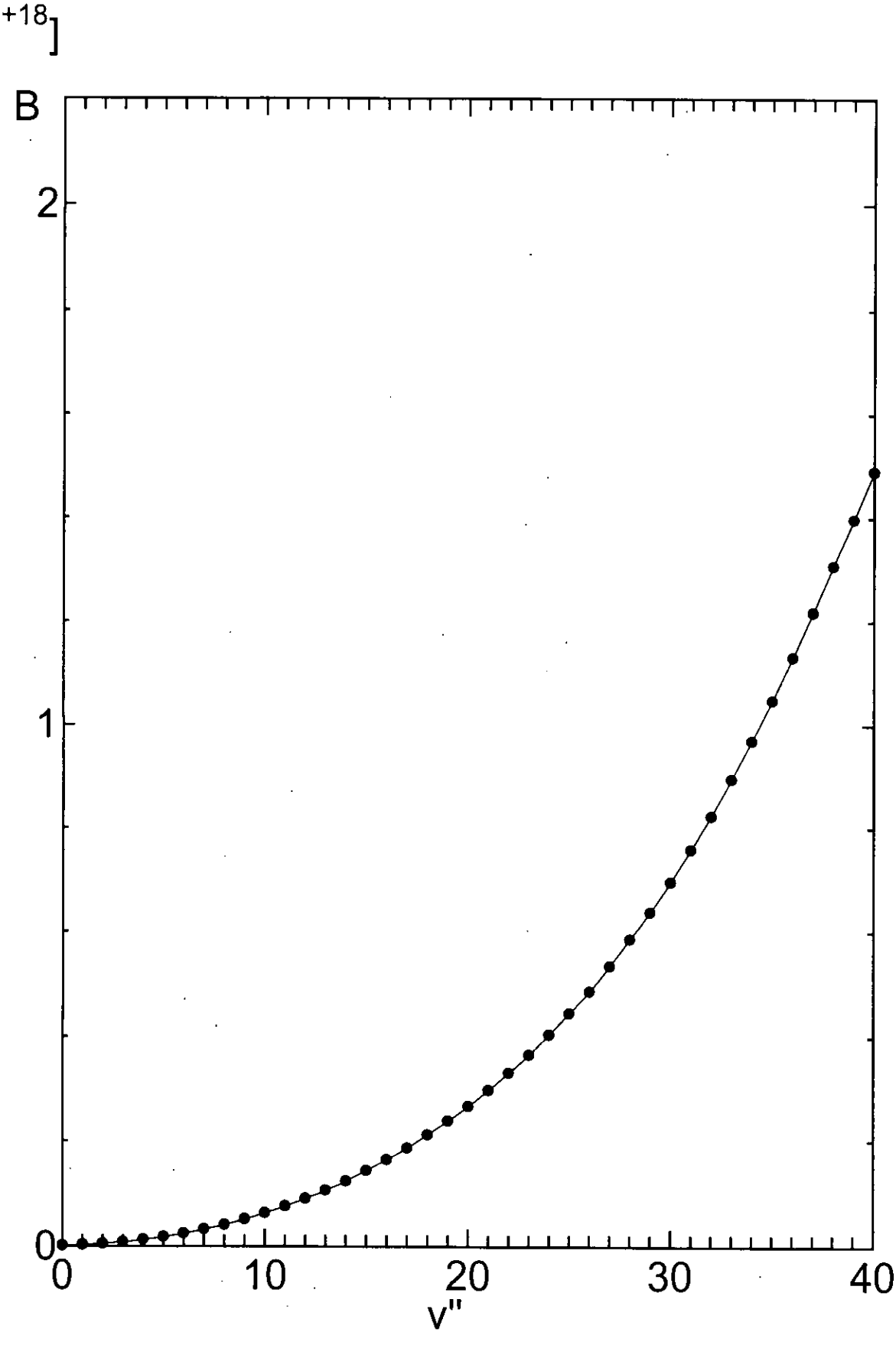

Fig. 5.3 $\Delta v = 3$

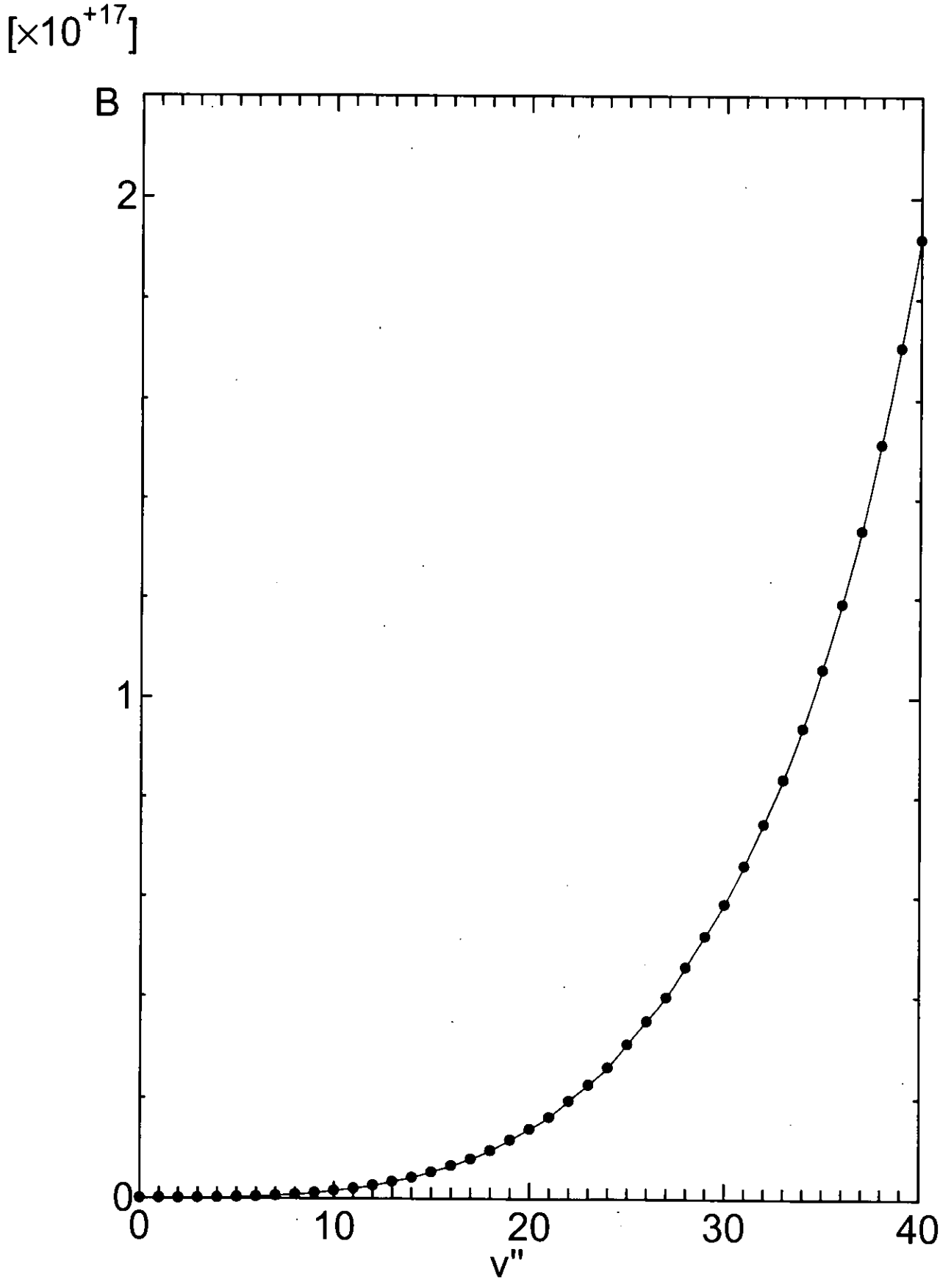

Fig. 6.1 $\Delta v = 1$

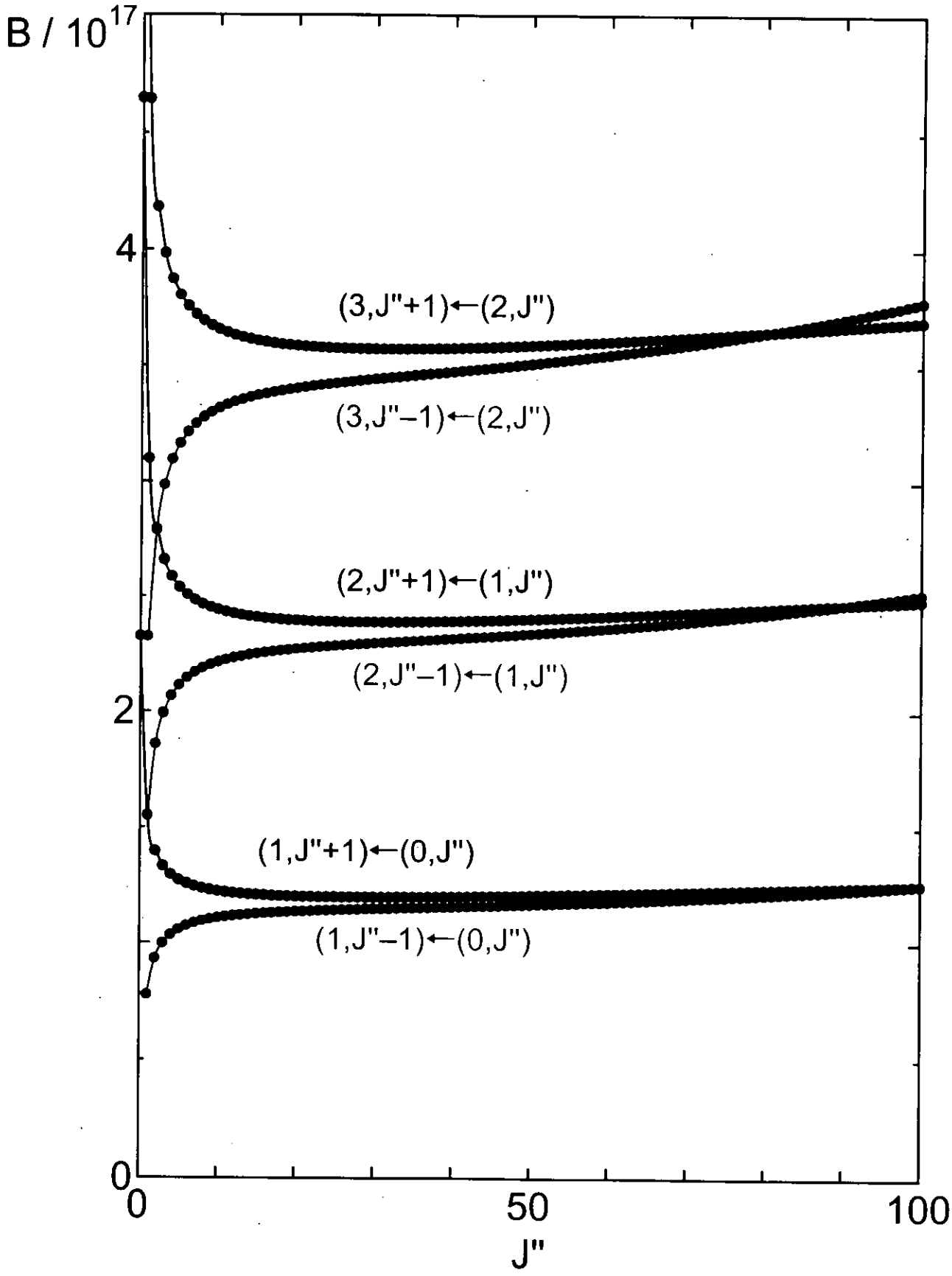

Fig. 6.2 $\Delta v = 2$

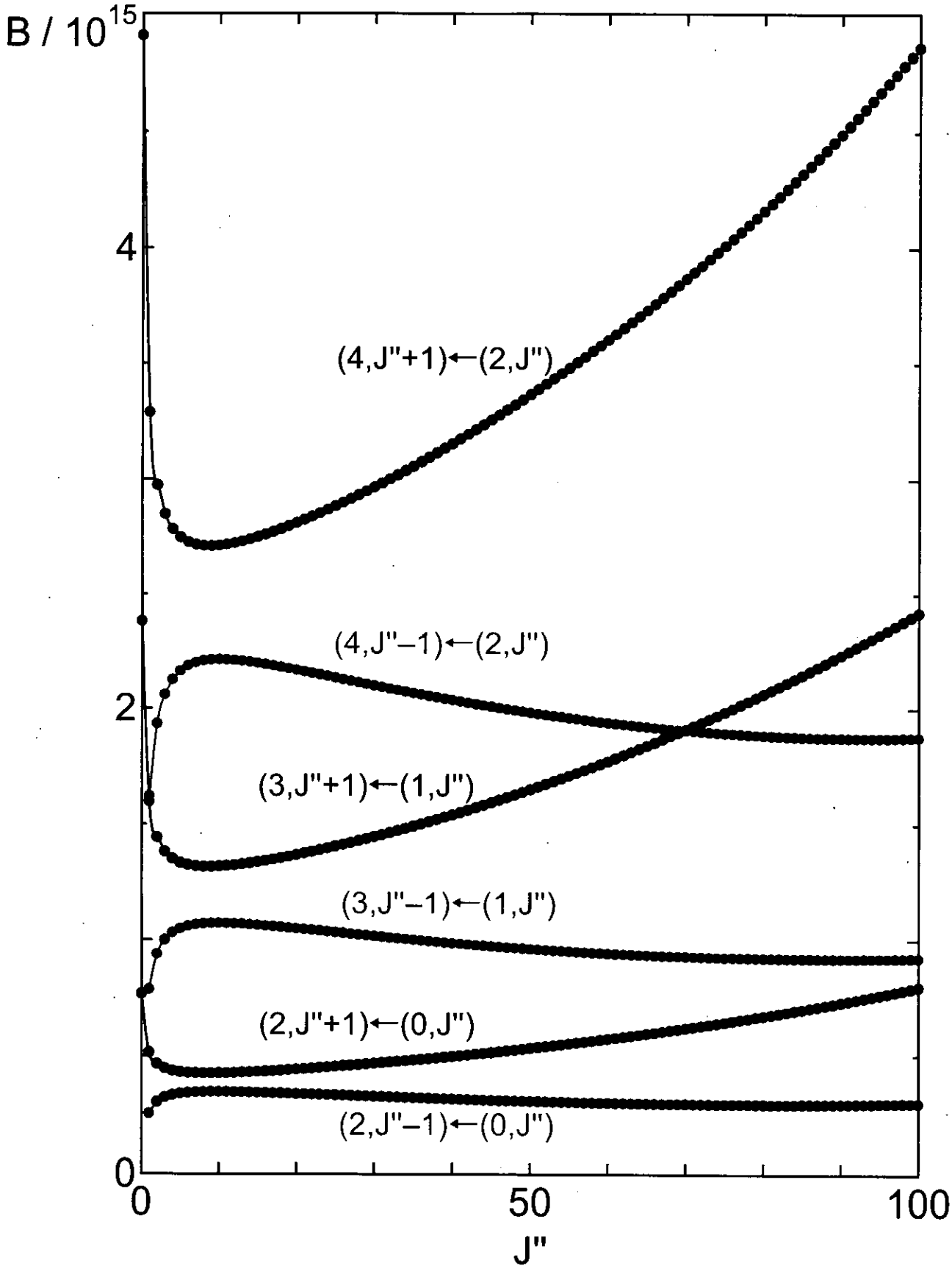

Fig. 7

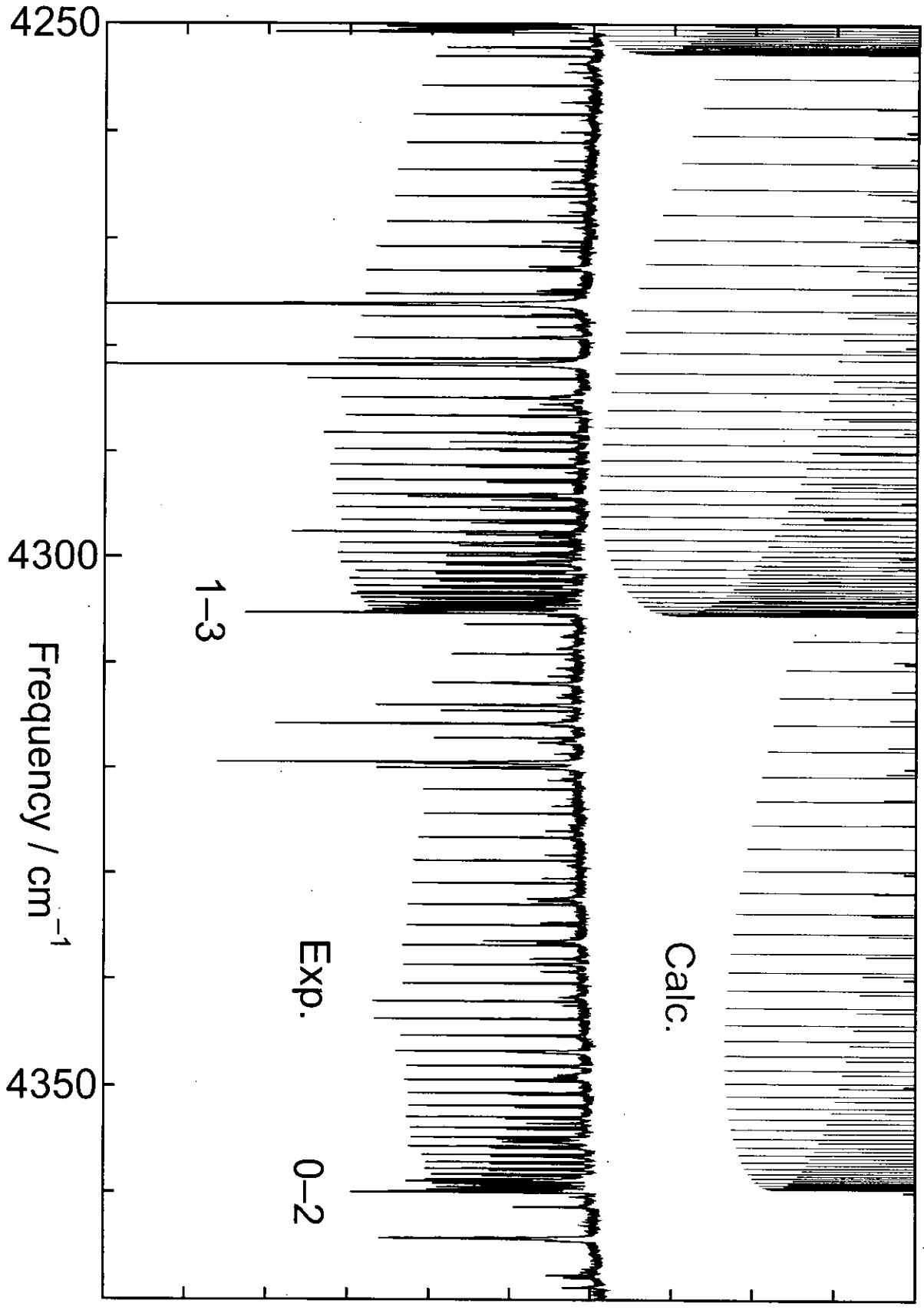

Fig. 8.1 0–2 transition

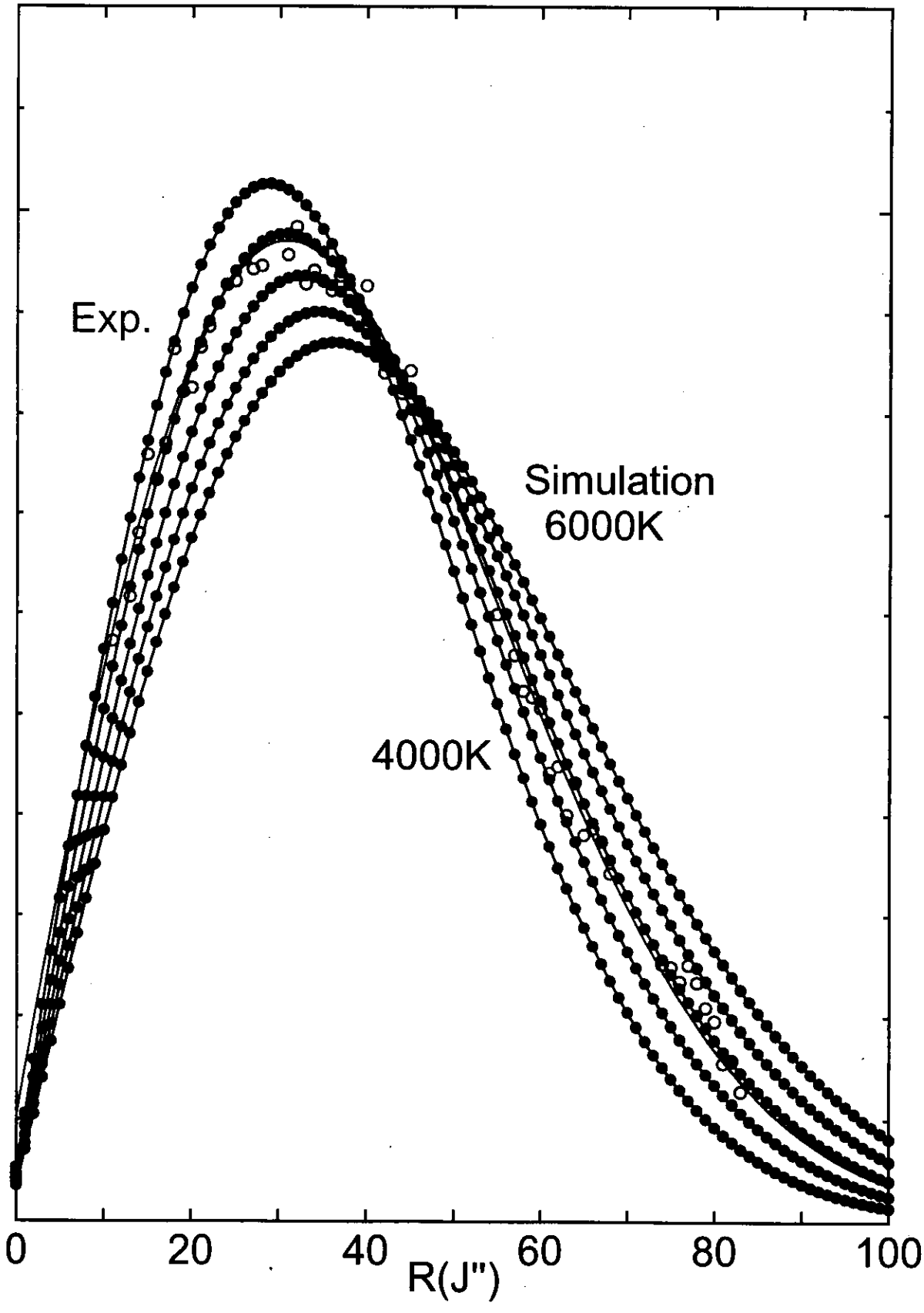

Fig. 8.2 2–4 transition

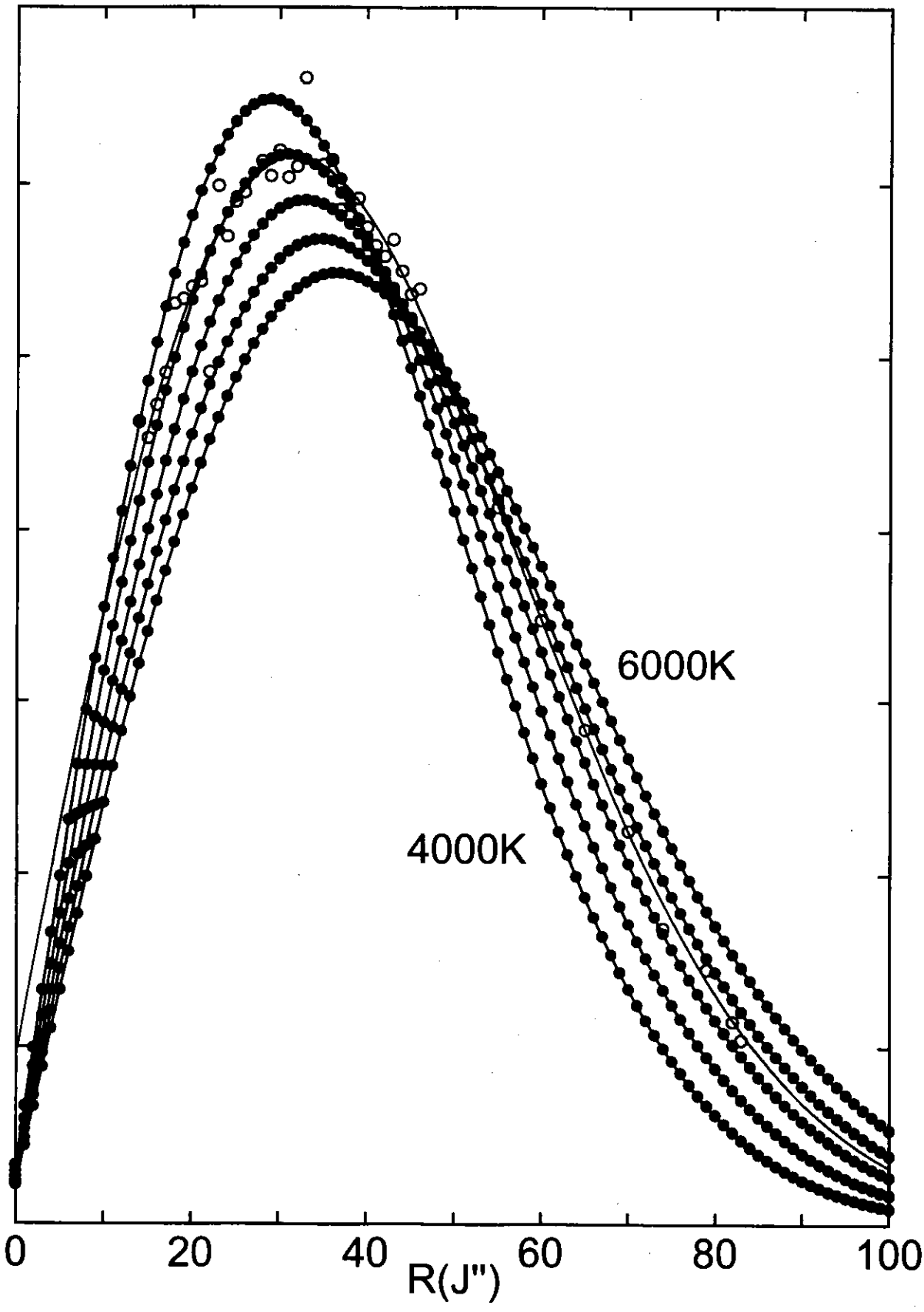

Table 1 The calculated and experimental spectroscopic constants. Langhoff and Bauschlicher's calculated result are also shown.

	r_e(Å)	$\omega_e(\mathrm{cm}^{-1})$	$\omega_e x_e(\mathrm{cm}^{-1})$	$\omega_e y_e(\mathrm{cm}^{-1})$	$D_e(\mathrm{cm}^{-1})$
Langhoff and Bauschlicher	1.132	2152.7	13.35	0.0170	88559
Present	1.130	2171.5	13.07	0.0112	89032
Exppriment	1.128	2169.4	13.32	0.0133	89446

Chapter 5

Accurate potential energy and transition dipole moment curves for several electronic states of N_2^+

1 Introduction

Nitrogen molecule is one of the most important diatomic molecules in atmospheric chemistry on our earth due to its ubiquitous presence in the atmosphere. Many experimental and theoretical studies have devoted to the molecular ion N_2^+. Experimentally, the ionic states of nitrogen molecule was observed by the visible and ultraviolet photoelectron, and pulsed field ionization photoelectron (PFI-PE) spectroscopies. For instance, Potts and Williams observed $X^2\Sigma_g^+$, $A^2\Pi_u$ and $B^2\Sigma_g^+$ states of N_2^+ [1]. Baltzer et al [2] observed photoelectron spectra of the $C^2\Sigma_u^+$, $D^2\Pi_g$, $2^2\Pi_g$, $F^2\Sigma_g^+$ and $3^2\Sigma_g^+$ states of N_2^+. Rotationally resolved PFI-PE spectra has been observed by F. Merkt and coworkers [3].

There are also many theoreticalc studies for the N_2^+ and its vibronic states. Recently, Langhoff and coworkers calculated potential energy and dipole moment functions of the $X^2\Sigma_g^+$ [4], $A^2\Pi_u$ [4], $B^2\Sigma_u^+$ [5] and $C^2\Sigma_u^+$ states [5] of N_2^+ and the radiative lifetimes of the vibrational levels of the $A^2\Pi_u$ and $B^2\Sigma_u^+$ states with reasonable accuracy.

In this study, the adiabatic potential energy and dipole moment curves of several doublet states of N_2^+ and the vibrational levels of each state were calculated. Spectroscopic constants were obtained from the potential energy curves and the calculated vibrational levels. From the obtained dipole moment function and vibrational levels, Einstein's A coefficients of the transition from vibrational levels of the excited states were evaluated, and the lifetime of the vibrational levels of the $A^2\Pi_u$, $B^2\Sigma_u^+$ and $C^2\Sigma_u^+$ states of N_2^+ were calculated and compared with available

calculated results and experimental data.

2 Calculation

Multireference configuration interaction (MRCI) calculations were performed for several electronic states of N_2^+. Two types of basis sets were employed. The one was derived from the Huzinaga (8s,5p) [6] contracted to [5111/2111], and two d function and one f function by Noro et al [7] were augmented; the basis set becomes [5111/2111/21/2]. We call it Noro basis set. The other was augmented valence quadruple zeta (aug-cc*p*VQZ, AVQZ) basis set of Dunning [8], which was employed to obtain accurate potential energy and property curves for the $X^2\Sigma_g^+$, $A^2\Pi_u$, $B^2\Sigma_u^+$ and $C^2\Sigma_u^+$ of N_2^+.

MRCI calculations were performed with MOLPRO internally contracted CI method [9][10]. The reference configurations were all electronic configurations generated from [$1\sigma_g^2$, $1\sigma_u^2$, $2\sigma_g^{0-2}$, $2\sigma_u^{0-2}$, $3\sigma_g^{0-2}$, $1\pi_u^{0-4}$, $1\pi_g^{0-4}$, $3\sigma_u^{0-2}$]. The calculations were performed under D_{2h} symmetry. The valence-type vacant orbitals, $1\pi_g$ and $3\sigma_u$, were determined by the VALVAC [11] (valence-type-vacant) method of Iwata. The method requires only a single Fock matrix generation after the closed shell SCF calculation, and provides us with a proper anti-bonding nature of molecular orbitals in the MRCI calculations.

Vibrational energies and wavefunctions on each adiabatic potential energy curve were calculated by solving the one-dimension nuclear Schrödinger equation with the FEM1D program of Kimura et al [12]. The integration region was between 1.6 a.u.

and 10.0 a.u.. Vibrational spectroscopic constants ω_e and $\omega_e x_e$ were obtained using the least-squares fitting of $\Delta G_{v+1/2} = G(v+1) - G(v)$, $G(v)$ being the vibrational energy relative to the lowest vibrational level. $G(v)$ is expressed as

$$G_v = \omega_e \left(v + \tfrac{1}{2}\right) - \omega_e x_e \left(v + \tfrac{1}{2}\right)^2 + ...$$

The dipole moment function of each state and the transition moment function between the states were evaluated, and by integrating them over the vibrational wavefunctions, Einstein's A coefficients of the vibrational transitions as well as the vibronic transitions were evaluated.

3 Results and discussion

All calculated results are compared with those of Langhoff and coworkers, and with experimental data ([4][5] and the references therein)

Figure 1 shows the potential energy curves (PEC) of the $X^2\Sigma_g^+$, $A^2\Pi_u$, $B^2\Sigma_u^+$ and $C^2\Sigma_u^+$ states of N_2^+ calculated by AVQZ basis set. Figure 2 shows the potential energy curves (PEC) of the other low-lying doublet states of N_2^+. The horizontal lines on each potential energy curve are the calculated vibrational levels. Equilibrium bond length, excitation energy, dissociation energy, and vibrational constants are also calculated from the potential energy curves, and are summarized in Table 1. The $X^2\Sigma_g^+$, $A^2\Pi_u$ and $B^2\Sigma_u^+$ states dissociate to $N^+(^3P)$+$N(^4S)$ or to $N^+(^2D)$+$N(^4S)$. From the figures, all of the calculated potential energy curves properly converge to the correct dissociation limit. The calculated energy difference at the dissociation limit between $N^+(^3P)$+$N(^4S)$ and $N^+(^2D)$+$N(^4S)$ is 19685 cm^{-1}. This is in good

agreement with the corresponding experimental value 19227.9 cm^{-1}.

Table 1 shows the electronic and vibrational spectroscopic constants of N_2^+. Potential energy curve and $\Delta G_{v+1/2}$ plot was fitted and vibrational spectroscopic constants ω_e, and $\omega_e x_e$ were obtained. R_e is equilibrium internuclear distance for each state. Experimental data are also shown. T_e is adiabatic excitation energy from the $X^2\Sigma_g^+$ state, and v_{00} is the 0-0 transition energy. D_e is adiabatic dissociation energy, and D_{00} is the dissociation energy from the $v = 0$ level. The values in parentheses are the present results with the Noro basis set. Only the $X^2\Sigma_g^+$, $A^2\Pi_u$, $B^2\Sigma_u^+$ and $C^2\Sigma_u^+$ states, the results by AVQZ basis set were given. For the $2^2\Pi_g$ state, ω_e and $\omega_e x_e$ is not obtained because the potential energy curve of the $2^2\Pi_g$ state has the shape of very shallow double minuma and the curve is far from the Morse potential energy curve. The calculated spectroscopic constants both for the Noro and AVQZ sets well reproduce experiment both for the Noro and AVQZ sets. The results also give a good prediction to the highly excited states when no experimental data are available.

Fgure 3 shows $\Delta G_{v+1/2} \equiv G(v+1) - G(v)$ for the $X^2\Sigma_g^+$, $A^2\Pi_u$, $B^2\Sigma_u^+$ and $C^2\Sigma_u^+$ states, plotted against $v + 1/2$. Dashed lines and a solid line are the least-squares fitted lines below $v \leq 10$ to determine spectroscopic constants ω_e and $\omega_e x_e$. The calculated $\Delta G_{v+1/2}$ are compared with experimental data and with those of Langhoff et al, if available. The agreement between the AVQZ result and experimental data are excellent for all of four states. The differnce in our result and experimental ω_e is only 3 cm^{-1} for the $X^2\Sigma_g^+$ and $A^2\Pi_u$ states. The calculated result by the AVQZ basis

set can reproduce experimental data quantitatively. The result by the NORO basis set and Langhoff et al are almost in the same accuracy; they are also in reasonable agreement with the experimental data. For the $X^2\Sigma_g^+$ state, experimental data shows that $\Delta G_{v+1/2}(3)$ and $\Delta G_{v+1/2}(4)$ deviates from the fitting line. This is due to the existence of the vibrational levels $v = 0$ and 1 of the $A^2\Pi_u$ state shown in Fig.1.

For the $B^2\Sigma_u^+$ and $C^2\Sigma_u^+$ states, the calculated and experimentally obtained $\Delta G_{v+1/2}$ plots deviates downward from the linear lines. The adiabatic potential energy curve of the $C^2\Sigma_u^+$ state shows that there is a strong coupling with the $B^2\Sigma_u^+$ state. Becauseof the configuration mixing, two curves cannot be approximated by a Morse functions. Therfore, the linear fitting of ΔG fails. In Fig. 3.3 and 3.4, both theoretical and experimental ΔG are fitted to quadratic forms of $(v + 1/2)$.

Table 2 shows the weights of the main ellectron configurations. Three bond lengths, 2.1 a.u.(Franck-Condon region of photoexcitation), 4.0 a.u.(intermediate) and 10.0 a.u.(near dissociation limit) are considered. The weights, $\sqrt{\sum(\mathbf{C}_{\mu,I})^2}$, are also shown, where the sum is taken over the configuration state functions (CSF) having the same electron configuration.

In near equiblium region, the main electronic configuration for the $B^2\Sigma_u^+$ state is a single hole configuration $(2\sigma_u)^{-1}$. And some small contribution is noticed from two-hole one-electron configurations, such as $(3\sigma_g)^{-1}(1\pi_u)^{-1}(1\pi_g)^1$, and the main electronic configuration for the $C^2\Sigma_u^+$ states is $(3\sigma_g)^{-1}(1\pi_u)^{-1}(1\pi_g)^1$. As the bond length increases, the mixing between $B^2\Sigma_u^+$ and $C^2\Sigma_u^+$ states becomes significant. At 4.0 a.u. the main configuration for both states are $(3\sigma_g)^{-1}(1\pi_u)^{-1}(1\pi_g)^1$ and

$(3\sigma_g)^{-1}(1\pi_u)^{-3}(1\pi_g)^3$. At 10.0 a.u., near the dissociation limit, the main configuration becomes $(3\sigma_g)^{-2}(1\pi_u)^{-2}(1\pi_g)^2(3\sigma_u)^1$.

Figure 4 shows the transition dipole moment functions between the $X^2\Sigma_g^+$ and $A^2\Pi_u$ states, between the $X^2\Sigma_g^+$ and $B^2\Sigma_u^+$ states, and between the $X^2\Sigma_g^+$ and $C^2\Sigma_u^+$ states calculated by the AVQZ basis set. Langhoff et al also calculated the transition dipole moment functions. The shapes of their curves are in agreement with ours, but in detail the bond length dependence of the functions is different. By evaluating the calculated dipole moment function, Einstein's A coefficient between vibronic levels are evaluated and the lifetime of the vibronic levels are estimated.

Table 3 shows the calculated lifetime of the vibrational levels of the $A^2\Pi_u$ state of N_2^+. Virational levels up to $v = 10$ are calculated and compared with the experimental data by Cartwright and by Peterson and Mosely. Previously calculational ones by Langhoff et al are also compared. Both calculated results are in excellent agreement with the both experimental data by Cartwright and by Peterson and Mosely within the experimental error. The agreement implies that the calculated Einstein A coefficients to the lower electronic states are accurate. In the calculation of the lifetime of the vibrational levels, Einstein's A coefficients of all transitions to the lower states has to be evalulated. In the calculation of Einstein's A coefficients, vibrational energies and their wavefunctions, and transition dipole moment functions have to be accurately evaluated.

Table 4 and 5 show the calculated lifetime of the vibrational levels of the $A^2\Pi_u$, $B^2\Sigma_u^+$ and $C^2\Sigma_u^+$ states of N_2^+. The calculated results are compared with the calcula-

tional results by Langhoff et al. For the $B^2\Sigma_u^+$ states, the lifetime of the vibrational up to $v = 10$ are calculated. For the $C^2\Sigma_u^+$ states, the lifetime of the vibrational levels are calculated only up to $v \leq 9$, because the adiabatic potential energy curve shows that there are only vibrational levels up to $v = 9$. Both calculated results agree well with each other. Experimentally, emission spectra of vibronic transitions $X^2\Sigma_g^+ \leftarrow A^2\Pi_u$ and $X^2\Sigma_g^+ \leftarrow B^2\Sigma_u^+$ are observed from aurora afterglow or lightning on earth. With calculated Einstein's A coefficients and experimentally observed rovibrational absorption intensity, the concentration of N_2^+ molecule can be measured.

4 Conclusion

With MR-SDCI calculations using an extended basis set, the potential energy curves of several doublet states of N_2^+ are obtained, and spectroscopic constants and vibrational levels are compared with recent experimental data. The calculated spectroscopic constants and radiative lifetime of emission quantitatively reproduce experimental data within experimental errors. With the calculated results and the experimentally observed emission spectra from aurora afterglow and lightning on earth, the concentration of N_2^+ on earth can be measured.

References

[1] B. Wannberg, D. Nordfors, K. L. Tan, L. Karlsson and L. Mattsson, J. Electron Spectroscopy and Related Phenomena **47,** 147 (1988).

[2] P. Baltzer, M. Larsson, L. Karlsson, B. Wannberg and M Carlsson Göthe, Phys. Rev. A **46**, 5545 (1992).

[3] F. Merkt and T. P. Softley, Phys. Rev. A **46**, 302 (1992).

[4] S. R. Langhoff, Charles W. Bauschlicher Jr. and HHarry Partridge, J. Chem. Phys. **87**, 4716 (1988).

[5] S. R. Langhoff, Charles and W. Bauschlicher Jr. J. Chem. Phys. **88**, 329 (1988).

[6] S. Huzinaga, J. Andzelm, M. Klobukowski, E. RadzioAndzelm, Y. Sakai and H. Tatewaki, eds. Physical Sciences Data, Vol. 16, *Gaussian basis sets for molecular calculations* (Elsevier, Amsterdam, 1985)

[7] T. Noro, M. Sekiya and T. Koga, Theor. Chem. Acc. **98,** 25 (1997).

[8] T. H. Dunning Jr, J. Chem. Phys. **90,** 1007 (1989).

[9] H. -J. Werner and P. J. Knowles, J. Chem. Phys. **89,** 5803 (1988).

[10] P. J. Knowles and H. -J. Werner, Chem. Phys. Lett. **145,** 514 (1988).

[11] S. Iwata, Chem. Phys. Lett. **83,** 134 (1981).

[12] T. Kimura, N. Sato, and S. Iwata, J. Comp. Chem. **9,** 827 (1988).

Figure Caption

Figure 1. The potential energy curves (PEC) of the $X^2\Sigma_g^+$, $A^2\Pi_u$, $B^2\Sigma_u^+$ and $C^2\Sigma_u^+$ states.

Figure 2. The potential energy curves (PEC) of the other low-lying doublet states of N_2^+.

Figure 3. $\Delta G_{v+1/2} \equiv G(v+1) - G(v)$ plot for the $X^2\Sigma_g^+$, $A^2\Pi_u$, $B^2\Sigma_u^+$ and $C^2\Sigma_u^+$ states, plotted against $v + 1/2$.

Figure 4. The transition dipole moment functions between the $X^2\Sigma_g^+$ and $A^2\Pi_u$ states, between the $X^2\Sigma_g^+$ and $B^2\Sigma_u^+$ states, and between the $X^2\Sigma_g^+$ and $C^2\Sigma_u^+$ states calculated by the AVQZ basis set.

Fig. 1

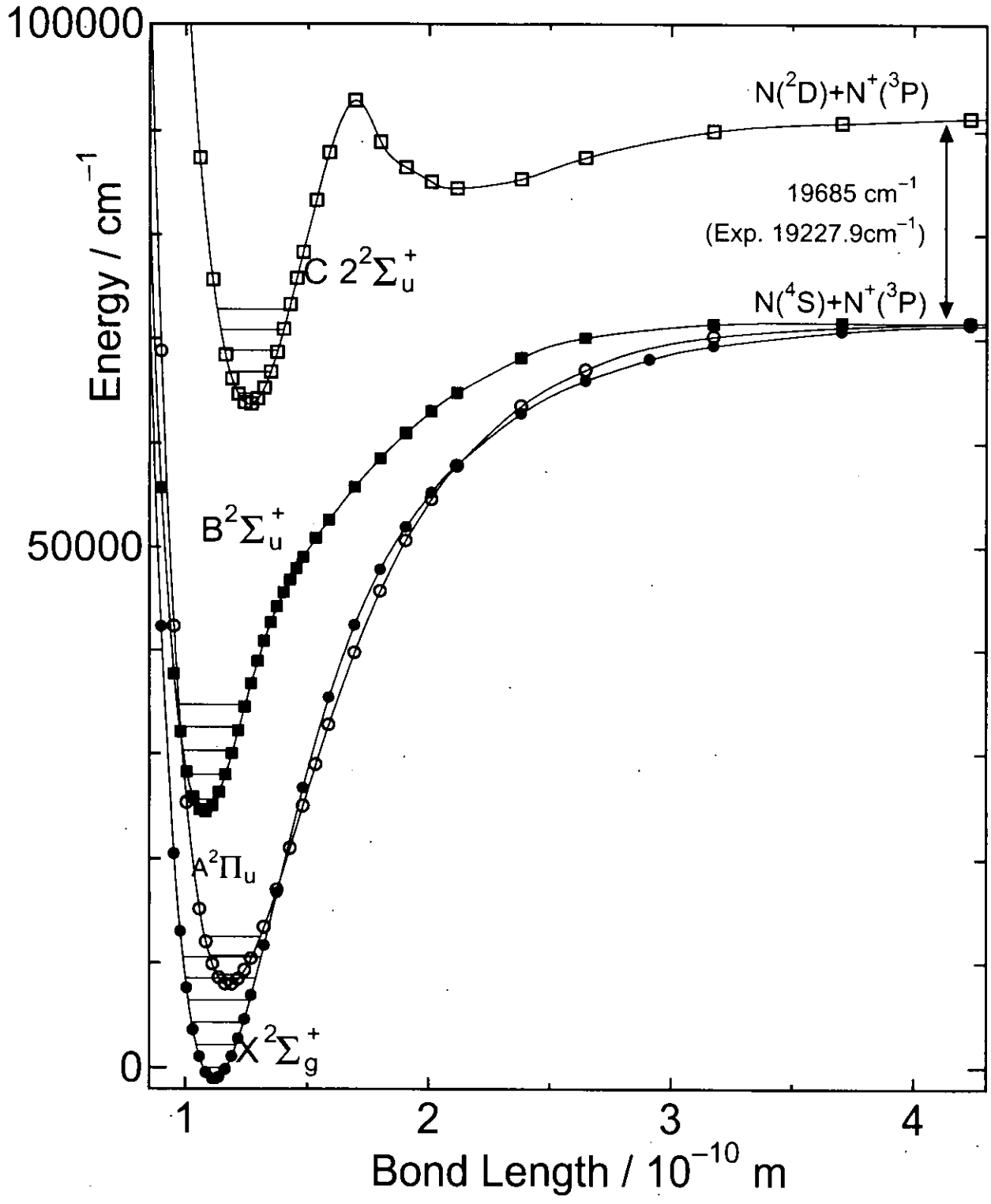
100000
50000
0
Energy / cm^{-1}
N(^{2}D)+N$^+$(^{3}P)
19685 cm^{-1}
(Exp. 19227.9cm^{-1})
N(^{4}S)+N$^+$(^{3}P)
C $2^2\Sigma_u^+$
B$^2\Sigma_u^+$
A$^2\Pi_u$
X$^2\Sigma_g^+$
1
2
3
4
Bond Length / 10^{-10} m

Fig. 2

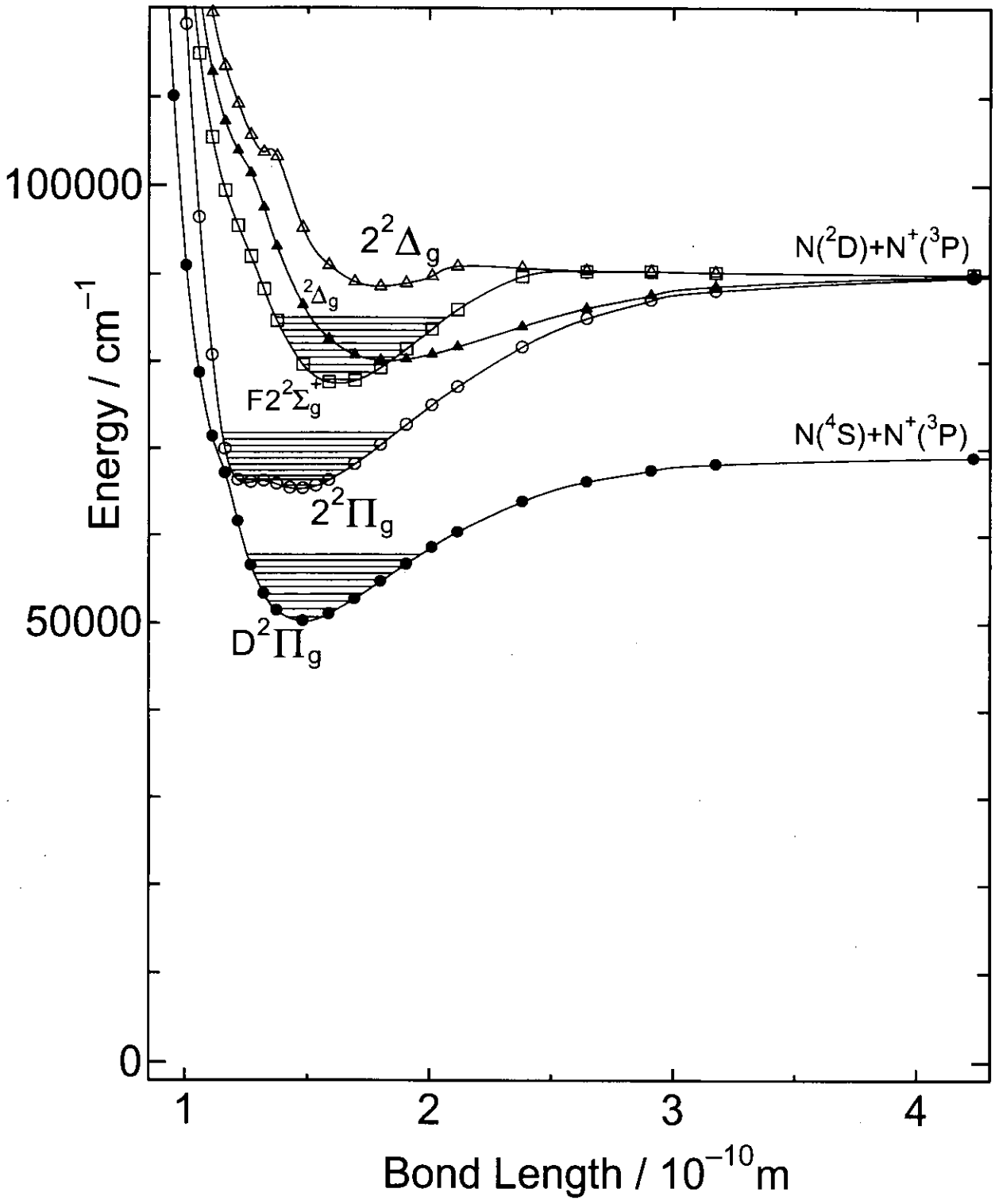
100000
50000
0
Energy / cm^{-1}
1
2
3
4
Bond Length / 10^{-10}m
$2^2\Delta_g$
$^2\Delta_g$
$F2^2\Sigma_g^+$
$2^2\Pi_g$
$D^2\Pi_g$
N(^{2}D)+N$^+$(^{3}P)
N(^{4}S)+N$^+$(^{3}P)

Fig. 3.1 X state

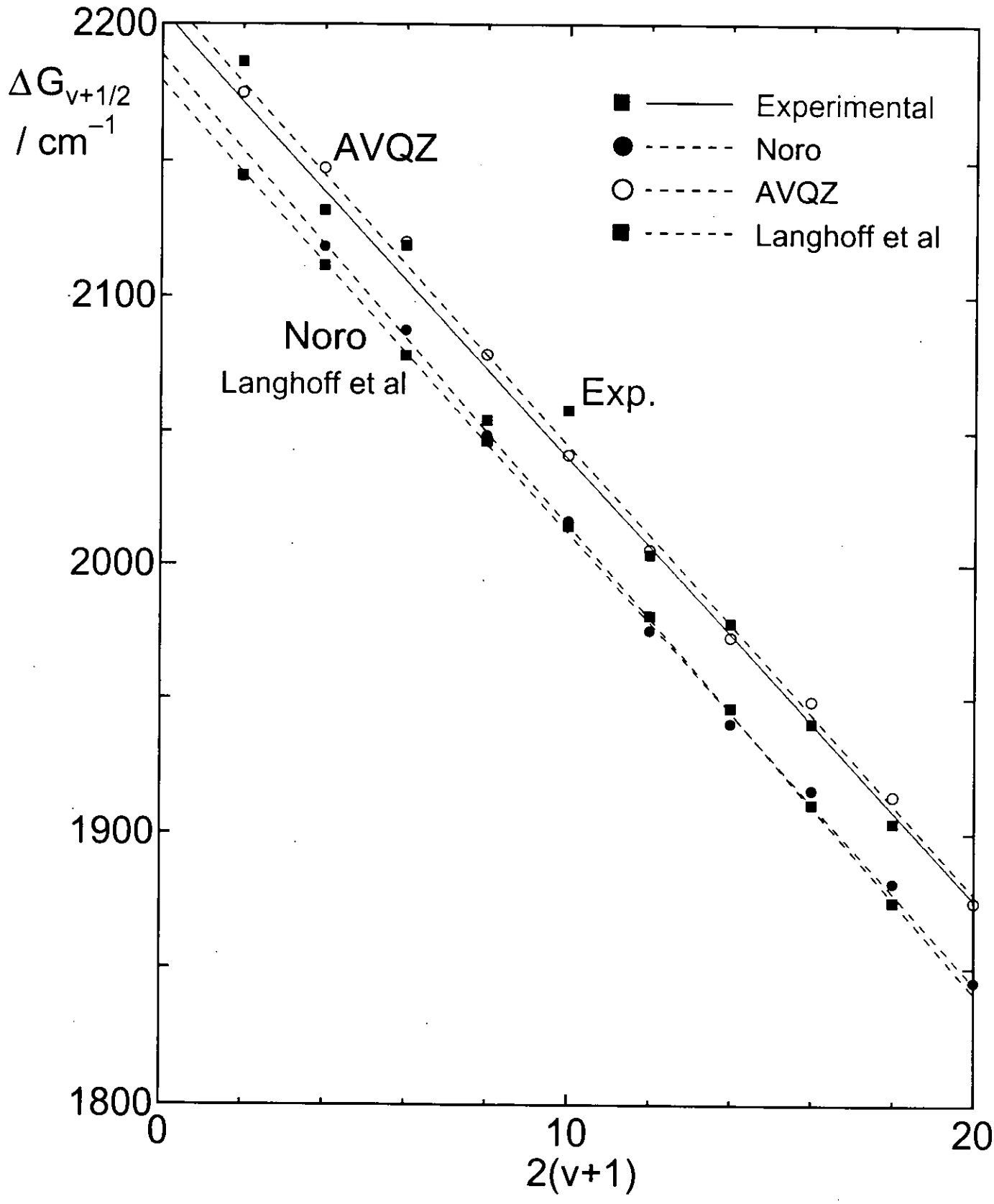

Fig 3.2 A state

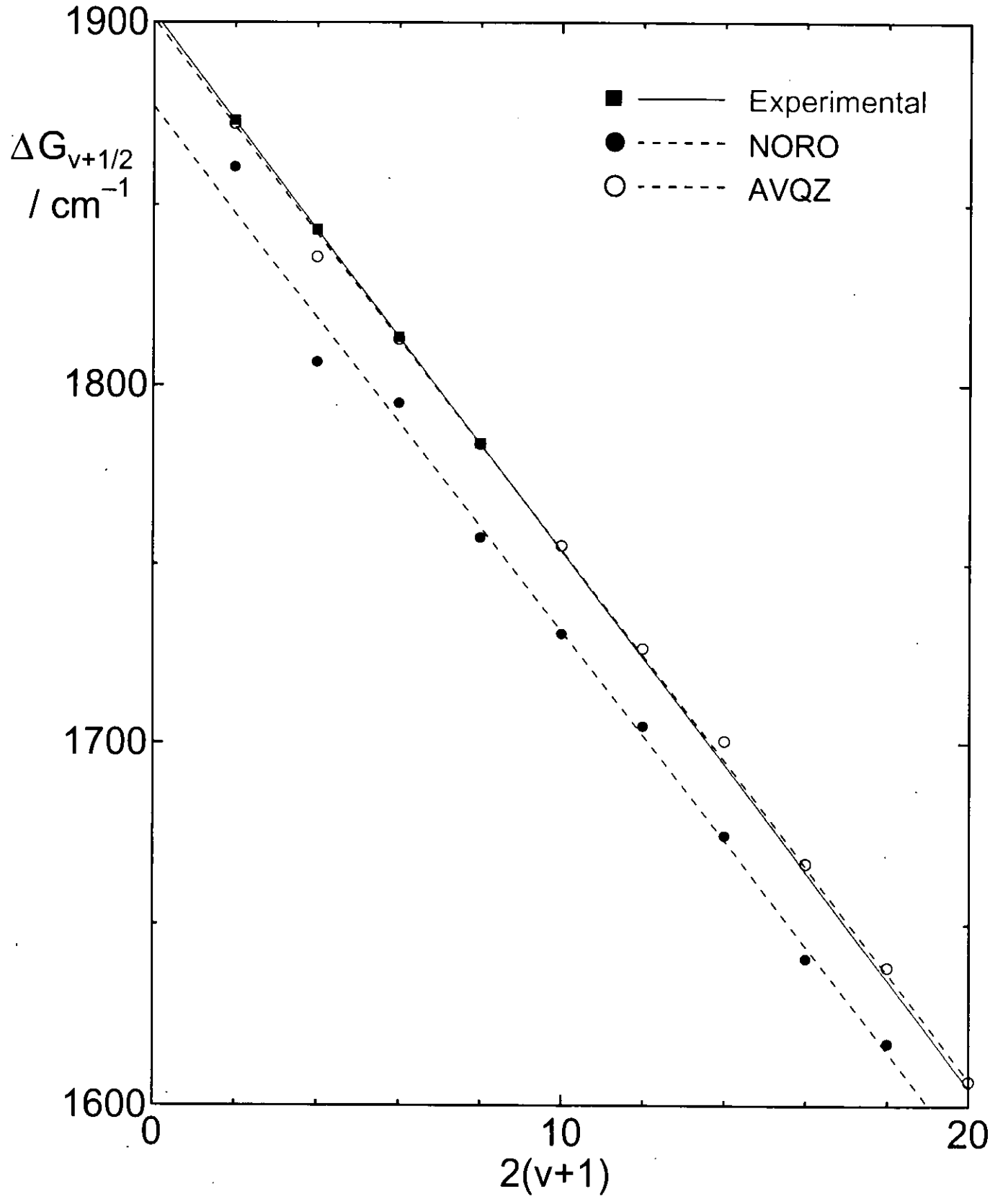

Fig 3.3 B state

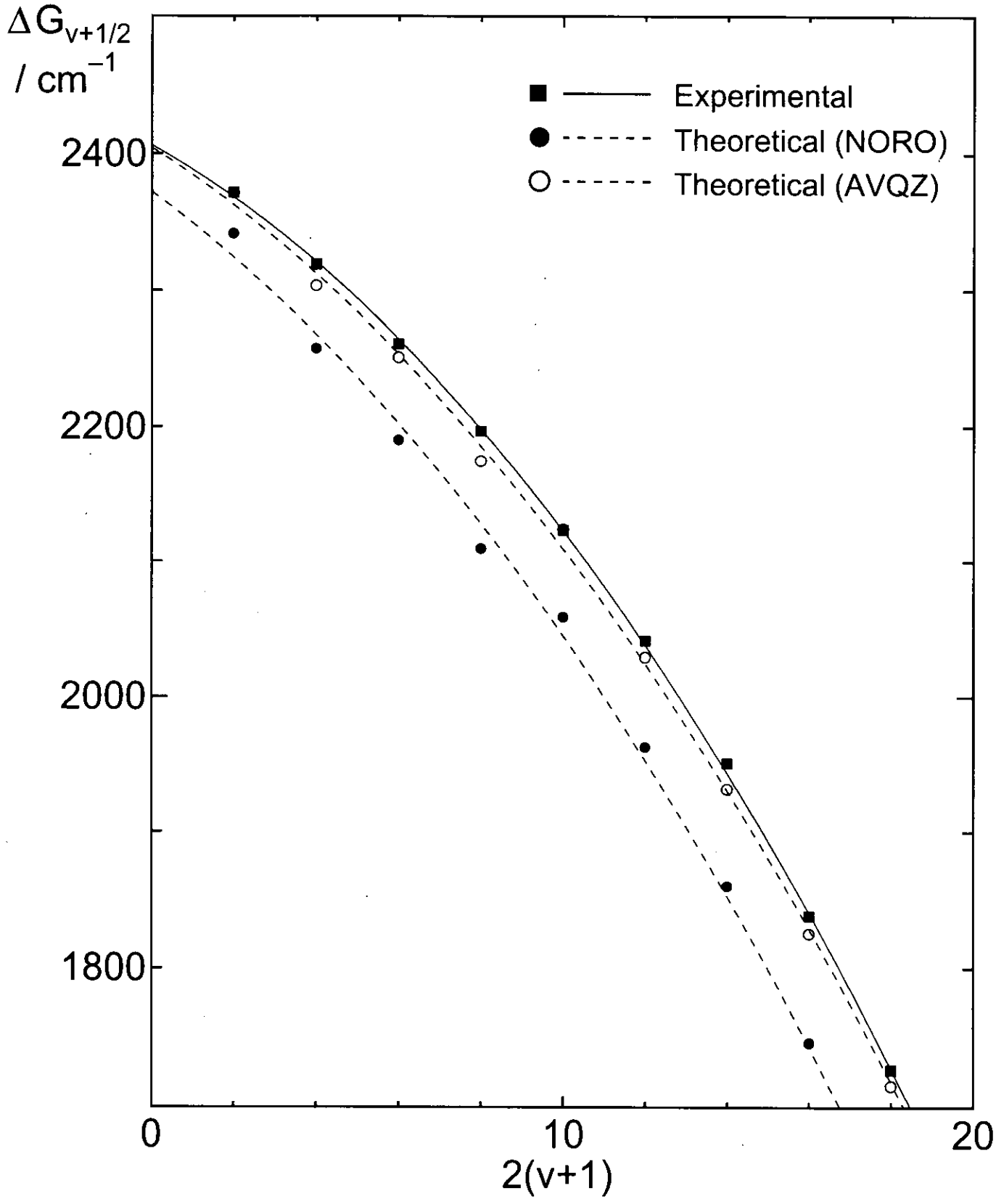

Fig 3.4 C state

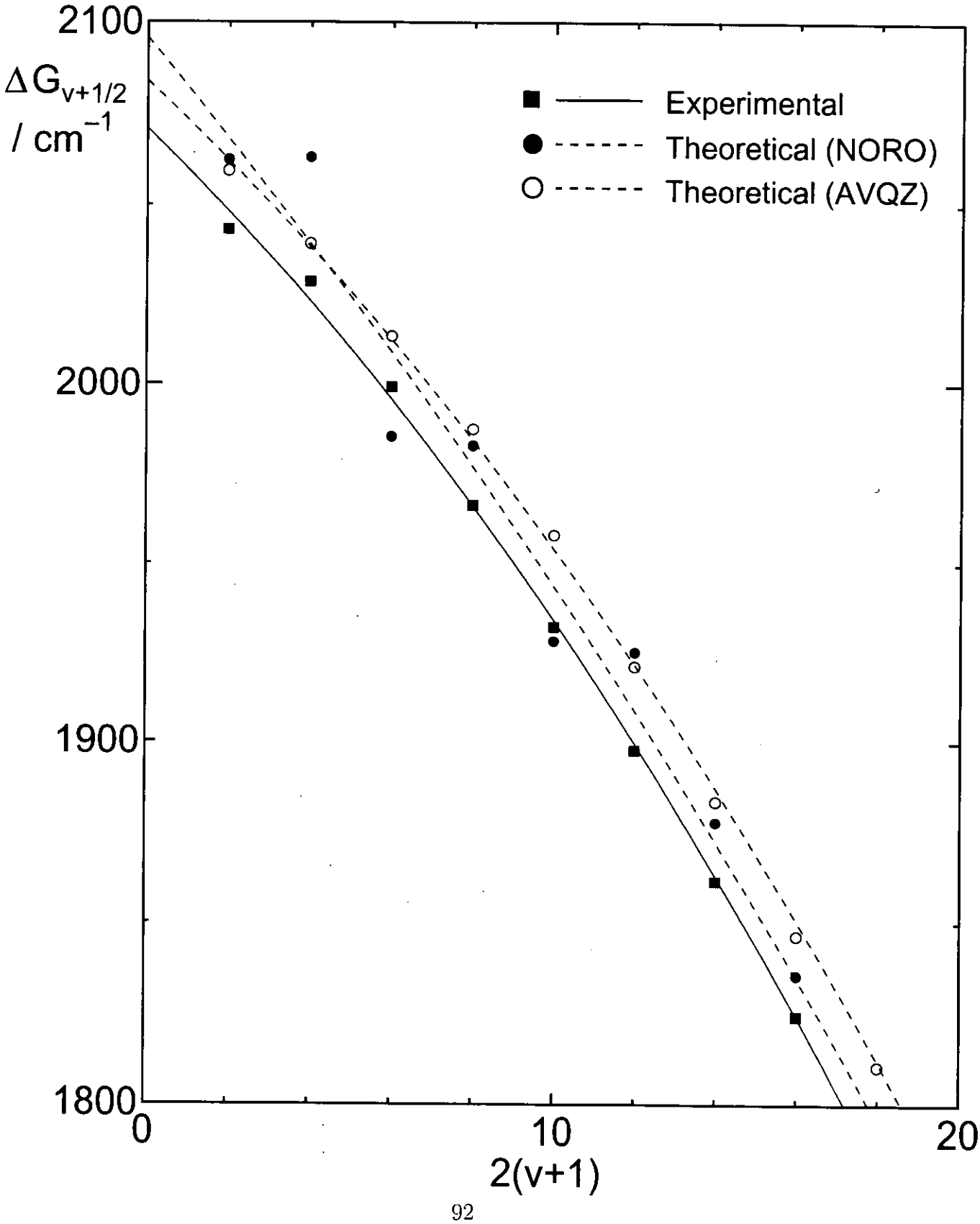

Fig. 4

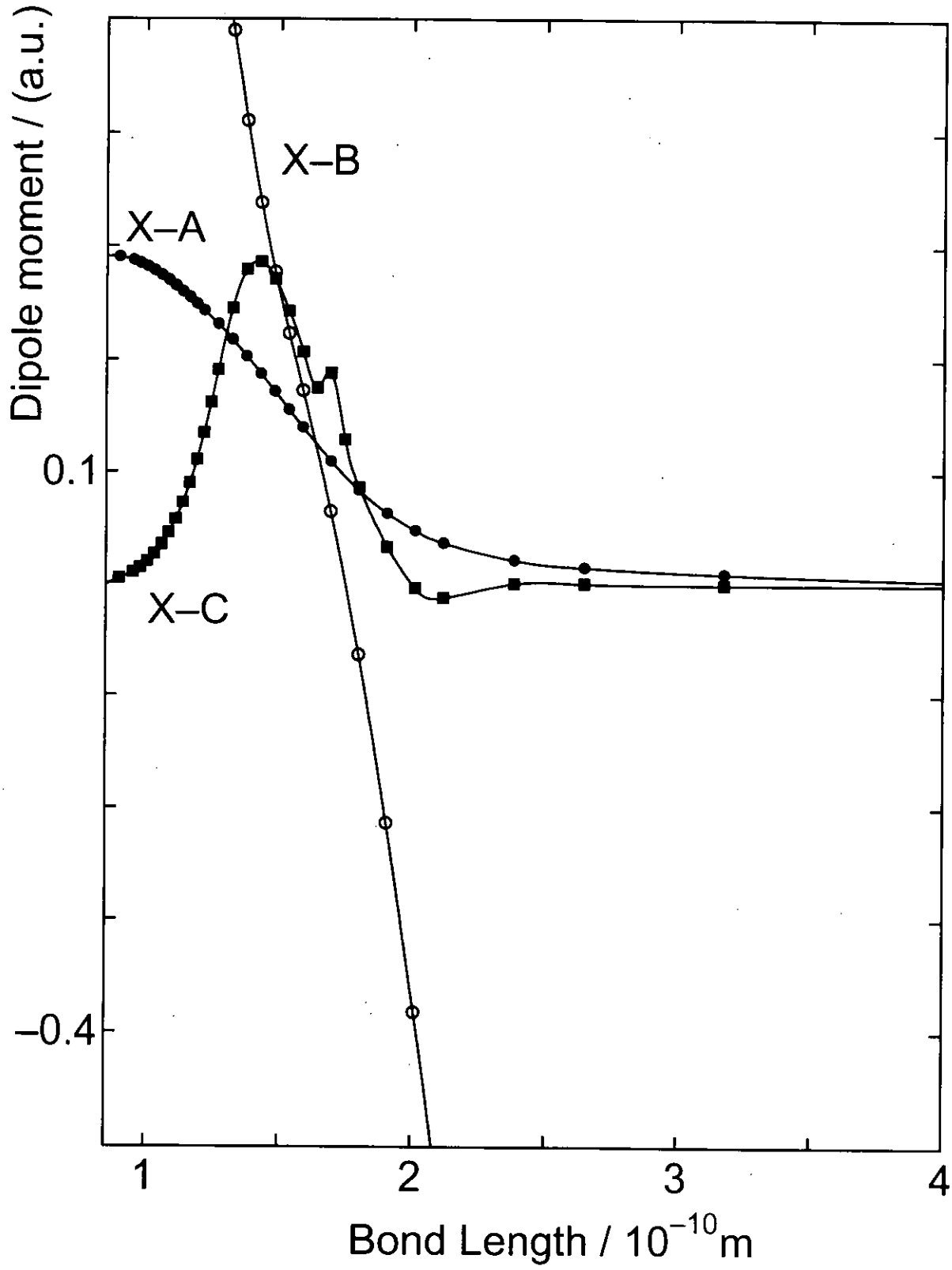

Table 1 Electronic, vibrational, and rotational spectroscopic constants N_2^+. Potential energy curve and $\Delta G_{v+\frac{1}{2}}$ plot was fitted and spectroscopic constants were obtained.

state		R_e/A *exp*	R_e/A *present*	T_e/cm^{-1} *exp*	T_e/cm^{-1} *present*	$\omega_e/\mathrm{cm}^{-1}$ *exp*	$\omega_e/\mathrm{cm}^{-1}$ *present*	$\omega_e x_e/\mathrm{cm}^{-1}$ *exp*	$\omega_e x_e/\mathrm{cm}^{-1}$ *present*	D_{00}/cm^{-1} *exp*	D_{00}/cm^{-1} *present*
N_2^+	$X^2\Sigma_g^+$	1.11642	1.119	0	0	2207.0	2209.6	16.10	15.88	70266	71747
			(1.125)		(0)		(2189.1)		(17.43)		(69490)
N_2^+	$A^2\Pi_u$	1.1749	1.178	9167	8983	1903.7	1901.1	15.02	14.70		62863
			(1.183)		(8710)		(1877.1)		(14.58)		(60780)
N_2^+	$B^2\Sigma_u^+$	1.074	1.077	25461	25507	$2419.8^{(a)}$	$2435.7^{(a)}$	$23.17^{(a)}$	$32.20^{(a)}$		46063
			(1.083)		(25994)		(2426.5)		(43.16)		(43390)
N_2^+	$C^2\Sigma_u^+$	1.262	1.263	64608	64825	$2071.5^{(a)}$	$2101.5^{(a)}$	$9.29^{(a)}$	$12.09^{(a)}$		26576
			(1.262)		(64556)		(2111.9)		(17.42)		(25618)
N_2^+	$D^2\Pi_g$	1.471	(1.477)	52318	(51338)	907.7	(896.5)	11.91	(11.59)		(18974)
N_2^+	$2^2\Pi_g$		(1.458)		(66940)		()		()		(24285)
N_2^+	$F^2\Sigma_g^+$		(1.630)		(78720)		(907.6)		(11.18)		(12123)
N_2^+	$2^2\Pi_u$		(1.879)		(77287)		(690.7)		(7.80)		(24285)
N_2^+	$1^2\Delta_u$		(1.361)		(64989)		(1122.0)		(14.11)		(25609)
N_2^+	$2^2\Delta_u$		(1.334)		(70378)		(1380.7)		(22.19)		(20111)
N_2^+	$1^2\Sigma_u^-$		(1.342)		(65268)		(1284.0)		(14.03)		(25222)
N_2^+	$2^2\Sigma_u^-$		(1.329)		(70378)		(1389.4)		(21.37)		(29575)
N_2^+	$1^2\Delta_g$		(1.831)		(81230)		(537.6)		(6.76)		(9671)

(a) The spectroscopic coefficients $\omega_e y_e$ by the quadratic fitting were $-1.56\ \mathrm{cm}^{-1}$(exp.) and $-1.43\ \mathrm{cm}^{-1}$(present) for the $B^2\Sigma_u^+$ state, and $-0.39\ \mathrm{cm}^{-1}$(exp.) and $-0.36\ \mathrm{cm}^{-1}$(present) for the $C^2\Sigma_u^+$ state.

Table 2 The lifetime (in μ scc.) of the vibrational levels of the $A^2\Pi_u$ state of nitrogen.

v	exp[a]	exp[b]	present	Langhoff et al [c]
0	16.57	.	16.98	16.04
1	13.88	13.9 ± 1.0	13.97	13.47
2	12.04	11.9 ± 0.4	11.93	11.74
3	10.70	10.7 ± 0.4	10.50	10.49
4	9.68	9.7 ± 0.4	9.49	9.54
5	8.89	9.1 ± 0.4	8.70	8.81
6	8.25	8.4 ± 0.5	8.10	8.24
7	7.72	7.8 ± 0.5	7.58	7.78
8	7.28	7.3 ± 0.5	7.15	7.40
9	6.91		6.77	7.10
10	6.58		6.54	6.85

(a) The data by Cartwright in Reference 4.
(b) The data by Peterson in Reference 4.
(c) Reference 4.

Table 3 The lifetime (in n sec.) of the vibrational levels of the $B^2\Sigma_u^+$ state of nitrogen.

v	present	Langhoff et al [a]
0	59.97	59.1
1	59.40	58.7
2	59.25	58.7
3	59.52	59.2
4	60.34	60.4
5	61.81	62.4
6	64.39	65.5
7	68.04	70.1
8	72.85	76.9
9	79.83	86.2
10	88.96	

(a) Reference 5.

Table 4 The lifetime (in n sec.) of the vibrational levels of the $C'^2\Sigma_u^+$ state of nitrogen.

v	present	Langhoff et al [a]
0	80.40	65.1
1	74.96	62.6
2	72.41	60.9
3	69.89	59.5
4	68.58	58.5
5	68.32	57.9
6	68.60	57.5
7	68.71	
8	70.72	
9	71.40	

(a) Reference 5.

Chapter 6

General conclusion

More accurate calculations than the previous studies for diatomic molecules and molecular ions were performed. The potential energy and dipole moment curves of the electronic states up to several electronic excited states of molecular ions were obtained. Rovibrational levels and wavefunctions for each calculated potential energy curve were also calculated. Vibrational spectroscopic constants and vibrational levels were compared with the recent experimental data. The calculated spectroscopic constants are in excellent agreement with the experimental data. By using the obtained rovibrational wavefunctions and the calculated dipole moment functions, Einstein's A and B coefficients of the rovibronic transition were calculated. The radiative lifetimes of vibronic excited levels were evaluated using Einstien's A and B coefficients and compared with the available experimental data. For the $X^1\Sigma^+$ state of neutral CO, the spectral intensity of absorption bands was simulated and compared with the recentlly observed rovibrational spectra from the sun.

All the calculated results well reproduced the experimental data. Especially, when the AVQZ basis set was used, the agreement with the experimental results were much better than the previous calculated results. The calculated results not only reproduced the trends but also quantitatively agreed with experimental data.

With these accurate theoretical A and B coefficients for the rovibronic transitions, if the absolute intensities of the emission and absorption spectra are experimentally determined for a target system, we can quantitatively monitor the target. This can provide a new important technique in atmospheric chemistry.

Acknowledgment

The author would like to express his sincere thanks to all the people who extended their support and cooperation for the completion of this work. The present work of the author is carried out under the guidance of Professor Suehiro Iwata.

The author wish to thank all the members of Professor Iwata's group, Mr. Takeshi Tsurusawa, Dr. Tsutomu Ikegami, Dr. Katsuhiko Satoh, Dr. Tomohiro Hashimoto, Dr. Feiwu Chen and Dr. Salai Cheettu Ammal, and also the previous members worked with Professor Iwata during his Doctor's course, Prof. Seiichiro Ten-no, Dr. Hidekazu Watanabe, Dr. Yumin Li, Dr. Jong Keun Park, Dr. Pradipta Bandyopadhyay, Dr. So Hirata, Dr. Andreas Fielder, Dr. Jan Hrusak, Prof. Fernando Ornellas and Mr. Tadayoshi Suzuki. The author also expresses his thanks to all the collaborators of Professor Iwata's group and to all the members of the other theoretical groups in IMS.

The author is grateful to Professor Cheuk Y. Ng(Iowa State University) for providing the photoelectron spectra before publication, which were used in Chapter 2 and 3, and also for useful discussions. The author acknowledges the help of Dr. Tsutomu Ikegami, who provided a spectrum of two strongly coupled diabatic states used in Chapter 3.

Finally, The author would like to express his sincere thanks to Prof. Hajime Kato in Kobe University, for his continuing encouragement during his Ph. D works.